NSF/CEE-81036

PB82-122391

The John A. Blume Earthquake Engineering Center

Department of Civil Engineering
Stanford University

# A BAYESIAN GEOPHYSICAL MODEL FOR SEISMIC HAZARD

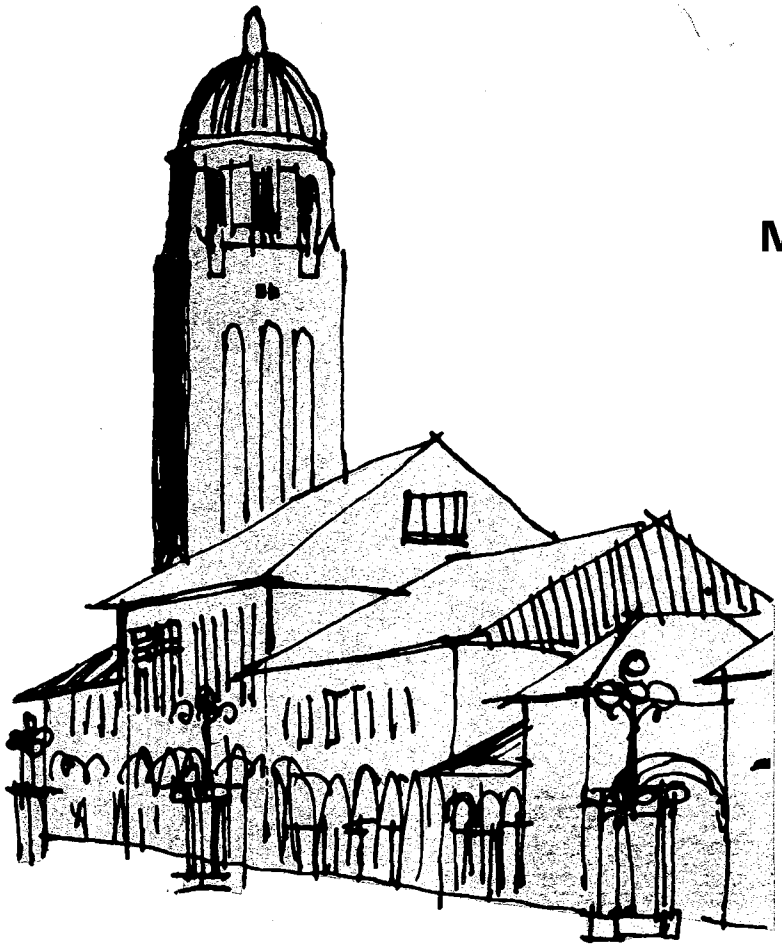

**Martin W. McCann, Jr.**

**A report on a research project partially supported by the National Science Foundation Grant ENV77-17834 and the U. S. Geological Survey Contract No. 17767**

**Report No. 47**

**May 1981**

*The John A. Blume Earthquake Engineering Center* was established to promote research and education in earthquake engineering. Through its activities our understanding of earthquakes and their effects on mankind's facilities and structures is improving. The Center conducts research, provides instruction, publishes reports and articles, conducts seminars and conferences, and provides financial support for students. The Center is named for Dr. John A. Blume, a well-known consulting engineer and Stanford alumnus.

*Address*

The John A. Blume Earthquake Engineering Center
Department of Civil Engineering
Stanford University
Stanford, California 94305

# A BAYESIAN GEOPHYSICAL MODEL FOR SEISMIC HAZARD

Martin W. McCann, Jr.

The John A. Blume
Earthquake Engineering Center
Dept. of Civil Engineering
Stanford University
Stanford, CA 94305

A Report on a Research Project
Partially Support by the
National Science Foundation
Grant ENV77-17834

and the

U.S. Geological Survey
Contract No. 17767

May 1981

Any opinions, findings, conclusions or recommendations expressed in this publication are those of the author(s) and do not necessarily reflect the views of the National Science Foundation.

Acknowledgements

I wish to express my sincere gratitude to my advisor Professor Haresh C. Shah for his support and encouragement during the course of this research.

I also wish to thank Professor David M. Boore for many helpful discussions and for reading the manuscript.

I also thank Professor James M. Gere for reading the manuscript and making many helpful suggestions.

I thank Professor Robert J. Geller for suggesting the use of the normal mode method.

I thank Nancy Novak for typing the manuscript.

The partial support of the National Science Foundation under grant ENV 77-17483 and the U.S. Geological Survey under contract no. 17767 is gratefully acknowledged.

I also wish to thank my parents for their support and encouragement in all my undertakings.

My deepest thanks goes to my wife Maggie for her understanding and patience.

TABLE OF CONTENTS

## LIST OF FIGURES

# CHAPTER I - INTRODUCTION

Earthquakes are a manifestation of the earth's geologic development. Their occurrence has been a topic of concern to man for thousands of years. This led to the development of earthquake engineering which seeks to define the expected hazard due to earthquakes and to control and reduce the consequences of these events to man's environment. These goals entail two central ideas, that of seismic hazard and seismic risk. In earthquake engineering these concepts are defined as follows: seismic hazard is the "expected occurrence of future seismic events", and seismic risk is the "expected consequence to future seismic events." This report deals with seismic hazard and the methods by which it is described.

## I.1 ELEMENTS OF SEISMIC HAZARD ANALYSIS

Seismic hazard analysis is concerned with modeling of earthquake occurrences on seismic sources and with defining the distribution of seismic intensity in the region surrounding the source.

The modeling of seismic occurrences has developed considerably in the last fifteen years. The probabilistic models that have been used to describe the future occurrence of earthquakes are the stationary Poisson model, (Cornell, 1968; Shah et al., 1975), the nonstationary Poisson model, (Savy, 1979), and Markov chain models, (Vagliente, 1973; Kiremidjian, 1979). Bayesian techniques have also been developed to update occurrence and magnitude information, (Benjamin, 1968; Esteva, 1969; Mortgat, 1976; Campbell, 1977).

The second aspect of seismic hazard analysis is that of describing the ground shaking intensity given the occurrence of an event. The methods employed in this area are strictly empirical, (McGuire, 1974; Shah et al., 1975; Idriss, 1978). Seismic intensity models consist of a description of the event size, a transmission path model, and a method of characterizing ground shaking. Both instrumental and subjective measures of the ground shaking hazard have been employed in seismic hazard analysis.

The complete probabilistic methodology for describing the seismic hazard at a site is a convolution of the effects due to all seismic sources for a future time period, (Cornell, 1968). The overall methodology is given graphically in terms of peak value characterizations of the ground shaking intensity in Figure I.1.1. Similarly Table I.1.1 presents a general summary of deterministic and probabilistic methods of seismic hazard analysis.

This report deals with the methods of defining the ground shaking hazard for application to seismic hazard analysis. The next section reviews the current methods of modeling strong ground motion.

## I.2 MODELING OF STRONG GROUND MOTION

A critical part of a seismic hazard analysis is the model used to describe the ground shaking intensity for an event. Strong ground motion due to earthquakes is the result of the dislocation on a fault and the propagation of seismic waves through a nonhomogeneous earth. The recorded strong motion time history has been considered in the past as a sample realization of a random process, (Housner and Jennings, 1964).

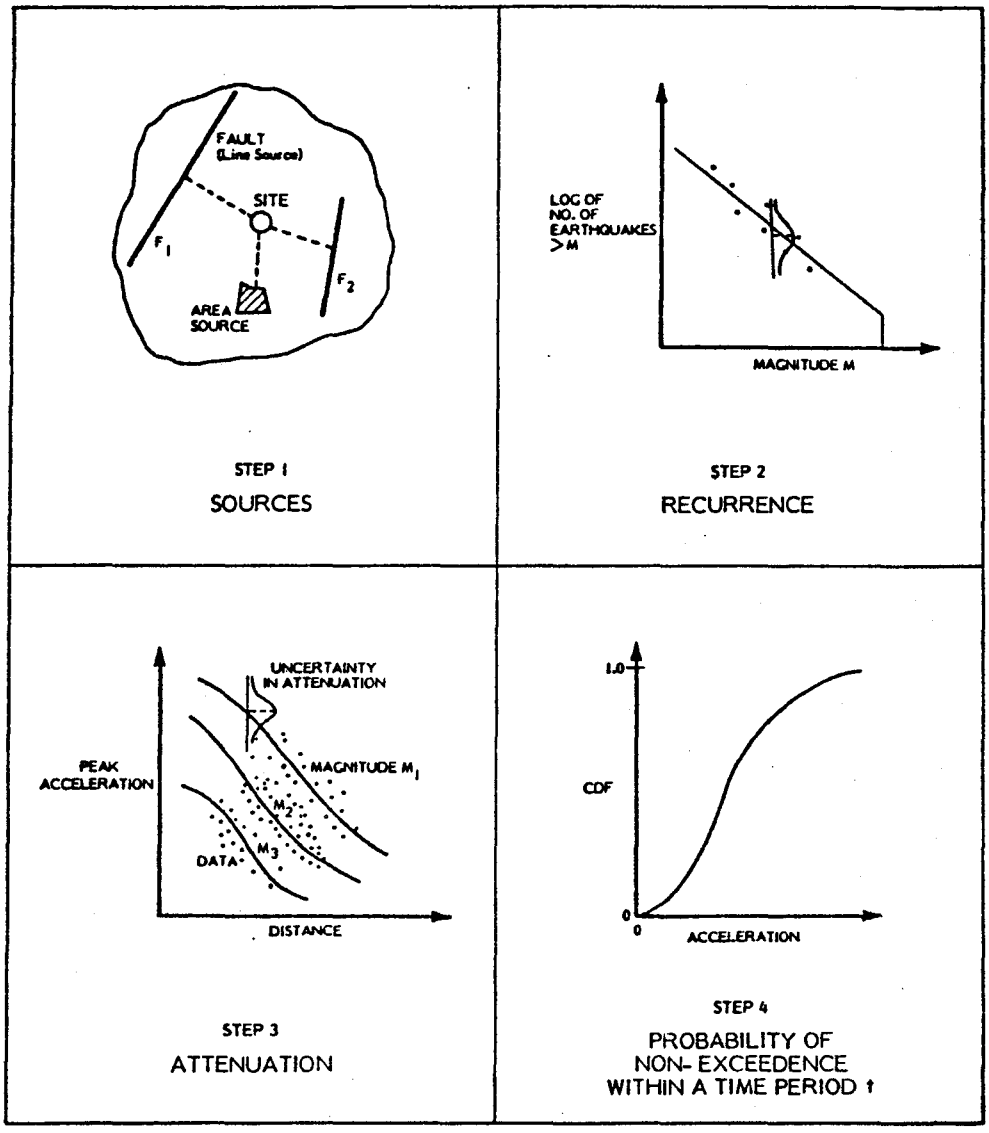


Figure I.1.1 A graphical summary of seismic hazard analysis in terms of peak value characterizations of strong ground motion. (from Mortgat, 1976)

## Table I.1.1
## Seismic Hazard Analysis

| | | Seismic Source Modelling | Data Analysis | Information from Seismology and Geology (Subjective Input) | Occurrence Model | Attenuation Relation |
|---|---|---|---|---|---|---|
| Deterministic Approach | | The source considered is the one that governs the biggest impact at a site. Deterministically determined source location based on geological and seismological information. | Deterministic selection of maximum credible event, maximum probable event or some limit state event. | Directly considered in source model and in selecting the size of the design earthquake. | None | Only mean value function or some arbitrarily biased function. |
| Probabilistic Approach | Classical Non-Bayesian Model | Deterministically determined. Geological and seismological information incorporated in this modeling. | Analysis of the available data base including correction for incompleteness and bias in the data. | Directly and informally incorporated in the source model and in the analysis of data. | Poisson or Markov or extreme value | Scatter in attenuation is incorporated by assuming a distribution on the ground motion parameter at a given distance - given site. |
| | Bayesian Model | Based on past seismic history and geologic evidence, source is modelled deterministically | Analysis of the available data base including correction for incompleteness and bias in the data. | Information generated through geological evidence and seismological models (theoretical as well as emptrical) is combined with the historical and seismological data base. A "priori" information to supplement the seismological data | Model accepting Bayesian input at two levels<br>• earthquake occurrence (Poisson)<br>• earthquake size (Bernoulli) | A Bayesian combination of empirical data based attenuation and seismologically based theoretical attenuation; scatter taken care of by assuming distribution on the ground motion parameter. |

However, as each earthquake is studied more is learned about strong ground motion and the degree of uncertainty associated with it is slowly reduced, (Savage, 1966; Aki, 1967, 1968; Heaton and Helmberger, 1977; etc.). The state of practice in modeling strong motion for prediction has developed along simplified empirical lines. This has been due in part to the complicated nature of the process and our level of understanding. McCann (1980) has discussed the various empirical methods used in attenuation studies. This approach to ground motion modeling has a number of drawbacks, which will be discussed in the next section.

## I.3 PROBLEM IDENTIFICATION

The state of the art in modeling strong ground motion is based on simplified techniques and depends completely on observations from past earthquakes. Also, the simplest parameters have been used to define the intensity of acceleration time histories. These methods are a major part of a seismic hazard analysis with virtually all types of hazard analyses being based on these techniques, from probabilistic seismic zone mapping, (Shah et al., 1975), to deterministic approaches of developing design loads.

The model used to define the propagation of seismic wave energy, the magnitude and distance model, makes a number of assumptions about the earthquake process. For example, this approach defines seismic events of the same Local Richter magnitude to be identical in terms of the mean level of ground shaking produced, neglecting the fault type, the dynamics of the fault rupture, and the regional transmission path. Similar statements can be made about the parameters that have been used to model

the intensity of ground shaking. That is, it can also be questioned as to whether peak values realistically represent the intensity of ground shaking, (Arias, 1970; Housner, 1975; Hanks and Johnson, 1976).

The improvement of these modeling techniques for use in seismic hazard analysis is the subject of this work. The problem to be addressed is discussed in the next section.

## I.4 PROBLEM FOCUS

This research work is concerned with the development of an improved methodology for modeling strong ground motion for application in seismic hazard analysis. Of interest is the means of modeling the fault rupture as well as the propagation of seismic waves in the earth.

Earthquakes represent a complicated release of elastic wave energy throughout the earth. The variability of simple empirical models to realistically predict future strong ground motion accentuates the complexity of the problem. The focus of this work is to develop a probabilistic model that takes into account the earthquake source and the transmission of seismic waves in a practical manner. This work will also consider an alternative means of characterizing the intensity of ground shaking. The improved seismological understanding of strong ground motion in recent years has not yet been incorporated into current modeling methods. Therefore the developments in this work will serve as a beginning to the improvement of this state of affairs.

## I.5 SCOPE OF THIS RESEARCH

In this work a method is developed for the probabilistic estimation

of strong ground motion. The method is based on an event defined according to its size and seismotectonic properties. A major aspect of this research will be to take into account the information available for estimating future strong ground motion. In carrying out these objectives, this research work develops in the following manner.

A Bayesian model is developed in Chapter II that is designed to incorporate the information from empirical studies as well as theoretical seismological models into the estimate of future strong ground motion. The methodology presented in this chapter defines what information is available and compares it to that used in the current state of practice.

The normal mode method is the theoretical seismological model selected to provide additional input on strong ground motion into the Bayesian model. The method is described in Chapter III for obtaining the Fourier transform of acceleration due to a propagating line segment.

To demonstrate the capability of the normal mode technique to model strong motion, the model is used in Chapter IV in a deterministic manner. An Imperial Valley earth structure is chosen for which the modal characteristics are determined. The model is first used to demonstrate the effects of various source parameters on ground motion, after which recorded displacement and acceleration motion are modeled for two events in this area.

Chapter V describes the Monte Carlo simulation used to generate observations of ground motion acceleration that represent realizations of a random fault rupture process.

Examples demonstrating the probability model of Chapter II are presented in Chapter VI. A sensitivity study is performed to identify the effects of the various source parameters on the predicted strong motion.

Chapter VII presents the conclusions of this work and recommendations for future research.

# CHAPTER II - A PROBABILISTIC MODEL FOR GROUND MOTION SPECTRA

## II.1 INTROUCTION

Probabilistic methods, contrary to a common misconception do not provide a decision regarding the selection of possible alternatives, but are however, a means of information processing. Decision analysis on the other hand is concerned with the problem of making a choice between alternatives whose outcome is uncertain. In this chapter a probabilistic model is developed which attempts to include available information in estimating the ground shaking due to a seismic event. The model is founded on the Bayesian view of probability and uses Bayes theorem to combine different sources of information.

The use of Bayesian analysis in engineering is not new, (Benjamin and Cornell, 1970). In seismic hazard analysis in particular, Bayesian methods have been used in modeling of earthquake occurrences and event sizes, (Benjamin, 1968; Esteva, 1969; Mortgat, 1976; Campbell, 1977; Eguchi and Wiggins, 1979). It would appear that Bayesian models are introduced as a method for combining two sources of information. Although true, this does not begin to illustrate the concept of probability endorsed by Bayes theorem, or its rational approach of introducing new information to apriori beliefs. For this reason a review of Bayesian probability is presented.

Section II.3 begins the study of strong ground motion modeling with a review of what is known about the earthquake process, and the methods used to model it. The state of practice in strong motion modeling is

then reviewed in a Bayesian context. This serves to define the transition from the state of knowledge about earthquake ground motion to the simplified models that have become the state of practice in earthquake engineering. The result of this review illustrates the need to access the other sources of information that are available, but as yet not taken into account.

The remaining sections present a Bayesian model for incorporating new information into the estimate of strong motion at a site. To implement the model, the root mean square acceleration is used as the avenue for carrying out the updating process. The result of the model is a probabilistic power spectral density function at the site, due to events of a given size.

## II.2 BAYESIAN ANALYSIS - A REVIEW

This section presents a review of the basic concepts of Bayesian analysis. It will outline the Bayesian or subjective view of probability, as opposed to the once very strongly held frequency definition. Although for many years controversial, Bayesian probability makes the formation of inferences from data straight forward and allows the consideration of problems that would be otherwise untouchable. It should become clear to the reader that the true contribution of Bayes is not expressed in the simple equation that bears his name, but rather in the concept of probability being endorsed. In words, what Bayes theorem does is to describe the way in which we learn from our experiences, making clear the fact that probability assignments define one's degree of belief, and are always conditional on the state of information.

## II.2.1 HISTORICAL REVIEW

For many centuries the definition of probability was centered around the concept of relative frequency. The probability of an event was defined to be the relative number of occurrences of an event in a sequence of trials. This view was held by statisticians to be the meaning of probability. Even to the beginning of this century this was the most commonly held definition. Statistics developed under this "frequentist" concept, but problems existed and there were matters that could not be properly addressed under this theory. As a result, other schools of thought developed hoping to bridge the gap left by the frequentist approach. Of these, the Bayesian or subjective school has taken the leading role in the present day advancement in probability theory, particularly with respect to applications in business, science and engineering. The subjective view defines probability as the degree of belief that the event of interest will take place. Subjective probability, or personal probability as it is sometimes called, (Savage, 1961), is the view associated with Bayes theorem.

In 1763 an essay by the Reverend Thomas Bayes was published two years after his death. The essay presented for the first time what is known as Bayes theorem. A simple mathematical fact based on the fundamentals of probability, this theorem introduced a revolutionary concept in probability theory. However, the suggestion that subjective input is incorporated in a probability statement seemed to oppose all goals of objectivity being sought in statistics. Thus, for many years this view was rejected. Statisticians simply refused to consider what it actually meant. Not until the early twentieth century was an effort made

to understand what Bayes theorem and subjective probability had to offer. The early investigators into subjective probability were De Finetti (1951), Good (1965), and Savage (1961),(1962), among others.

## II.2.2 BAYES THEOREM

Bayes theorem is a simple mathematical statement of the way in which we learn from new experiences. To illustrate the derivation of Bayes theorem, consider two events, A and B. From the conditional probability theorem, the probability of event B occurring, given that event A has taken place, is denoted $P[B|A]$, and is defined as,

$$P[B|A] = \frac{P[B \cap A]}{P[A]} \qquad \text{(II.2.1)}$$

where $A \cap B$ is read, A intersection B, meaning A and B occur at the same time. It should be clear that, $P[B \cap A] = P[A \cap B]$, thus $P[A \cap B]$ can be rewritten,

$$P[A \cap B] = P[A|B]\ P[B] \qquad \text{(II.2.2)}$$

Substituting this result into eq. (II.2.1),

$$P[B|A] = \frac{P[A|B]\ P[B]}{P[A]} \qquad \text{(II.2.3)}$$

Eq. (II.2.3) is known as Bayes theorem and an uncontested result of the

fundamental theories of probability. In words, eq. (II.2.3) can be expressed in the following manner,

$$P[\text{hypothesis}|\text{data}] = \frac{P[\text{data}|\text{hypothesis}]\ P[\text{hypothesis}]}{P[\text{data}]} \qquad \text{(II.2.4)}$$

where the terms in eq. (II.2.4) are defined as follows; P[hypothesis|data] is known as the posterior or updated probability, in this case on event B, given the new information that event A has occurred. P[hypothesis] is defined simply as the apriori probability that the hypothesis is true, or in this case that event B will occur. P[data|hypothesis] expresses the likelihood that the data would be observed given that the hypothesis is true, or in the present example, this can be stated as the probability of event A occuring given that event B has occurred. P[data] is essentially a normalizing constant as was P[A] in eq. (II.2.1). The controversy over Bayes theorem lies with the prior probability, P[B].

The prior probability on the occurrence of an event may range from total ignorance, to a belief that the event will certainly occur. What Bayes theorem suggests is that apriori probabilities represent the information at hand before the data are available. The apriori information may be a purely subjective opinion about the event, or it may be the result from a previous experiment. The slightest suggestion that subjective input be permitted into a field where total objectivity is the goal was considered preposterous by statisticians. The concept of subjective probability however, was not the only problem. If one were to

accept this idea, the question would soon be raised as to how probability is defined. Certainly it could no longer be defined in a relative frequency sense, since the weight of ones' opinions cannot be counted like the number of heads in a coin tossing experiment. These pitfalls led to the virtual banishment of Bayes theorem from application and research in the years following its publication. There were short lived comebacks, but not until the early part of this century did a serious effort sustain itself in the study of Bayes theorem. This rebirth has continued to the present, extending into many fields of research and application.

The view of probability associated with Bayes theorem can be explained in the following way. A probability is the measure of one's state of information about something. The actual numerical measure is the encoding of this state of information, (Tribus, 1969; Jaynes, 1958; Howard, 1968). This definition recognizes all forms of information, from purely subjective opinion to "objective" data. The first and most important step before applying Bayes' probability theory, is to understand this concept of probability. Once this transition has been made, the understanding and use of Bayes theorem is straightforward.

One of the important elements in employing Bayesian probability is the methodology that results. It is a rational and consistent means of taking into account new information in the development of updated or refined probability assignments. Quite simply, Bayes theorem describes the development of updated opinions based on recent information. Jaynes (1958) points out that very often in science the key to a problem is not a new mathematical tool but rather a new viewpoint, a new way of

reasoning. In fact, Jaynes makes this statement while discussing his own development in the area of statistical mechanics. Indeed this has been the case in probability theory as well. As demonstrated previously, the mathematical tools for deriving Bayes theorem were available, namely conditional probability. The breakthrough by Bayes was not in deriving an equation but in the definition of probability he presented. Therefore to summarize Bayesian analysis is to present what has developed as a result of this new viewpoint. The basic concepts of Bayesian analysis are now summarized.

Bayesian probability is consistent with the fundamental theorems of probability, and therefore if more than one method of solving a problem is available, both methods should give the same result. Another important aspect of Bayesian analysis is that of updating current probabilities given new information. This implies that each source of information made available, be used in its entirety in developing a probability statement. If this is not the case, then the posterior probability statement will be inconsistent or incomplete, (Jaynes, 1958; Savage, 1961). Bayesian analysis does not replace or improve what have been the fundamentals of probability theory, but instead enhances its realm of application. What it does do in all instances is impart a consistent and rational method to probabilistic analysis. Finally, this methodology does not replace the fact that an infinite sample of the variable of interest will give the best estimate of the parameters of a distribution.

## II.3 A REVIEW OF THE STATE OF INFORMATION FOR MODELING EARTHQUAKE STRONG GROUND MOTION

This section presents a review of the information that is available on strong ground motion. As discussed in the previous sections, probability assignments are merely the encoding of the state of information. Consequently, this represents a major part in the development of a Bayesian probability model, the assessing of available information on the event of interest. This section will review the sources of information on strong ground motion, both empirical and theoretical, and form the basis for a review of ground motion modeling from a Bayesian perspective. This leads to the development of a probability model for estimating strong ground motion.

### II.3.1 THE EARTHQUAKE PROCESS

An earthquake can be defined as the complex release of elastic strain energy in the form of seismic waves. In this section a summary is presented of the state of knowledge of those characteritics of the earthquake process that are believed, through theoretical understanding and observation, to have first order effects on strong ground motion. This summary will refer to many works that have observed a given effect or have demonstrated its potential importance in theoretical studies. This will not be an indepth coverage, but by reference and a simple review, the current understanding of the earthquake process will be summarized.

Figure II.3.1 presents an example of a typical source site arrangement from a crossection view of the earth. With the aid of this

figure the basic understanding of the earthquake process is presented. An earthquake can be considered in two parts, the source and the transmission path. Figure II.3.1 shows an earth structure whose properties vary laterally and with depth. The earthquake hypocenter and epicenter are shown for a particular fault with different slip directions. Below the figure are listed three categories, source effects, transmission path and local site conditions. For each group, a summary of its major characteristics are given.

Starting with the seismic source, dislocation theory requires that the shear dislocation on the fault be described as a function of space and time, (deHoop, 1958). This is of course impossible to predict beforehand or to derive for a past event. Therefore the source dislocation is usually described by other parameters such as seismic moment and average values of stress drop, dislocation, rupture velocity, etc. (Haskell, 1964; Aki, 1966; etc.). Below the entry for the dislocation function, $D_o(x,y,z,t)$, other characteristics commonly used to define the earthquake source are given. References are listed for each parameter, where the effect on ground motion has been demonstrated. Identifying the earthquake source and the details that define it, in effect emphasizes the obvious fact that the forcing function in a vibrations problem is of first order importance.

The next category is the transmission path traveled by seismic waves, which can be described completely by the earth structure. This accounts for the mechanical properties of the material, as well as geologic structures. As shown in Figure II.3.1 the mechanical properties are defined in terms of the seismic wave velocity and density

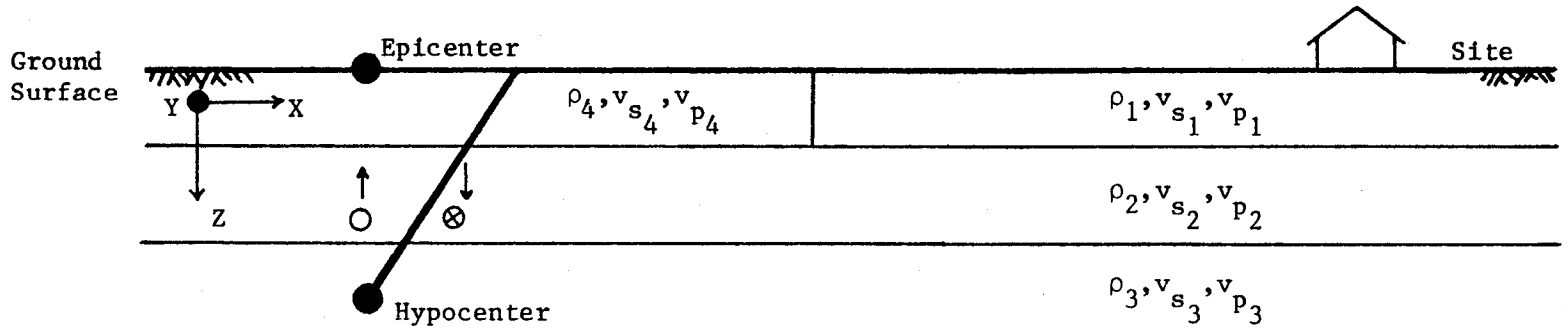


SEISMIC SOURCE

- $D_o(x,y,z,t)$, Haskell (1964)
  - rupture velocity
    Savage (1966),
    Swanger & Boore (1978), and
    Boore & Joyner (1978)
  - rise time
    Haskell (1964)
  - $D_o$ - ave. dislocation
  - $M_o$ - seismic moment
  - $\overline{\sigma}$ - effective stress
  - $\Delta\sigma$ - ave. stress drop
    Keillis-Borok (1959),
    Aki (1966), and Brune (1970)

TRANSMISSION PATH

- earth structure
  - $v_s(x,z)$ - shear wave velocity
  - $v_p(x,z)$ - compression wave velocity
  - $\rho(x,z)$ - density
  - $Q(x,z)$ - specific attenuation
  - distance

  Heaton & Helmberger (1977), and
  Geller, Frazier, & McCann (1979)

LOCAL CONDITIONS

- soil-structure effects
  Crouse & Jennings (1975),
  Hradilek & Luco (1970),
  Boore et al. (1978), and
  this work, Chapter IV

Figure II.3.1 A summary of the earthquake process.

distribution as a function of depth. The importance of the transmission path on the waveform produced at a site cannot be over emphasized. The fact that the fundamental dynamic characteristics of a system are an integral part of what determines the response, does not require a detailed discussion. However the degree to which this has been neglected in ground motion studies requires its emphasis. The importance of the transmission path has been pointed out in many studies and will be demonstrated later in this work.

The local site conditions are often identified as a separate category when in fact it is merely the final part of the transmission path. Therefore in this discussion the local conditions refer to soil-structure effects that determine the input motion to a structure. The filtering effect of structure imbedment has been observed and studied analytically.

In summary, this section has graphically and by reference attempted to identify the basic parts of the earthquake process that are recognized to play a major role in generating strong ground motion. The sections to follow briefly discuss empirical and theoretical modeling of the earthquake process. It should be noted that no attempt was made in this section to quantify these factors, but rather by a general coverage to demonstrate apriori to the prediction of future ground motion, what is known.

### II.3.2 EMPIRICAL METHODS

This section addresses empirical techniques of modeling ground motion intensity. This review will describe that part of the available

information on earthquake ground motion that is incorporated in empirical models. The discussion will be concerned with instrumentally recorded measures of earthquake intensity.

Empirical models consist of three main parts: a measure of the size of the earthquake that produces the observed motion, the parameter(s) describing the ground shaking intensity, and a transmission path model. The earliest work in this area began with simple models to describe what has come to be known as the attenuation of strong ground motion. The general form of these models has not changed appreciably, and can be expressed in the following manner,

$$\text{ground motion parameter} = f(M,d,c_i) \qquad \text{(II.3.1)}$$

The ground motion parameter is defined as a function of earthquake magnitude M, distance d, and other parameters $c_i$, such as local soil condition, or higher order functions of magnitude. A large percentage of attenuation models are functions of magnitude and distance only, (Idriss, 1978). A common functional form for eq. (II.3.1) is,

$$\ell n y = A + B\ M + Cg(d) + f'(x_i) \qquad \text{(II.3.2)}$$

where $\ell n$ is the logarithm, y denotes the strong motion parameter and A, B, and C are constants derived from a statistical analysis of strong motion data. The term f'(x) may be a binary or other function dependent

on subsurface conditions, (Trifunac and Brady, 1975). The function g(d) defines the distance dependence and is often of the form $\ell n$ (d). This function has been allowed to take many other forms in order to model attenuation of ground motion intensity. Idriss (1978) presents a summary of a number of works and the functional forms they used.

In a comprehensive review of the methods of modeling earthquake ground motion, Idriss (1978) addressed many of the features of the earthquake process presented in the previous section. In his review, the importance of other factors, besides magnitude and distance were recognized, as was the potential of other means of characterizing strong ground motion. However, based on available data, there is an insufficient statistical base upon which well founded conclusions on the influence of these parameters can be made. Therefore, what was a fundamental understanding of the earthquake process, has been reduced to the conceptual model in eq. (II.3.1), and the common functional form of eq. (II.3.2). The drawbacks of this model are clear. This is not to imply that empirical models do not provide any insight into ground motion attenuation, indeed they are very informative. To abandon such efforts would be to ignore the only real link to the earthquake process. In terms of those parameters being used to model the process, a great deal has been discovered, (Hanks and Johnson, 1976; Boore et al., 1978; etc.). However, these methods should be assessed based on the current understanding and/or beliefs as expressed in section II.3.1.

To summarize the information as processed through empirical modeling techniques, the following general observations are made. The available data of strong earthquake ground motion represents a sparse sampling of

the multi-dimensional earthquake process. As evident from the parameters used in empirical studies, the most reliable information is available for magnitude, distance, and local site conditions. Even for these factors, the amount of data is far from sufficient. In essence what is taking place is a form of aliasing in the parameter domains of magnitude, distance, and soil condition, and a spatial averaging of the effects due to other parameters. Therefore conclusions or statements concerning ground motion attenuation are in fact general statements related only to the parameters sampled and represent an averaging of the other factors not considered. For example, the radiation pattern effect is never considered in strong ground motion studies. Therefore attenuation laws based on magnitude and distance, result in an averaging of the effects due to source radiation. Similarly, this can be said of the other properties not considered. For the parameters that are investigated a spatial aliasing occurs, since in no instance does sufficient data exist.

Figure II.3.2 presents the view of seismic attenuation as accounted for by empirical models. This states that earthquakes of the same magnitude, and recorded at the same distance from the source on an alluvial, stiff, or rock site, produce the same average intensity. It should be pointed out that recent models do consider the uncertainty about the mean, (McGuire, 1974). However, this uncertainty is due in part to the aliasing effect as well as the statistical uncertainty. This type of modeling is not consistent with what is understood about the earthquake process.

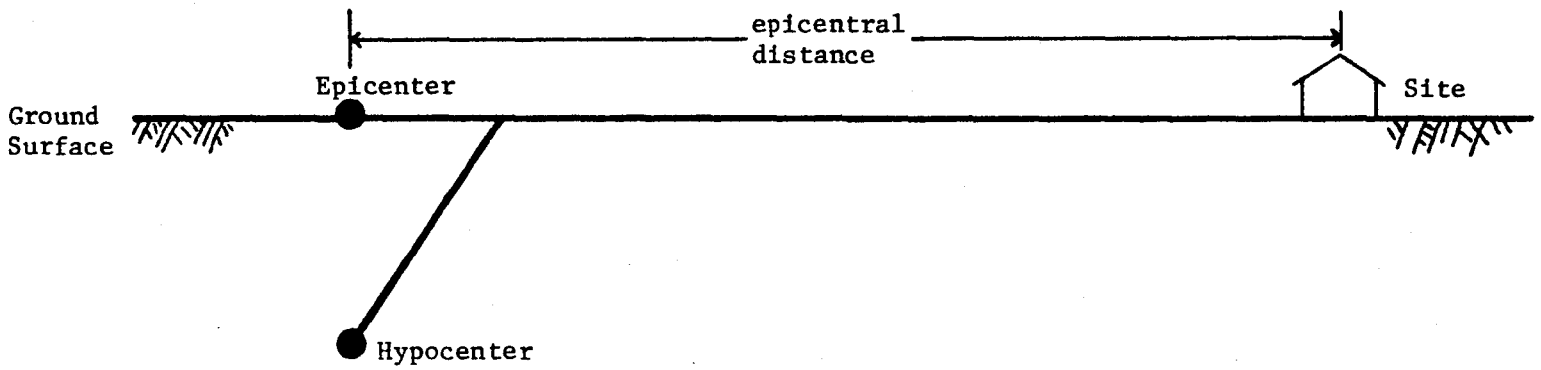


| Source Effects | Transmission Path | Local Site Conditions |
|---|---|---|
| • Richter Magnitude | • distance | • alluvial, stiff, or rock sites |

Figure II.3.2 Currently used earthquake model.

## II.3.3 THEORETICAL MODELING OF SEISMIC EVENTS

Keeping in mind that the reviews presented in this and the previous section are for the purpose of demonstrating the degree to which available information on strong ground motion is used, theoretical modeling techniques are considered next. Two types of seismological modeling or analysis tools are of interest in this work; seismic spectrum scaling laws and time domain waveform modeling based on dislocation theory.

The use of seismic spectrum scaling laws was discussed by McCann (1980). In addition to that discussion, it is stated that scaling law relationships provide one method of obtaining a set of static, average measures or summaries of a seismic event. For major events this type of analysis is usually carried out, (Kanamori and Anderson, 1975). The data used in these studies are usually teleseismic or other data bases and therefore estimates of source parameters independent of the strong motion data can be obtained.

The second form of modeling used in seismology is the use of wave propagation models and shear dislocation theory. A few of the methods commonly adopted are the generalized ray technique, (Heaton and Helmberger, 1978), the normal mode method, (Takeuchi and Saito, 1972; Swanger and Boore, 1978), the finite element method, (Archuleta and Frazier, 1978), etc. These models have been used to understand the dynamics of fault rupture and wave propagation in the earth. They have the demonstrated capability to reproduce observed strong motion displacements, (Heaton and Helmberger, 1978; Swanger and Boore, 1978; Archuleta, 1979; etc.). Modeling past events also provides estimates of source parameters such as seismic moment, average stress drop, fault

rupture dimensions, rupture velocities, dislocation rise times, etc. For a major, well instrumented earthquake, a number of investigative teams employing different techniques will study the recorded ground motion. Consequently the parameters of the event become "reasonably" well constrained. In general, estimates of seismic moment will be determined to within a factor of two or better, and similarly for stress drop, (Wyss, 1977). The estimates of source parameters depends very much on the degree of strong motion instrumentation and scientific interest in the event. For example, large earthquakes along the Aluetian Trench are not given the attention that similar sized events in the Imperial Valley get. However, for those events for which there is overwhelming interest and more importantly adequate instrumentation, excellent understanding of the earthquake can be attained. The 1971 San Fernando earthquake has been studied for many years, and the recent Imperial Valley earthquake may be one of the finest instrumented events and therefore is being studied by a number of investigators using different data sets and methods, (Kanamori, 1980; Archuleta and Sharpe, 1980).

The point of this discussion is to present the fact that through the many sources of available ground motion data and the different methods of analysis, information about earthquake dynamics is available. This information extends considerably beyond the magnitude, distance, and peak value summaries which are standard in earthquake engineering. Kanamori and Anderson (1975) and Geller (1976) for example have summarized, for a number of world wide events, some of the standard seismological parameters derived from scaling law relations and dynamic source models. At the present time, in only a few cases are the parameters of events

well constrained. The basic reason being insufficient instrumentation, thus limiting the ability to constrain model solutions.

### II.3.4 BAYESIAN REVIEW OF THE STATE OF THE ART OF MODELING STRONG GROUND MOTION

In view of the uncertainties in trying to model future strong ground motion it is of no surprise that probabilistic methods are used. As pointed out in the previous sections, empirical and theoretical methods of modeling strong ground motion are blanketed in a veil of uncertainty and inadequate information. Thus the development of probabilistic models was a natural course. A fundamental aspect of modeling strong motion is the fact that the set of strong motion records does not represent a complete or sufficient ensemble of realizations of the earthquake process. Therefore, a basic belief of seismologists and engineers is that levels of ground shaking intensity higher than those that have been observed to date are possible even though such motion has not been recorded. The assigning of non-zero probabilities based on few or no observations of ground motion implies a definition of probability other than the relative frequency concept. The differences in the definition of probability were discussed in the section on Bayesian analysis. Here the intent is to take a Bayesian view of what has transpired in ground motion modeling to produce the state of practice.

Engineers by the nature of their profession are Bayesian. Their job calls for the application of physical laws, often on the basis of too little information. Invariably, "engineering judgement" comes into play, representing the engineer's degree of belief in a particular outcome.

This judgement, combined in some way with the available data, leads to a decision. Formally this is Bayesian analysis, and "engineering judgement" is the engineers subjective probability or apriori information. It was suggested in section II.2 that the introduction of Bayesian probability was not represented by the simple equation known as Bayes theorem, but by the philosophy of reasoning and analyzing uncertain information. This same approach is taken here. That is, the discussion to follow will develop an interpretation of the state of practice in modeling strong ground motion. It should be noted that modeling as referred to here, means the methods applied in earthquake engineering, thus the use of the term state of practice. It is the improvement of these methods to which this work is addressed.

Section II.3.1 covered briefly, current understandings of the earthquake process. These have been developed from observation and theory, and were summarized in Figure II.3.1. This represents apriori to modeling of future ground motion, the available information.

From section II.3.2 two ideas or concepts were presented. The first being the type of empirical models used to predict earthquake ground shaking, and second, the fact that empirical models are the only ones used in seismic hazard analysis. Section II.3.3 summarized the fact that seismologists, through various theoretical techniques, derive information about the earthquake process beyond the standard observed or derived parameters used in engineering applications.

In the process of adopting empirical models, a tremendous transition has taken place between what is understood about the earthquake process

(Figure II.3.1) and how the earthquake is modeled in seismic hazard analysis, (Figure II.3.2). This section attempts to interpret this transition.

To proceed with this review, the seismic hazard problem is defined in the following way. A particular site is defined, for which the future ground shaking hazard is to be assessed. This information defines the tectonic and geologic environment and the particular hazard. The parameter to define the ground shaking hazard is left undefined so that the discussion can remain general. This discussion is refined further, by considering a single event of a given size. The problem is reduced to one of estimating the ground shaking hazard for a given seismic event. The complete seismic hazard is derived by applying the total probability theorem for all event sizes.

To solve this problem, the seismic hazard analyst must define what is given, determine its degree of importance, and quantify these factors to develop the estimate of strong ground motion. Before the model is developed, the analyst recognizes that the size of the earthquake and the type of event play a role in defining the expected motion. Similarly, since the geology of the region is known, and fundamental wave propagation theory would predict that the medium of transmission is important in the estimated response, the analyst feels that this should also be viewed as relevant input. It is assumed that the analyst's understanding of the seismic event, prior to the hazard analysis, is summarized by Figure II.3.1. The problem, it is recalled, is to estimate the strong motion due to the defined event, in terms that have been left open for this discussion. An apriori or subjective probability statement

will simply be the encoding of this initial information about the expected ground motion.

Based on the understanding of the earthquake as presented in section II.3.1, the analyst makes an implied probability assignment. That is, for the problem at hand some method of describing ground motion intensity must be developed. The analyst proceeds to ask what can be said about the expected ground shaking given his particular apriori knowledge. Based only on the understanding of Figure II.3.1 it would be very difficult indeed to define a probability distribution on the ground shaking parameter. To realize this, two fundamental questions can be asked. What is the expected value of ground shaking intensity, and second, how does the distribution vary about the mean. Keep in mind that the response to these questions is based on the information in Figure II.3.1 and not on any form of analysis, empirical or otherwise. Possibly an estimate of the mean value could be made, but around the mean the distribution would change slowly, and the result will be a probability density function that has considerable variation, (Savage, 1961). The result of this exercise of encoding the state of prior information, is shown in Figure II.3.3, where the prior probability density function is denoted $f'(x)$, for a general ground motion parameter $x$. The actual process of encoding prior probabilities is an interesting and complex subject. The mechanics of this is not covered in this work and the reader is referred to studies in this specific area, (Morris, 1971).

Recognizing the wide variation in this estimate, the hazard analyst looks to observations of similar processes to help improve the

probability assignment on the expected ground motion. Statistical

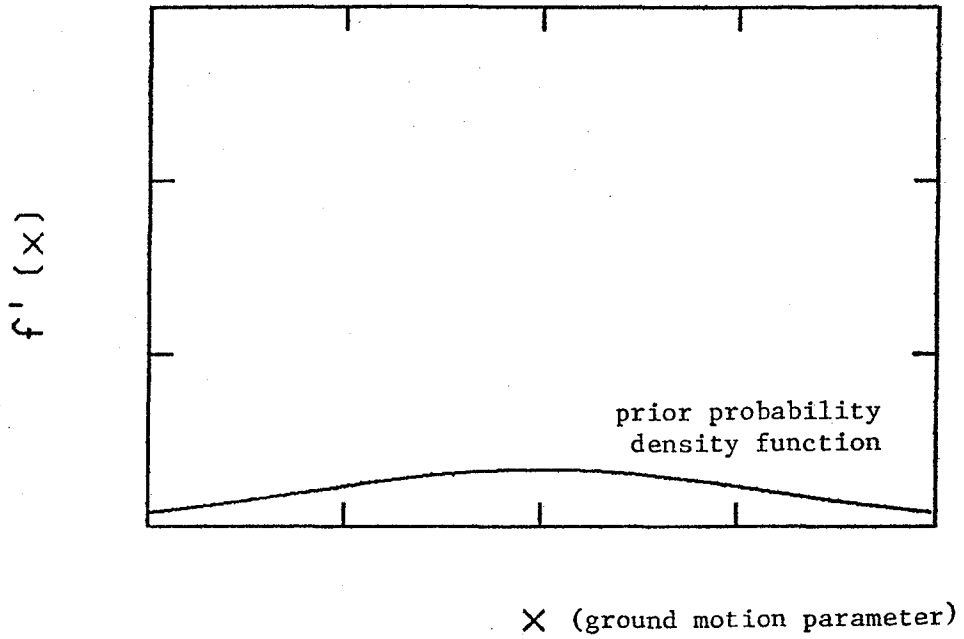


Figure II.3.3 Prior probability density function for a ground motion parameter x.

analyses of strong motion data are performed, and an empirical model is developed, as described in section II.3.2. This analysis provides a probability statement on the ground motion parameter for an event of the same size and at a distance equal to that for the site being studied. Bayes theorem is applied to combine the apriori probability, f'(x), and the data based information. The data based probability assignment is denoted L(x) and is called the likelihood function. Applying Bayes theorem,

$$f''(x) = N\, L(x)\, f'(x) \qquad \text{(II.3.3)}$$

where f"(x) is the posterior or updated probability density function on

the ground motion parameter x. It represents the analysts prior information, f'(x), and the results of empirical attenuation studies,

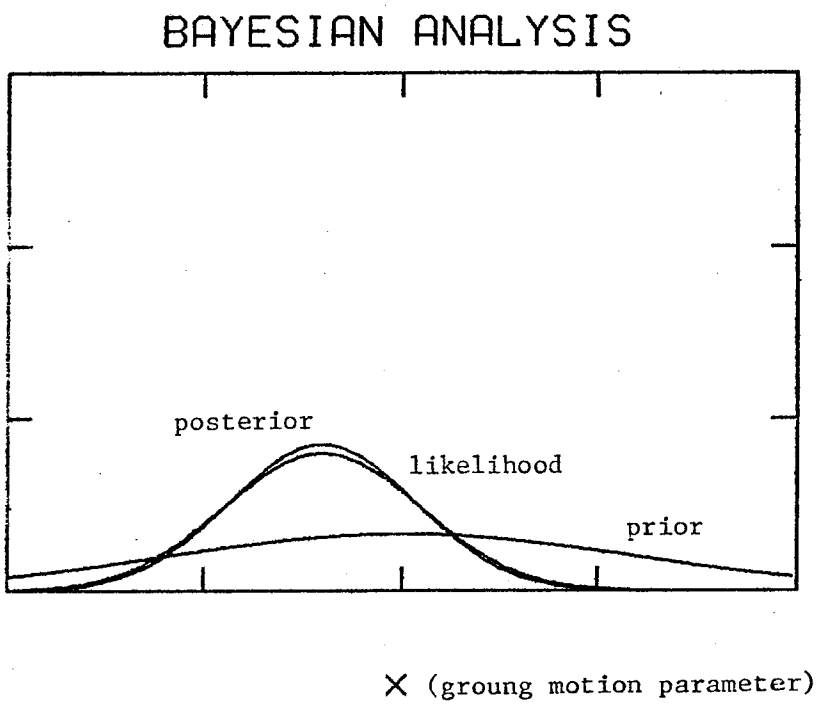


Figure II.3.4 An example of a Bayesian analysis for the case of a diffuse prior. The posterior probability is data based in this case.

L(x). The result of this analysis is shown graphically in Figure II.3.4. Recalling that the priori probability was very vague (had a wide distribution), the result of the analysis is dominated by L(x). Distributions of this type are called diffuse priors, (Benjamin and Cornell, 1970), and f"(x) is known as a data based posterior distribution.

What is accomplished by this exercise? Why go through this detail when the result is based solely on the data anyway? The reasons are many, and lie at the heart of Bayesian analysis. Every probability statement is based on any and all available information, regardless of

how vague, or whether it is derived from the observations of an experiment or from personal opinion. Therefore, defining a prior probability function sets in motion the information processing, and the evaluation of alternatives. Savage (1961) goes as far as to say that the encoding of prior information requires an honest evaluation of what is known and the degree of belief in this knowledge. Secondly, it results in a defined realm of what is considered likely to occur by the analyst, and begins a consistent approach to the problem. Note that an engineer or scientist will always have a personal bias about what results are expected. In discussing this subject, Savage (1961) recognizes the difficulty in defining what our apriori understandings and expectations are. As pointed out earlier, Bayesian probability requires that all information be made available, or the resulting probability statement will be incomplete. It is apparent from the strong motion modeling techniques in current use that the likelihood function, $L(x)$, is based on a limited description of the seismic event, in view of what seismologists have learned from this same data set.

To summarize the Bayesian review of the state of practice, the following comments can be made. First, current methods of predicting ground motion are in fact posterior probability estimates of the ground shaking hazard. Having defined what is known about the earthquake process, it is recognized that current methods represent an incomplete description of the seismic intensity. That is, for the earthquakes observed to date, the magnitude, distance, and peak value attenuation relations do not represent a statement based on a complete use of all the information derived from this data base. This will be referred to as the

stage I Bayesian analysis. The sections to follow develop a method to include all sources of information into the state of practice.

## II.4 A PROBABILITY MODEL FOR STRONG GROUND MOTION

In this section a method is developed that provides a probabilistic power spectral density at a site. The method is a Bayesian approach to updating ground motion estimates as obtained from current empirical methods. The model is founded on the discussion in the previous sections that define the earthquake process and the current state of practice. The Bayesian model developed here is unlike typical applications of Bayes theorem. That is, Bayes theorem is used in this work to update the estimate of ground motion at a site based in part on the data base used during the stage I analysis. However, much of the information which has been derived from this data base, (section II.3.3), has not been utilized. This is due to the recentness of these findings and the tendency for change being slow. Therefore instead of applying Bayes theorem in series with previous results, in which new and independent information is incorporated, a different viewpoint is required. The methodology presented here employs Bayes theorem in a parrallel sense, from an information processing point of view. To summarize this idea, Figure II.4.1 presents a diagram of the information flow.

The objectives of this model are twofold. The first is to present a model that in an information processing sense will provide a probability statement based on the complete set of available information. Secondly, sufficient apriori information exists that would indicate that some of the parameters of the earthquake process not taken into account have

INFORMATION DIAGRAM

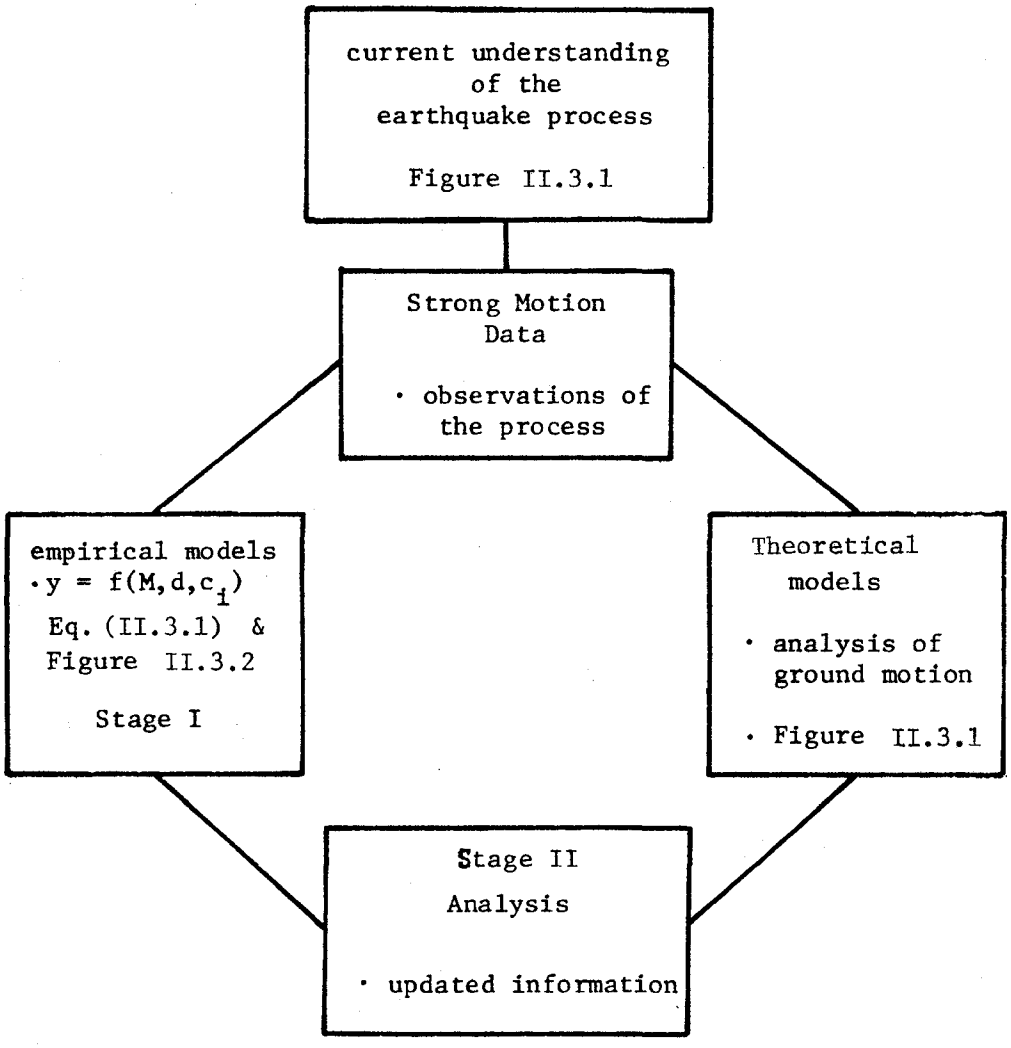


Figure II.4.1 Diagram describing the flow of information available to model future earthquake ground motion.

first order effects on the ground motion and in given circumstances will greatly effect the ground motion prediction. The model to be used will allow for this possibility.

### II.4.1 A BAYESIAN APPROACH TO GROUND MOTION MODELING

In Bayesian analysis, new information about a process is usually derived from an experiment or a new set of observations. In the present case, the strong motion data base represents the only observations of earthquake ground motion. The number of observations is quite limited in view of the complexity of the process. Ideally, additional samples of the process would allow a more thorough statistical analysis to be performed taking into account each parameter of the earthquake. Clearly, earthquakes cannot be repeated, or triggered at will so as to collect additional data. The solution proposed here to the problem of acquiring additional observations involves performing numerical experiments of the earthquake process. A mathematical model of the earthquake source and propagation path are used that employs as part of its input, the information which is available but not yet incorporated into the estimate of ground motion. The observations of the process are generated for a stochastic rupture model from a Monte Carlo simulation. The simulation generates observations of the earthquake defined in the current problem, (see section II.3).

This proposed solution can be stated as follows. For the situation described, current modeling procedures will predict the expected ground motion based solely on the magnitude of the event, and the source-site distance. The review presented in section II.3 showed that parameters of

the process other than magnitude and distance are important, and that not including these factors results in an incomplete probability assessment. Therefore, since a very limited strong motion data base restricts further statistical analysis, the solution proposed is to generate a data set for the present set of circumstances. A simulation provides an ensemble of realizations of strong motion recordings at the site. From this data base, a likelihood function on the ground motion parameter can be generated. Employing Bayes theorem, this additional information can be combined with the previous probability assignment. This second application of Bayes theorem constitutes an incorporation of the factors of recognized importance, which to date have been neglected.

To summarize the basic concept, a model is developed to incorporate in a realistic manner information about the earthquake source and transmission media in the estimate of strong ground motion. Due to the limited number of observations of earthquake ground motion, empirical modeling techniques consider a minimum number of parameters of the earthquake process. Using a mathematical model, observations of the process can be generated by a Monte Carlo simulation for a stochastic fault rupture. From these realizations a likelihood function on the ground motion parameter is derived and combined with the posterior distribution of the stage I analysis by Bayes theorem. This second application of Bayes theorem will be referred to as the stage II analysis. The next section discusses how this concept is carried out.

### II.4.2 A PROBABILISTIC MODEL FOR GROUND MOTION SPECTRA

The previous section outlined the development of a model for

updating ground motion predictions using Bayes theorem. In this section a specific approach will be taken that uses the root mean square acceleration as the ground motion parameter. Exploiting its dual role as a time domain as well as a frequency domain summary, the root mean square is used as a spectral intensity measure. An appropriate theoretical model is used to model the propagation of seismic waves from the earthquake source. The result of carrying out the proposed model will be a probabilistic power spectrum at the site. Recall that this discussion is carried out, given that a seismic event has occurred and is specified in the manner of a standard seismic hazard analysis, by event size, earthquake fault and site location, (Mortgat, 1976).

McCann (1980) studied the root mean square acceleration and duration as an alternative means of characterizing strong ground motion. The basic theoretical properties of the rms made it an attractive parameter to employ in ground motion studies. One of the results of that study were attenuation relations for rms acceleration. That analysis corresponds to the stage I analysis discussed in this chapter.

Before proceeding, it is important to define the random variable of interest and what the uncertain parameter(s) are. The random variable is the rms acceleration at a site, which is some distance r from the source. It is assumed in this work that the mean rms acceleration, $\mu$, is the unknown parameter and that the variance, $\sigma^2$, is known and determined from the stage I analysis. The Bayesian method considers the parameter(s) of a distribution to be random, (Benjamin and Cornell, 1970), and therefore the analysis is carried out to update the distribution on the mean rms value at the site. The probability density function on the rms

acceleration is conditional on knowledge of the mean and is denoted $f(r|\mu)$. Having defined the random variable and the uncertain parameter, the stage I analysis is summarized as follows, $f_1'(\mu)$ is the prior probability density function on the mean rms acceleration with a mean and variance denoted $\mu_1'$ and $\sigma_1'^2$. The likelihood function is $L_1(x|\mu)$ with mean m and variance $s_1^2$. The posterior distribution is $f_1''(\mu)$ with mean and variance denoted $\mu_1''$ and $\sigma_1''^2$, respectively. The variance of the process, which is assumed known, and determined from the stage I analysis is denoted $\sigma^2$.

Having defined the random variable and its distribution, the Bayesian analysis proceeds as follows. The posterior from stage I, serves as the prior distribution for the second stage analysis. That is, $f_1''(\mu)$ is equal to $f_2'(\mu)$, where $f_2'(\mu)$ is the prior information on the mean rms upon entering stage II. The parameters of the prior are also renamed as, $\mu_1'' = \mu_2'$, and $\sigma_1'' = \sigma_2'$.

To update this information, it was suggested that an appropriate mathematical model be used to generate additional observations of the process. A model is chosen that has the capability to consider the dynamic characteristics of the earthquake source, as well as the properties of the transmission path of the region. The theoretical model to be used in this study is discussed in Chapter III.

Although excellent models are available for modeling strong ground motion, the problem of prediction is quite another story. The details of the fault rupture are not known beforehand. However, information is available on the possible values the parameters of the rupture process

may take on, (Kanamori and Anderson, 1975; Geller, 1976; Seih, 1979). Therefore the rupture on a fault is considered a stochastic process, (Boore and Joyner, 1978; Savy, 1978), with the parameters of the source as random.

For each simulation of fault rupture, the theoretical model will generate a power spectral density at the site. At the end of the simulation an ensemble of power spectra is obtained. Recalling the frequency domain definition of the root mean square, realizations of the rms acceleration are also determined. For the $i^{th}$ simulation the rms acceleration is,

$$rms_i = \left\{ \int_o^{2\pi f_{max}} G(\omega)_i \, d\omega \right\}^{\frac{1}{2}} \qquad \text{(II.4.1)}$$

where $f_{max}$ is the maximum frequency in the spectrum, and $G(\omega)_i$ is the one-sided power spectral density realized as a result of the $i^{th}$ simulation. From the ensemble of rms values, the likelihood function on the mean rms acceleration is determined. This is denoted $L_2(z|\mu)$ and is the likelihood of observing the sample z, given the true value of $\mu$.

Also from the simulation, an ensemble of spectral shapes is observed. For the $i^{th}$ simulation, the spectrum shape is defined as,

$$N(\omega)_i = \frac{1}{(rms_i)^2} G(\omega)_i \qquad \text{(II.4.2)}$$

Similarly, the probability distribution on spectral shape can be determined, and is denoted, $f(N(\omega_j))$. $N(\omega)$, the spectral shape function, has unit area and can be considered as the distribution of the mean square acceleration as a function of frequency.

Having developed the likelihood function on the mean rms value, this new information is combined with the prior distribution on the mean rms through Bayes theorem. The posterior probability density function on the mean becomes,

$$f_2''(\mu) = N\, L_2(z|\mu)\, f_2'(\mu) \qquad \text{(II.4.3)}$$

This is shown graphically in Figure II.4.2. The posterior distribution on the mean is the result of incorporating the available information on strong ground motion.

Recalling that the original distribution on the rms acceleration was conditional on knowledge of the mean value, $f(r|\mu)$, applying the total probability theorem, the unconditional distribution on rms acceleration, $f(r)$, is derived. This is shown in eq. (II.4.4).

$$f(r) = \int_0^\infty f(r|\mu)\, f_2''(\mu)\, d\mu \qquad \text{(II.4.4)}$$

Combining the distribution on the rms acceleration and the probabilistic spectral shape obtained from the simulation, a probabilistic power spectrum can be derived by a standard change of variable, (Benjamin and

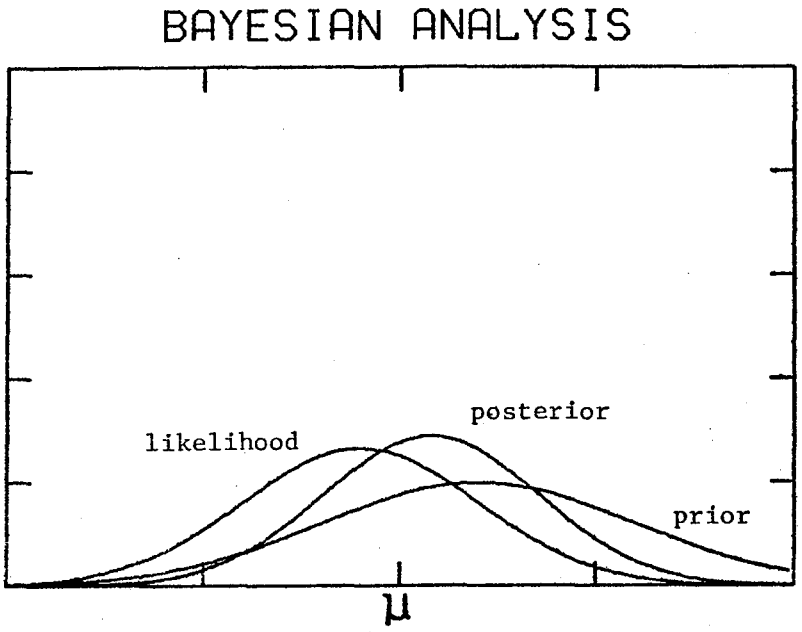


Figure II.4.2 A graphical presentation of the second stage Bayesian analysis.

Cornell, 1970). This is shown in eq. (II.4.5),

$$S(\omega) = rms^2 \cdot N(\omega) \qquad \text{(II.4.5)}$$

where $S(\omega)$ is the power spectrum at the site. The probability density function on $S(\omega_j)$ is $f(S(\omega_j))$, which is the probability density on the spectral ordinate $S(\omega_j)$ at frequency $\omega_j$. Knowledge of $f(S(\omega_j))$ makes it possible to provide consistent risk spectra for design, where each spectral ordinate has the same probability of being exceeded, (McGuire 1974).

In summary, a probabilistic model is presented that takes into

account information that can be derived from a seismological model. A Monte Carlo simulation is performed which generates observations of the earthquake process for the event of interest. This information is combined through Bayes theorem, with the prior knowledge from empirical models. The mean value of the rms acceleration is the uncertain parameter updated by Bayes theorem. With an updated distribution on the rms acceleration, the mean square acceleration is used as a spectral intensity which is distributed according to the spectral shape function derived from the simulation. The result is a probabilistic power spectrum from which consistent risk spectra can be defined.

### II.4.3 PROBABILITY MODEL

In the previous section the probabilistic method for deriving an updated distribution on the root mean square acceleration was presented. The development presented the mathematical relationships needed to carry out the updating process. This section presents the probabilistic aspect of the model. To demonstrate the methodology a conjugate prior analysis is used, which is a standard approach in Bayesian analysis, (Raiffa and Schlaiffer, 1961). The meaning and implications of this approach are discussed.

The probability model is based on the root mean square acceleration. In the stage I analysis presented in section II.3.4, the posterior probability distribution was data based, and therefore of the form of the likelihood function. For the event and site that were defined, the likelihood function is derived from statistical studies of strong motion data. This analysis defined the rms acceleration as a function of

distance. It should be pointed out that the probability density function derived from the attenuation model is not a likelihood function in the strictest sense, but should be more properly defined as a data based distribution, (Benjamin and Cornell, 1970).

A conjugate prior analysis is used in this work. What this means is the following, of the many possible distributions that could be used to define the prior probability density function, the natural conjugate of the likelihood function is selected. The natural conjugate combines with the sample likelihood to provide a mathematically tractable solution for the posterior distribution. The conjugate prior analysis in fact results in a posterior distribution of the same form as the prior probability density function. The advantage of this approach lies in the closed form solution, which obviates expensive, tedious numerical integrations, and statistical derivations of probability distributions. Also for model development and testing, reasonable first order analyses can be made using this approach.

In Section II.3.2 the assumed form of the attenuation law, eq. (II.3.2) implies that the ground motion parameter, in this case the rms acceleration, is Log-Normally distributed. In this analysis the mean of the rms distribution is uncertain, and therefore the probability density function on the mean is of interest. It is assumed in this work that the distribution on the mean rms value, is Normal. This assumption therefore implies that the posterior probability of stage I is also Normal. The parameters of the posterior distribution are the mean and standard deviation, denoted $\mu_1''$ and $\sigma_1''$.

The posterior probability density function on the mean rms from the stage I analysis is defined as,

$$f_1''(\mu) = N(\mu_1'', \sigma_1'') \qquad \text{(II.4.6)}$$

where the symbolic notation, N(m,s), is used to denote the Normal distribution with mean m and standard deviation s. Since the parameters from the regression analysis are derived for the logarithm of the variable, the parameters of the distribution on the variable itself must be determined. For the particular case where the random variable is the mean, the approximation of assuming a Normal distribution is reasonable, (Benjamin and Cornell, 1970).

The sample likelihood represents the likelihood of observing the sample set z, given the true value of the mean. In this case the samples of the process are obtained from the Monte Carlo simulation. Thus for a sample set z, where

$$z = (z_1, z_2, z_3, \ldots z_n) \qquad \text{(II.4.7)}$$

the likelihood function, $L_2(z|\mu)$ is determined. To facilitate the use of a conjugate prior analysis, the generating process of the root mean square is assumed to be Gaussian. Therefore from the definition of the likelihood function,

$$L_2(z|\mu) = \prod_{i=1}^{n} f(z_i|\mu) \qquad \text{(II.4.8)}$$

where $f(z_i|\mu)$ is the probability distribution on the rms evaluated at $z_i$. The likelihood function on the mean becomes,

$$L_2(z|\mu) = N(\bar{z}, \frac{\sigma}{\sqrt{n}}) \qquad \text{(II.4.9)}$$

where $\bar{z}$ is the sample mean, n is the number of samples of the rms acceleration, and $\sigma/\sqrt{n}$ is the standard deviation of the distribution on the mean. Recall that the variance of the process is assumed known, thus $\sigma$ is used in the likelihood function.

The assumption that the generating process is Normal is clearly an approximation. However, since the distribution of the mean value and not the variable itself is of interest, the degree of approximation is not critical. From the simulation, only an estimate of the mean value is required.

Also during the simulation the spectral shape function was determined. From this ensemble the probability density on the spectral ordinates can be derived. In this work this distribution is assumed to be Gamma type. This is consistent with theoretically predicted distributions of spectral ordinates and observations for earthquake spectra, (Bendat and Piersol, 1971; Kiremidjian, 1976). The distribution on spectral shape, $f(N(\omega_j))$ is,

$$f(N(\omega_j)) = \frac{\lambda^k \omega_j^{k-1} e^{-\lambda\omega_j}}{\Gamma(k-1)} \qquad \text{(II.4.10)}$$

with parameters $\lambda$ and k. The mean and variance of this distribution are,

$$E[N(\omega_j)] = \frac{k}{\lambda}$$

$$\sigma^2_{N(\omega_j)} = \frac{k}{\lambda^2} \qquad \text{(II.4.11)}$$

The parameters $\lambda$ and k are determined from sample estimates of the mean and variance. There will be a probability distribution function corresponding to each ordinate of $N(\omega)$.

Given the prior, $f_2'(\mu)$, and the sample likelihood, $L_2(z|\mu)$, Bayes theorem is applied to determine the posterior distribution on the mean rms. Applying eq. (II.4.3), the posterior, $f_2''(\mu)$ is, (Ang and Tang, 1975),

$$f_2''(\mu) = N\, L_2(z|\mu)\, f_2'(\mu)$$

$$= N \frac{1}{\sqrt{2\pi}\sigma''} \sqrt{n}\, \exp\left(-\frac{1}{2}\left(\frac{\mu - \bar{z}}{\sigma/\sqrt{n}}\right)^2\right) \frac{1}{\sqrt{2\pi}\sigma_2'} \exp\left(-\frac{1}{2}\left(\frac{\mu - \mu_2'}{\sigma_2'}\right)^2\right)$$

$$\text{where: } N = \int_{-\infty}^{\infty} L_2(z|\mu)\, f_2'(\mu)\, d\mu \qquad \text{(II.4.12)}$$

and the mean and standard deviation are given as,

$$\mu_2'' = \frac{[\bar{z}/(\sigma/\sqrt{n})^2] + [\mu_2'/(\sigma_2')^2]}{[1/(\sigma/\sqrt{n})^2] + [1/(\sigma_2')^2]}$$

$$\sigma_2''^2 = \frac{(\sigma_2')^2\, (\sigma/\sqrt{n})^2}{(\sigma_2')^2 + (\sigma/\sqrt{n})^2} \qquad \text{(II.4.13)}$$

Equation II.4.13 illustrates that the updated estimate of the mean rms value is a weighting of the prior and likelihood mean values, depending on their respective variances.

Given updated information on the mean, the total probability theorem can be applied to obtain,

$$f(r) = \int_{-\infty}^{\infty} f(r|\mu)\ f_2''(\mu)\ dr \qquad \text{(II.4.14)}$$

where $f(r|\mu)$ was assumed Normally distributed in this analysis with parameters $\mu$ and $\sigma$. The integration over $\mu$ yields, (Ang and Tang, 1975),

$$f(r) = N(\mu_2'', \sqrt{\sigma^2 + \sigma_2''^2}) \qquad \text{(II.4.15)}$$

The result of the Bayesian analysis is then an updated distribution on the root mean square acceleration which is approximated in this work by a conjugate prior analysis, where the prior and the generating process are assumed Normal. The probability distribution on the power spectral density is found by applying eq. (II.4.5). This final result is obtained by numerical integration in order to determine $f(S(\omega_j))$ at each spectral ordinate.

## II.5 SUMMARY

In this chapter a Bayesian probability model for estimating a probabilistic power spectrum at a site is presented. The model is based

on the use of the root mean square acceleration as a spectral intensity measure. The mean rms acceleration at a site is the uncertain parameter updated through the use of a theoretical model to generate observations of the earthquake process. These additional realizations constitute a numerical experiment from which the likelihood function on the mean is derived. Bayes theorem is used to combine prior information on ground motion as derived from empirical attenuation studies and the likelihood information determined from the simulation. The result of the analysis is a probabilistic power spectrum at the site.

# CHAPTER III - DETERMINING THE FOURIER TRANSFORM OF ACCELERATION BY THE NORMAL MODE METHOD

## III.1 INTRODUCTION

This chapter describes the theoretical model that is used to generate the Fourier transform of acceleration at a site. The information obtained from this model is used in the Bayesian analysis discussed in Chapter II. The technique adopted is the normal mode method in which the free oscillation modes of the earth are determined and used to obtain the response of the earth to the dislocation on a fault. The application of normal mode methods in seismology has been a topic of considerable interest for many years. The method has been applied to the problem of finding the periods of free oscillation of the earth, in the analysis of surface waves for flat or spherical, multilayered earth structures, and in modeling of strong ground motion displacements. It has also been applied to the development of earth models and the investigation of earthquake source mechanisms. Modal superposition is familiar to both engineers and seismologists in modeling the dynamic response of linear elastic systems.

In section III.2 a general review of normal mode analysis and wave propagation is presented. This section will develop the background for understanding the use of normal mode techniques in seismology and describe seismic waves traveling in a dispersive medium. The normal mode method of dynamic analysis is outlined in section III.3, illustrating the principle of modal superposition.

The remaining sections present the method for the case of earthquake ground motion in a spherical earth. The model is described in two parts, the first is an explanation of the computational procedure for identifying the earth's eigenfrequencies and eigenfunctions, and the second presents the derivation of the Fourier transform of acceleration at a site due to the rupture of a single fault segment. The model derivation is based on the work of Kanamori (1970), Takeuchi and Saito (1972), Fukao and Abe (1971), among others. This presentation is not a contribution of this work, since it is available in the geophysical literature, however for completeness and understanding, the major details of the model derivation are presented. The application of this particular procedure for modeling strong motion acceleration is however a new development.

## III.2 NORMAL MODE ANALYSIS IN SEISMOLOGY

Modal superposition methods have been employed by Fukao and Abe (1971), Hermmann and Nuttli, (1975a), (1975b), Kanamori and Stewart, (1976), and Swanger and Boore (1978) with considerable success in modeling ground motion displacements. Gilbert and Dziewonski (1975) have studied the use of this method in determining earthquake source mechanisms. In this work the normal mode method is used to generate an ensemble of Fourier transforms of acceleration at a site, to provide updated information on strong ground motion as discussed in Chapter II.

The earth is a spherical structure which has three vibrational modes that distinguish its dynamic response. These modes are of the radial, torsional, and spheroidal type. The radial mode is often referred to as

the "breathing" mode of the earth since it corresponds to uniform radial displacement. This mode is actually a special case of the spheroidal modes. Torsional modes correspond to the twisting motion of the sphere, examples of which are given in Figure III.2.1a,b. Spheroidal modes represent a distorting of the spherical shape as shown in Figure III.2.1c. The mode shapes shown in the figure are representative of the surface distortions for long period modes. The same principle holds for frequencies in the range of interest for strong ground motion.

To describe the free oscillation modes of a sphere, three parameters are required as opposed to the single parameter needed in the case of a one dimensional system. In geophysics these parameters are denoted $\ell$, m, and n; where $\ell$ is the angular order and defines the surface oscillation as a function of latitude. The term m is the azimuthal order and characterizes the surface motion as a function of longitude, and the parameter n defines the modal depth dependence and is known as the mode or overtone number. A free oscillation mode of a sphere can be characterized by these parameters plus the designation whether torsional or spheroidal modes are being considered. The symbolic notation, as used in Figure III.2.1 is ${}_{n}^{m}T_{\ell}$ and ${}_{n}^{m}S_{\ell}$ for torsional and spheroidal modes respectively, where the longitudinal dependence was held constant, (Press, 1965).

Determining the free oscillations of a sphere has been a problem of interest in mechanics for many years. Love (1927) determined the period of the fundamental spheroidal mode of a sphere the size of the earth, with the rigidity of steel and a Poissons' ratio of 1/4 to be approximately one hour. Since that first calculation, numerous

investigators have made refined estimates using more realistic earth

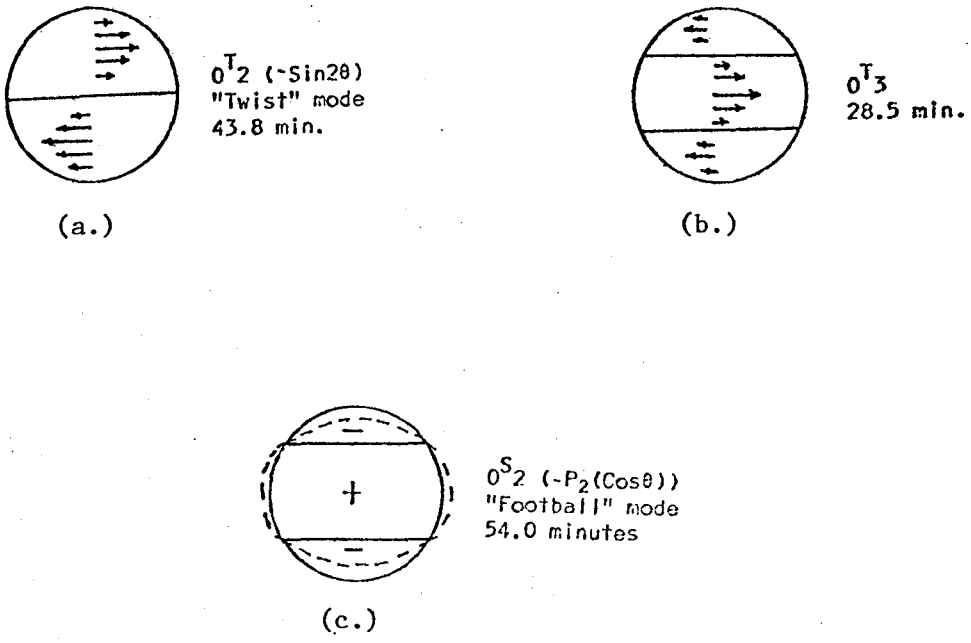


Figure III.2.1 Example of the free oscillation modes of the earth, (a.) torsional and (b.) spheroidal. (from Pilant, 1979)

models. The recording and verification of the fundamental spheroidal mode did not take place until 1960 with the Chilean earthquake, (Press, 1965). Subsequently, literally hundreds of modes have been observed, (Gilbert and Dziewonski, 1975). In the remainder of this section the normal mode method is discussed in relation to wave propagation.

The modes of a sphere, as pointed out, are of two independent types torsional, and spheroidal. As might be anticipated, particular wave types can be associated with the modes of vibration. For example, the fundamental torsional mode oscillations corresponds to Love surface waves, and similarly the fundamental spheroidal mode oscillation defines Rayleigh surface wave motion. As higher modes or overtones are

considered, the torsional modes correspond to SH body waves, (horizontally polarized shear body waves), and the spheroidal modes are P-SV waves, (compressional and vertically polarized shear waves). In engineering applications, horizontal motion is of prime importance and thus SH motion or the torsional modes are modeled in this work.

Surface waves are so called because they are constrained to travel on or near the earth's surface. There are two types of surface waves, Love waves which are SH waves traveling along the free surface, and Rayleigh waves whose particle motion is elliptical in a vertical plane in the direction of propagation. Rayleigh first suggested the existence of a special class of waves along boundaries of elastic solids in a homogeneous half space and thus one type bears his name. Love investigated the theory that a type of surface wave may exist having motion predominantly transverse to the direction of propagation. This phenomena had been observed, but not explained. Love proceeded to demonstrate the existence of surface waves of this type in the presence of a layer over a half space, and in the process discovered that these transverse surface waves are dispersive. That is, the propagation velocities are functions of wavelength. Similarly, Rayleigh waves are dispersive due to the heterogenity of the earth's properties with depth. Figure III.2.2 illustrates a typical example of Love wave dispersion curves for an Imperial Valley structure.

Dispersion curves describe wave velocity as a function of frequency or period. Note the two velocities shown, phase velocity, $c(\omega)$, and group velocity, $u(\omega)$. The phase velocity is defined as $\omega/k$, where $\omega$ is the circular frequency and k is the wavenumber. The wavenumber is a

spatial frequency and is defined as $2\pi$/wavelength. To measure the phase

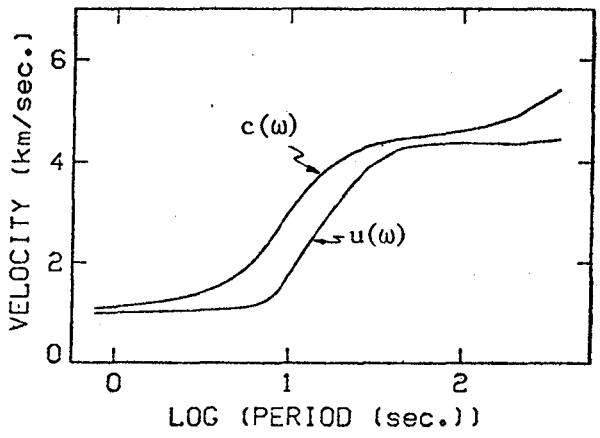


Figure III.2.2 An example of Love wave dispersion curves.

velocity, observations in the same direction, at distances $x_1$ and $x_2$ from a source must be made. The phase velocity is $x_2-x_1$, divided by the phase delay. The group velocity on the other hand, is the rate at which energy travels for a particular frequency group and is defined as $d\omega/dk$. The group velocity can be measured as the distance traveled, divided by the time of arrival of a wavegroup.

To demonstrate the concept of dispersion, a graphical example is given illustrating the definitions of phase velocity and group velocity. Consider the situation in Figure III.2.3. A point source is applied to the system with waveforms recorded at twenty stations starting at a distance of 40 km. and spaced at 1 km. increments. The phase velocity can be observed by considering two stations close to one another and measuring the phase delay of a particular peak or zero crossing. The phase velocity is then,

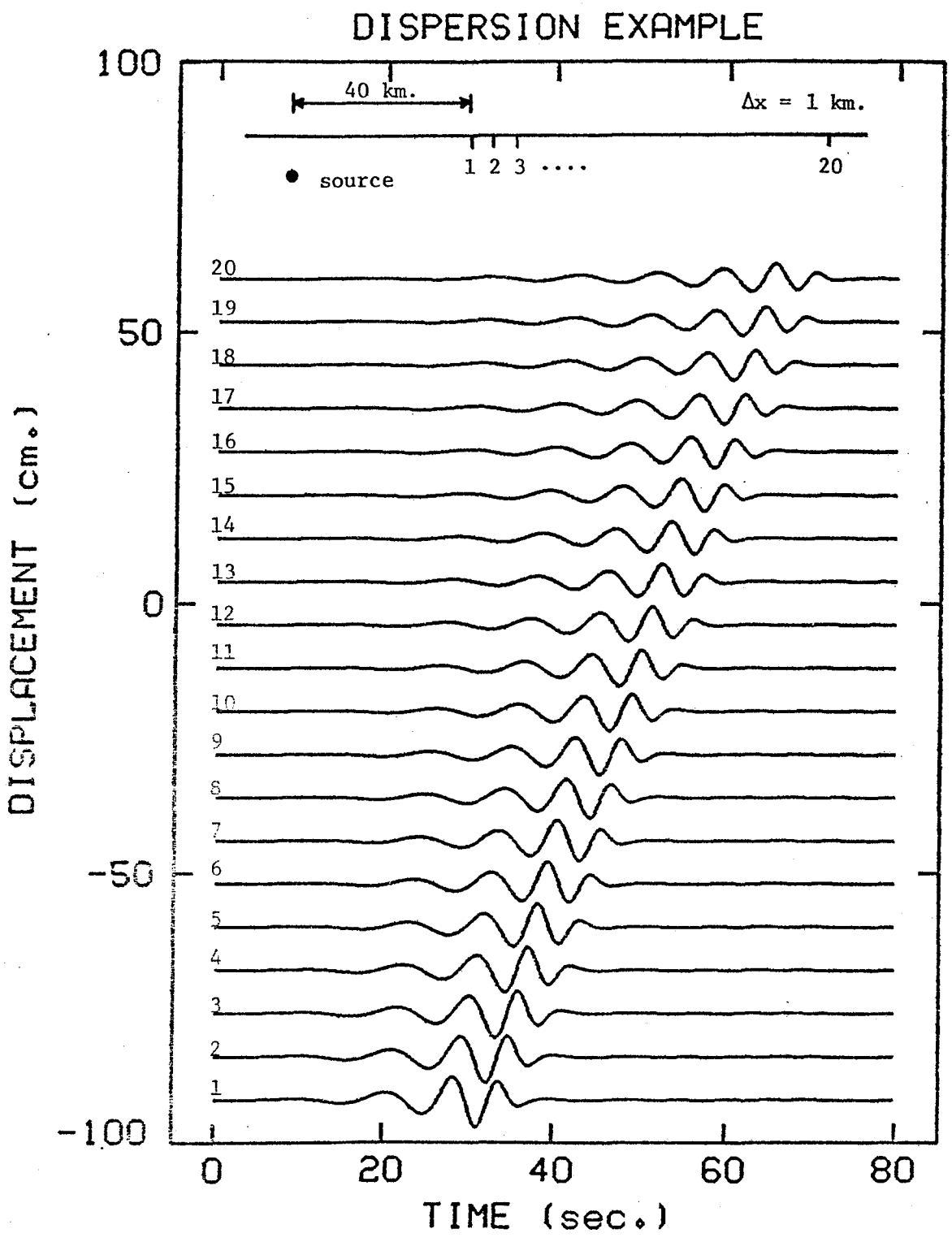


Figure III.2.3 An example demonstrating the dispersion of seismic waves. From these observations dispersion curves could be developed for phase and group velocity.

$$c(\omega) = \frac{x_2 - x_1}{t_p} \qquad \text{(III.2.1)}$$

where $x_2-x_1$ is the distance traveled by the wave, and the phase delay, $t_p$, is the delay of a particular peak traveling from point 1 to point 2.

The group velocity is defined as the source-site distance divided by the time of arrival of a wave group. The group velocity can be thought of as the velocity at which an envelope function for a given frequency group travels. Since energy is proportional to the amplitude squared, group velocity is often referred to as the velocity of energy flow. In Figure III.2.3 the phase and group velocities can be measured as the wave travels from the source.

A variational method is used in this work to determine the free oscillation modes and dispersion characteristics of a radially heterogeneous earth. Most applications of modal superposition techniques use a flat earth model. A spherical earth is considered in this work due to the stability of the variational method, and the availability of the computer algorithms. This is described in section III.4. The limitation of considering a laterally homogeneous earth is not viewed as a major handicap in modeling strong ground motion in view of the relative short distances, generally less than 100 kilometers, of interest in earthquake engineering. The advantage of having an earth model with radially varying characteristics is an important step towards the improvement of the state of the art in modeling strong ground motion for use in seismic hazard analysis.

## III.3 NORMAL MODE ANALYSIS

The normal mode method is discussed in a general way to outline the analysis procedure and to present its advantages in computing the response motion of a linear elastic system. The normal mode method of analysis is a popular computational technique in engineering, (Clough and Penzien, 1975), and seismology, (Kanamori and Stewart, 1976; Swanger and Boore, 1978). The method is based on the existence of normal modes of vibration of a system, each with a characteristic shape and frequency. The response of the system to arbitrary loads is defined as a weighted superposition of all modes.

Modal analysis is based on the principle that the response of a linear system can be composed of the superposition of the normal modes of the system. In structural engineering applications, the systems analyzed are often discrete and the number of modes equals the number of degrees of freedom associated with the individual masses. In seismology, a spherical or flat multilayered earth are examples of continuous systems where the method is applied. Normal mode analysis offers considerable advantage in that the modes and frequencies of vibration are calculated once, with the information then stored for repeated use. The response of the system to different loading functions is determined by the appropriate superposition of the modes. In the remainder of this section, the normal mode method is presented.

## III.3.1 DETERMINING THE FREE OSCILLATION MODES AND FREQUENCIES

Consider the equation of motion for the undamped free oscillations of a multi-degree of freedom system,

$$\underset{\sim}{M}\,[\ddot{U}(t)] + \underset{\sim}{K}\,[U(t)] = [0] \qquad \text{(III.3.1)}$$

where:

$\underset{\sim}{M}$ = mass matrix

$\underset{\sim}{K}$ = stiffness or rigidity matrix

$[\ddot{U}(t)]$, $[U(t)]$ = vectors of acceleration and displacement, respectively

$[0]$ = null vector

Assuming that in a normal mode the system response is harmonic, the displacement and acceleration of the $j^{th}$ mode is,

$$\begin{aligned} [U(t)]_j &= [Y]_j \sin(\omega_j t + \phi_j) \\ [\ddot{U}(t)]_j &= -[Y]_j\, \omega_j^2 \sin(\omega_j t + \phi_j) \end{aligned} \qquad \text{(III.3.2)}$$

where $[Y]_j$ is the maximum amplitude vector of the $j^{th}$ mode, $\omega_j$ is the angular frequency and $\phi_j$ the phase angle. Substituting eqs. (III.3.2) into (III.3.1) to obtain,

$$(\underset{\sim}{K} - \omega_j^2\, \underset{\sim}{M})\,[Y]_j = [0] \qquad \text{(III.3.3)}$$

which is a set of n simultanteous linear equations. The solution of these equations requires that the determinant of the expression on the left hand side is zero. This condition is given in eq. (III.3.4).

$$|\underset{\sim}{K} - \omega^2 \underset{\sim}{M}| = 0 \qquad \text{(III.3.4)}$$

An $n^{th}$ order algebraic equation in $\omega^2$ is obtained having n roots. The roots of this characteristic equation are the eigenfrequencies. For a given $\omega_j^2$, eq. (III.3.3) can be solved for $[Y]_j$ to within an arbitrary constant. The $[Y]_j$'s are the eigenvectors or modes of vibration.

It can be shown that the eigenvectors are orthogonal or normal to one another, (Clough and Penzien, 1975). The orthogonality property allows the problem of determining response to be decoupled into a set of n 2nd order differential equations, which are solved separately in the normal coordinate system, (Clough and Penzien, 1975). The final solution involves transforming the decoupled response in normal coordinates, back to the original coordinate system.

### III.3.2 RESPONSE TO A STEP FUNCTION FORCE

Consider the following example, where the response [U(t)] is desired due to a step function in time, [H(t)], which is applied to a discretized multi-degree of freedom elastic system. The undamped equation of motion for this system is,

$$\underset{\sim}{M}\,[\ddot{U}(t)] + \underset{\sim}{K}\,[U(t)] = [H(t)] \qquad \text{(III.3.5)}$$

By the orthogonality property of the normal modes, the mode shapes are used to define a generalized coordinate system where the total displacement is represented as a weighted superposition of the modes. Thus,

$$[U(t)] = \sum_{n=1}^{\text{modes}} [Y]_n\,[\Phi_n(t)] \qquad \text{(III.3.6)}$$

where $[Y]_n$ is the mode shape vector for the $n^{th}$ mode and $[\phi_n(t)]$ is the amplitude vector of the $n^{th}$ mode. Applying the orthogonality principle and substituting eq. (III.3.6) into the equation of motion, the following result is obtained,

$$\underset{\sim}{M}^{*}\,[\ddot{\Phi}(t)] + \underset{\sim}{K}^{*}\,[\Phi(t)] = [H^{*}(t)] \qquad \text{(III.3.7)}$$

where:

$$\begin{aligned} M^{*} &= \underset{\sim}{Y}^{T}\,\underset{\sim}{M}\,\underset{\sim}{Y} \\ K^{*} &= \underset{\sim}{Y}^{T}\,\underset{\sim}{K}\,\underset{\sim}{Y} \\ [H^{*}(t)] &= \underset{\sim}{Y}^{T}\,[H(t)] \end{aligned} \qquad \text{(III.3.8)}$$

Eq. (III.3.7) can be rewritten,

$$[\ddot{\Phi}(t)]_n + \omega_n^2\,[\Phi(t)]_n = \frac{[H^{*}(t)]_n}{M^{*}} \qquad \text{(III.3.9)}$$

which is the decoupled equation of motion for the $n^{th}$ mode. The solution for $[\phi_n(t)]$ is the result for a single degree of freedom oscillator, with natural frequency $\omega_n$, where,

$$[\Phi(t)]_n = \frac{[H^*(t)]_n}{\omega_n^2 \underset{\sim}{M}^*} (1-\cos\omega t) \qquad \text{(III.3.10)}$$

The total response, upon transforming the individual modal responses to the original coordinates, is,

$$[U(t)] = \sum_{n=1}^{\text{all modes}} [Y]_n \frac{[H^*(t)]_n}{\omega_n^2 \underset{\sim}{M}^*} (1-\cos\omega_n t) \qquad \text{(III.3.11)}$$

[U(t)] is the displacement response vector of the system due to a forcing function which varies stepwise. This exercise illustrates the principle of modal superposition to determine the response. A major advantage of modal analysis is that once the system is defined, that is once $\underset{\sim}{M}$ and $\underset{\sim}{K}$ are known, the eigenfrequencies and free oscillation modes can be determined and stored. The response of the system is found for any forcing function by applying eqs. (III.3.7) - (III.3.11). This same principle applies to normal mode analysis in seismology. That is, the determination of the earth's normal modes will be a function of the earth structure, and not the fault or event size.

## III.4 COMPUTATION OF NORMAL MODES AND DISPERSION CHARACTERISTICS FOR A SPHERICAL EARTH

In this section the computational method used to determine the free oscillation modes, and the frequency dependent phase and group velocities of a spherical earth model is presented. The previous sections described the general form of normal mode analysis and the fact that the earth is a dispersive medium having propagation velocities that vary with wavelength. A number of methods have been used in the past to compute the eigenfunctions and dispersion properties of surface waves for layered earth models, such as the Thomson-Haskell matrix method, (Harkrider, 1964). Routines are readily available for most techniques. In this work the variational approach developed by Wiggins (1976) is used. Geller (1979) suggests that variational methods offer considerable advantage over other techniques in terms of computational efficiency and accuracy. The method presented by Wiggins is a Rayleigh-Ritz procedure. The method is outlined in this section, describing the basic variational approach and solution technique for determining the normal mode eigenfrequencies and dispersion curves. In seismology the term overtone is often used to describe the higher order modes. The lowest order mode is the fundamental, with the higher modes denoted as the first, second overtones, etc.

The method presented by Wiggins is a Rayleigh-Ritz procedure that makes use of the principle that the Lagrangian remain stationary. In order to estimate the natural frequencies and normal modes of a system through the use of Rayleigh's principle, an assumption about the mode shape or an estimate of the eigenfrequency is required. This is true for

the earth or any elastic system. The method can be applied for the fundamental and any number of higher overtones.

The earth is assumed to be a radially heterogeneous sphere whose free oscillation modes are sought. The earth is described according to the radial variation of its density and elastic properties, or equivalently by its compressional and shear wave velocities. The earth also has boundary conditions at the outer surface and at the liquid-solid interface of the core-mantle boundary. These conditions are; zero stress at the outer surface and liquid-solid interface and displacement and stress continuity across internal boundaries such as between solid layers. Since the earth is modeled as a radially heterogeneous sphere, the eigenfunction will be a function of r, the radial coordinate only.

Following the formulation of Ritz, the eigenfunction can be considered as a linear sum of interpolation functions. Once the form of these functions has been chosen, potential and kinetic energy integrals can be found. Following Hamilton's principle, the solution for the eigenfrequencies corresponds to a minimizing of the Lagrangian. For the case of a radially heterogeneous earth, the Lagrangian is given by Takeuchi and Saito (1972) to be,

$$
\begin{aligned}
I &= \omega^2 I_1 - I_2 - (\ell-1)(\ell+2) I_3 \\
I_1 &= \int_o^a \rho(r)\, r^2 y_1^2(r)\, dr \\
I_2 &= \int_o^a \mu(r)\, (r\dot{y}_1(r) - y_1(r))^2\, dr \\
I_3 &= \int_o^a \mu(r)\, y_1^2(r)\, dr
\end{aligned}
\qquad \text{(III.4.1)}
$$

where a is the earth's radius, $\omega$ is the eigenfrequency, $y_1(r)$ is the depth dependent displacement eigenfunction, $\mu(r)$ is the shear modulus, $\rho(r)$ is the density, and $\ell$ is the angular order. Also in eq. (III.4.1), $\dot{y}_1(r)$ is $dy_1(r)/dr$. Applying the condition that the Lagrangian be stationary, the standard form of the eigenvalue problem is obtained. The solution for the eigenfrequencies and the eigenfunctions can be carried out by a standard eigenvalue solution routine.

A free oscillation mode, $y_1(r)$, is modeled as a linear sum of interpolation functions as shown in eq. (III.4.2).

$$y_1(r) = \sum_{i=1}^{m} c_i \, \phi_i(r) \qquad \text{(III.4.2)}$$

For a defined set of interpolation functions, $\phi_i(r)$, the $c_i$'s are the unknowns and can be considered as a set of generalized coordinates. For engineers this method is familiar as the basis of the finite element method of structural analysis. In practical problems the system, in this case the earth, is divided into segments, within which the eigenfunction is described by eq. (III.4.2). A set of natural coordinates is employed where the segments are of unit length. Substituting eq. (III.4.2) into eq. (III.4.1), Wiggins gives the following expression for the Lagrangian,

$$I = [c]^T \underset{\sim}{A}[c] - \omega^2 [c]^T \underset{\sim}{B}[c]$$

where:

$$\underset{\sim}{A} = A_1 + (\ell-1)(\ell+2) A_2$$

$$A_{1ij} = \int_o^a \mu(r) \, (r\dot{\phi}_i(r) - \phi_i(r)) \, (r\dot{\phi}_j(r) - \phi_j(r)) \, dr$$

$$A_{2ij} = \int_o^a \mu(r)\ \phi_i(r)\ \phi_j(r)\ dr \qquad \text{(III.4.3)}$$

$$B_{ij} = \int_o^a \rho(r)\ r^2\ \phi_i(r)\ \phi_j(r)\ dr$$

$$[c]^T = [c_1, c_2, \ldots . c_n]$$

where T denotes the transpose. Minimizing the Lagrangian with respect to the unknown generalized coordinate, [c], the standard form of the eigenvalue problem is obtained.

$$\underset{\sim}{A}[c] - \omega^2\ \underset{\sim}{B}[c] = [o] \qquad \text{(III.4.4)}$$

Summarizing the development of the solution for the normal modes to this point, a Rayleigh-Ritz method is used to set up the eigenvalue problem for an elastic sphere. The earth's structure is described by the variation of mass density and shear wave velocity with depth. For this system the eigenfunction is a function of depth, and is modeled as a series of segments. Within each segment the eigenfunction is described as a linear sum of interpolation functions. Substituting the discretized eigenfunction into the Lagrangian, eq. (III.4.3) was obtained. The remaining undefined components are the interpolation functions which are described next.

Wiggins has chosen to use Hermite polynomials as the interpolation functions. These functions in natural coordinates are,

$$\phi_1(x) = 3x^2 - 2x^3$$

$$\phi_2(x) = -x^2 + x^3$$

$$\phi_3(x) = 1 - 3x^2 + 2x^3$$

$$\phi_4(x) = x - 2x^2 + x^3 \qquad \text{(III.4.5)}$$

where $x = \frac{r-a}{b-a}$ for the radial interval r = a to r = b. The shape of the

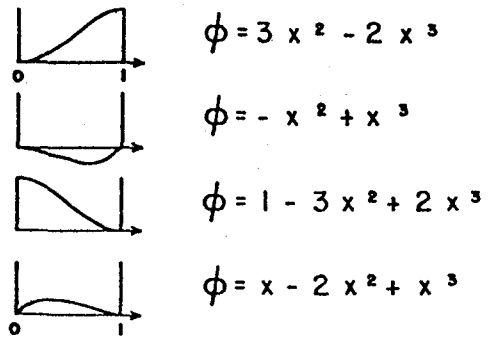


Figure III.4.1 The interpolation functions used to represent the eigenfunction, shown with their polynomial representation, (Wiggins, 1976).

interpolation functions are shown in Figure III.4.1. These interpolation functions have been chosen such that the slope or displacement is 0 or 1 at the ends. For systems with boundary conditions this choice is particularly advantageous. The boundary conditions at internal layer boundaries and at the earth's surface are met by appropriate modification of the A matrix. Conditions such as displacement and stress continuity at the boundary between layers and the requirement of zero stress at the free surface are taken into account and have been demonstrated by Wiggins (1976).

The solution for the eigenvalues and corresponding eigenvectors is carried out through the use of the inverse iteration method. For an initial estimate of $\omega_i$, the corresponding eigenvector is determined. If this is not the solution, the Rayleigh quotient gives the next estimate,

$\omega_{i+1}$,

$$\omega_{i+1} = \frac{[c]_i^T \underset{\sim}{A} [c]_i}{[c]_i^T \underset{\sim}{B} [c]_i} \qquad \text{(III.4.6)}$$

This process is repeated until the Lagrangian is stationary.

When a particular eigenfrequency and mode have been found, the group and phase velocities of the wave can be computed, (Takeuchi and Saito, 1972),

$$\begin{aligned} c(\omega) &= \frac{\omega a}{\ell + 1/2} \\ u(\omega) &= \frac{2\ell + 1}{2\omega} \quad \frac{I_3}{I_1} \end{aligned} \qquad \text{(III.4.7)}$$

where $u(\omega)$ is the group velocity and $c(\omega)$ the phase velocity and a, $\ell$, and $\omega$ are as defined earlier.

To use the inverse iteration method of solving the eigenvalue problem, reasonably good estimates of the eigenvalue or eigenfunction must be made. For the fundamental mode this is not so critical, since given a poor eigenvalue estimate, the routine will generally find the fundamental eigenfrequency. For other modes the initial estimate must be within about 10% of the true value. To obtain accurate initial estimates of the eigenvalues the following technique is used. For a given angular order, the Lagrangian is calculated over a wide range of $\omega$'s, incrementing $\omega$ by 1 or 2 percent on each iteration. The routine identifies the eigenvalue number that the current value of $\omega$ is closest

to, (Wiggins, 1976).

This method of determining the normal modes of the earth has a number of specific advantages over other techniques that have been used in the past. Previous methods model the earth as a layered media whose elastic properties vary in a stepwise manner with depth. Realistically the earth would be better represented by a gradient of some form. Wiggins' routine allows for a linear variation of $\rho(r)$, $v_p(r)$ and $v_s(r)$ with depth. The method does not however, require that these properties be continuous across boundaries and therefore discontinuities can also be modeled.

To conclude, the Wiggins variational method offers an efficient, accurate method of determining the free oscillation modes and dispersion characteristics of a realistic model of the earth's structure.

## III.5 MOTION DUE TO A SINGLE FAULT SEGMENT

This section develops the acceleration motion at a site due to an arbitrary fault segment that propagates unilaterally along a line. The development follows that of Kanamori, (1970),

Fukao and Abe, (1971), Takeuchi and Saito, (1972), etc. in obtaining the Fourier transform of displacement due to a double-couple point source varying stepwise. The model is extended to consider a propagating line source, a dislocation time function that is a ramp, and acceleration motion. The development presented here will be for the transverse component of the SH motion.

The form of the torsional mode displacement motion, as derived from

the wave equation in spherical coordinates is,

$$
\begin{aligned}
U_r(r,t) &= 0 \\
U_\theta(r,t) &= \frac{1}{\sin\theta}\, y_1(r)\, \frac{\partial Y_{\ell m}(\theta,\phi)}{\partial \phi}\, e^{-i\omega t} \\
U_\phi(r,t) &= -y_1(r)\, \frac{\partial Y_{\ell m}(\theta,\phi)}{\partial \theta}\, e^{-i\omega t}
\end{aligned}
\qquad \text{(III.5.1)}
$$

where the spherical coordinates r, $\theta$, and $\phi$ are shown in Figure III.5.1. Eq. (III.5.1) defines the free oscillations of the earth when vibrating in a torsional mode. In the above equation, $y_1(r)$ is the depth dependent displacement eigenfunction and $Y_{\ell m}(\theta,\phi)$ is the spherical surface harmonic which is independent of depth and earth structure, and describes the oscillations of the surface of a sphere. Also, $\ell$ is the angular order number, m the azimuthal order number, and $\omega$, the eignfrequency. The radial displacement, $U_\theta(r,t)$ depends on m, and the transverse displacements will depend on $\ell$. For the torsional modes, the radial motion is negligible.

As pointed out in section III.2, the normal modes of the earth are defined by 2 parameters, n and $\ell$, for constant azimuthal order m. Therefore the modal properties to be described in this section, $y_1(r)$, $\omega$, $L_1(\omega)$, $L_2(\omega)$, etc., are functions of the mode, n, and the angular order $\ell$. To simplify notation the subscripts, n and $\ell$, are implied for the remainder of this discussion for frequency dependent functions.

The form of the spherical surface harmonics, $Y_{\ell m}(\theta,\phi)$, is given in eq. (III.5.2),

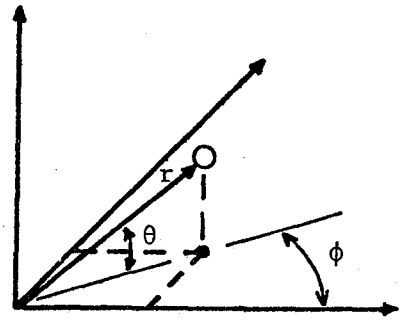


(a.)

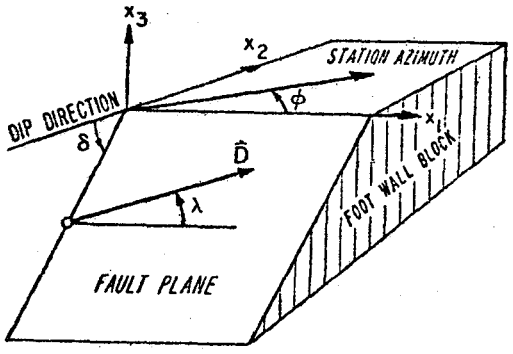


(b.)

Figure III.5.1 (a.) Polar coordinate system with parameters, $r, \phi, \theta$ and (b.) fault representation defining the slip vector D and slip angle $\lambda$ which is measured counter clockwise from the $x_1$ axis and the dip angle $\delta$ measured from the negative $x_2$ axis.

$$Y_{\ell m}(\theta,\phi) = (-1)^m \frac{2\ell+1}{4\pi} \frac{(\ell-m)!}{(\ell+m)!} P_\ell^m(\cos\theta)\, e^{im\phi} \qquad m \geq 0$$

$$= (-1)^m Y^*_{\ell m}(\theta,\phi) \qquad m < 0 \qquad \text{(III.5.2)}$$

where $P^m(\cos\theta)$ is the Legendre polynomial, which for an argument x, satisfies the differential equation,

$$P_n^m(x) = (1-x^2)^{\frac{m}{2}} \frac{d^m}{dx^m} p_n^m(x) \qquad m \geq 0 \qquad \text{(III.5.3)}$$

Knowledge of the displacement field as given in eq. (III.5.1) makes it possible to determine the potential and kinetic energy integrals as derived by Takeuchi and Saito (1972), and expressed in the previous section (see eq. (III.4.3)). After considerable algebra, equations (III.5.1) to (III.5.3) are solved to give the displacement due to a point source in terms of the normal modes of the earth. The total displacement motion is then expressed as a superpostion of each mode. The general form of the displacement, U (r,t), observed on the surface of the earth, and excited by a point double-couple source varying stepwise, is given by,

$$U(r,t) = \sum_n \sum_\ell \frac{(\varepsilon_{ij}(r_s)\, M_{ij})\, y_l(r_s)}{\omega^2\, y_l(r)^T\, \rho(r)\, y_l(r)} (1-\cos\omega t) \qquad \text{(III.5.4)}$$

where the forcing function $[H^*(t)]$ in eq. (III.3.11) is replaced by the term $\varepsilon_{ij}(r_s)M_{ij}$. This represents the forcing function of the earthquake applied at a point $r_s$. $\varepsilon_{ij}$ is the strain tensor at the source and $M_{ij}$ is the seismic moment tensor, (Geller, 1979).

Eq. (III.5.4) represents the solution for ground displacements by the normal mode method. After evaluating the strain tensors, the result for the transverse component, $U_\phi(r,t)$, is,

$$U_\phi(r,t) = \sum_n \sum_\ell y_1(r) \cos\omega t$$

$$(-L_1(\omega)q \frac{dP_\ell^1(\cos\theta)}{d\theta} + L_2(\omega)p \frac{dP_\ell^2(\cos\theta)}{d\theta}) \qquad \text{(III.5.5)}$$

The terms, p and q, in eq. (III.5.5) are geometric factors that depend on the fault mechanism and source site azimuth and are defined as, (refering to Figure III.5.1a,b),

$$q = -(\cos\lambda \cos\delta) \sin\phi + (\sin\lambda \cos 2\delta) \cos\phi$$
$$p = (\sin\lambda \sin\delta \cos\delta) \sin 2\phi + (\cos\lambda \sin\delta) \cos 2\phi \qquad \text{(III.5.6)}$$

$L_1(\omega)$ and $L_2(\omega)$ are the earthquake forcing functions for a given mode and angular order which are independent of source geometry, and defined to be,

$$L_1(\omega) = \frac{2\ell + 1}{4\pi\omega^2 I_1} \frac{y_2(r_s)}{\mu(r_s)}$$

$$L_2(\omega) = \frac{2\ell + 1}{4\pi\omega^2 I_1} \frac{y_1(r_s)}{r_s} \qquad \text{(III.5.7)}$$

where the subscript s denotes the value of the variable at the source depth. $I_1$ is the energy integral defined in eq. (III.4.1) and $y_2(r)$ is the depth dependent stress eigenfunction, defined as,

$$y_2(r) = \left(\frac{dy_1(r)}{dr} - \frac{y_1(r)}{r}\right) \qquad \text{(III.5.8)}$$

The equation for transverse displacement, eq. (III.5.6), is for a unit moment. Geller (1979) presents the modal amplitude factors $A_1(\omega)$ and $A_2(\omega)$ for the case of a moment tensor at the source, varying stepwise,

$$\begin{aligned} A_1(\omega) &= L_1(\omega)\ (-M_{r\phi} + M_{r\theta}) \\ A_2(\omega) &= L_2(\omega)\ (-M_{\theta\phi} + \tfrac{1}{2}\ (M_{\theta\theta} - M_{\phi\phi})) \end{aligned} \qquad \text{(III.5.9)}$$

where the moment tensors were, p and q, in the case of a unit moment without the azimuthal dependence $\phi$.

The time domain representation of the transverse component was given in eq. (III.5.5), where $U_\phi(r,t)$ was represented by a summation over the number of modes. To solve for $U_\phi(r,t)$, the asymptotic expansion of the Legendre polynomial is used, which is

$$P_\ell^m(\cos\theta) \simeq e^{im\pi}\, \ell^m \cos\left((\ell + \tfrac{1}{2})\,\theta\right) + \left(\tfrac{m\pi}{2} - \tfrac{\pi}{4}\right) \sqrt{\frac{2}{\ell\pi\sin\theta}} \qquad \text{(III.5.10)}$$

By a change of variable, the summation over $\ell$ in eq. (III.5.6) is replaced by an integral over, $\omega$, the frequency. The variable change, $k = (\ell + 1/2)/a$ and $d\ell = dk/(d\omega/dk)$, is used where k is the wavenumber and $d\omega/dk$ is recognized to be the group velocity $u(\omega)$. Expansion of eqs. (III.5.5) and (III.5.10) into complex form, and substituting eq. (III.5.10) into the new expression for $U_\phi(r,t)$, leads to the following result,

$$U_\phi(r,t) = \frac{1}{2\pi} \frac{1}{\sqrt{\sin\theta}} \sum_n \int_{-\infty}^{\infty} y_1(r)\, [p\, P^1(\omega) + iq\, Q^1(\omega)] \exp\left(-\tfrac{i\pi}{4}\right) \exp\left(-i\omega a\theta/c(\omega)\right) \exp\left(i\omega t\right) d\omega \qquad \text{(III.5.11)}$$

This is the Fourier transform integral for $U_\phi(r,t)$. Simplifying notation and identifying terms,

$$P^1(\omega) = -\sqrt{\frac{\pi}{2\ell}}\; \ell^2(\ell + \tfrac{1}{2}) \frac{a}{u(\omega)}\; L_2(\omega)$$
$$Q^1(\omega) = -\sqrt{\frac{\pi}{2\ell}}\; \ell(\ell + \tfrac{1}{2}) \frac{a}{u(\omega)}\; L_1(\omega) \qquad \text{(III.5.12)}$$

where $L_1(\omega)$ and $L_2(\omega)$ are the source terms which depend on source depth and the earth structure as defined earlier. Also,

$$C(\omega) = \frac{1}{\sqrt{\sin\theta}} \left[p\, P^1(\omega) + iq\, Q^1(\omega)\right]$$

$$\exp\left(-i\frac{\pi}{4}\right) \cdot \exp\left(-i\omega a\theta/c(\omega)\right) \qquad \omega \geq 0 \qquad \text{(III.5.13)}$$

$$C(-\omega) = C^*(\omega) \qquad \omega < 0$$

which is the Fourier transform of displacement due to a unit double couple source varying stepwise, and p and q are the geometric factors accounting for source-site azimuth and fault geometry. The $1/\sqrt{\sin\theta}$ term accounts for the geometric spreading of surface waves where $\theta$ is the source-site distance in radians.

In seismology, where the generation of synthetic seismograms is of interest, the source excitation terms are interpolated at equal spacing over the desired frequency range, and inverse Fourier transformation produces the time domain signal. In this work the frequency function is of interest and therefore $C(\omega)$ is used throughout the remainder of this chapter.

The solution derived to this point describes the displacement at a site due to a point source with a step function excitation. In this work acceleration motion due to the propagating rupture of a fault segment is desired. By the derivative theorem, the Fourier transform of acceleration, $A(\omega)$, is given by

$$A(\omega) = -\omega^2\, C(\omega) \qquad \text{(III.5.14)}$$

For other than the first point of rupture, the excitation due to a general segment will be shifted in time until the rupture reaches that

point. Denoting the time of rupture initiation at a segment j as $tr_j$, by the shift theorem the acceleration transform becomes,

$$A(\omega) = -\omega^2 C(\omega) e^{-i\omega tr_j} \qquad \text{(III.5.15)}$$

The Fourier transform of displacement derived previously was for a source dislocation function that varied stepwise in time. This is shown in Figure III.5.2a. In this work a ramp dislocation function, (Haskell, 1964), is used, as shown in Figure III.5.2b. Therefore to transform the results for a step function, to that for a ramp, the time domain function is convolved with what is known as the far field source function. This function is equal to the derivative of the desired source dislocation function. In this case the derivative of the ramp function is a box-car of duration equal to the time until the final dislocation, $D_o$, is reached (see Figure III.5.2b). The far field source function is shown in Figure III.5.2c. The time it takes to reach $D_o$ is known as the rise time and is denoted by $\tau$. In the frequency domain, the convolution with a box-car results in a multiplication with a sinc function, (sin x/x), the box-car transform. Thus $A(\omega)$ now becomes,

$$A(\omega) = -\omega^2 C(\omega) \frac{\sin(\tau\omega/2)}{\tau\omega/2} \exp(-i\omega(tr_j + \tau/2)) \qquad \text{(III.5.16)}$$

The acceleration spectrum is further modified due to the fact that the earthquake source is no longer a point but a propagating finite line

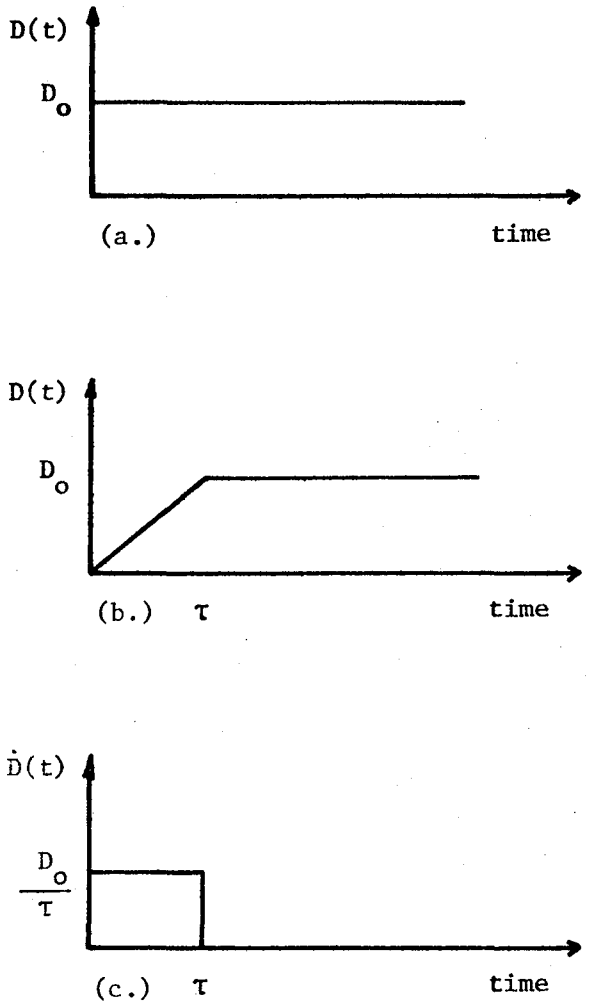


Figure III.5.2 Source dislocation functions varying as a (a.) step function, (b.) ramp function with rise time τ, and, (c.) the far field source time function.

source having a velocity $v_r$ over a length L. The effect due to rupture over a finite source is known as directivity and was first studied by Ben-Menahem (1961). The acceleration transform is modified due to this effect in a manner similar to that for a ramp dislocation. The directivity effect is

$$\frac{\sin(T_L\omega/2)}{T_L\omega/2}\, e^{-iT_L\omega/2} \qquad \text{(III.5.17)}$$

where $$T_L = \frac{L}{2}\left(\frac{1}{v_r} - \frac{\cos\phi}{c(\omega)}\right)$$

$\phi$ is the source-site azimuth, and $c(\omega)$ is the wave phase velocity. The resulting Fourier transform of acceleration due to a general fault segment is,

$$A(\omega) = -\omega^2\, C(\omega)\, \frac{\sin(\tau\omega/2)}{\tau\omega/2}\, \frac{\sin(T_L\omega/2)}{T_L\omega/2} \qquad \text{(III.5.18)}$$
$$\exp\left(-i\omega(tr_j + \tau/2 + T_L/2)\right)$$

The final factor to be included in the ground motion model is the anelastic attenuation of seismic waves. This is taken into account by a filter of the form,

$$\exp\left(\frac{-r\omega}{2Qu(\omega)}\right) \qquad \text{(III.5.19)}$$

where r is the source to site distance on the earth's surface in

kilometers, $\omega$ is the frequency, Q is the specific attenuation factor and $u(\omega)$ is the group velocity.

## III.6 SUMMARY

In this chapter the model for generating the Fourier transform of acceleration at a site was presented. The development was for a propagating line segment of arbitrary position in space and time where the motion is determined by the normal mode method. The modal superposition method permits modeling of a radially heterogenous earth with linear velocity gradients. The variational procedure of Wiggins was used to identify the eigenfrequencies and modes to permit calculation of the source excitation coefficients. The model presented is based on the method developed by a number of researchers, as cited, and extended by standard techniques to consider the directivity effect due to a propagating source, a ramp source time function, and acceleration motion. The normal mode method provides a realistic means of taking into account the earth structure and free surface in estimating strong ground motion. Also, since the eigenfrequencies and eigenfunctions are calculated once, the method is quite efficient in generating synthetic spectra or waveforms. The next chapter demonstrates various aspects of this model and applies it in modeling of strong ground motion from observed events.

# CHAPTER IV - THE NORMAL MODE METHOD: DETERMINISTIC MODELING

## IV.1 INTRODUCTION

Chapter III presented the normal mode method for determining ground motion due to a general fault segment. From this result an expression for the total motion due to the complete fault rupture can be given as the superposition of individual segment contributions. Although well founded theoretically, the usefulness of a wave propagation model is judged by its ability to reproduce recorded waveforms given the "proper" input. This statement is admittedly vague in its definition of model verification. The philosophy of scientific investigation, as discussed by Jeffreys (1961), involves the basic differences between inductive and deductive logic. In the present discussion, the following approach is taken. Observed ground motion data are modeled to demonstrate the ability of the normal mode method to reproduce the distribution of energy as a function of frequency. This is to say, that spectral levels are considered of prime importance in the present work. Although time domain comparisons are used throughout this chapter when modeling ground displacement and acceleration, spectral measures are more appropriate for defining the future seismic hazard. The reasons for this are related to the complex dependence of the waveform phase on the fault rupture and dispersion properties of the transmission medium. Thus spectral amplitudes, which are not dependent on phase, are adopted. Examples of these are the Fourier amplitude spectrum, power spectral density and peak response spectrum, (McGuire, 1974; Anderson and Trifunac, 1977; Savy, 1979).

This chapter has two objectives; to demonstrate the effect various source parameters have on ground motion, and then by modeling past events, the capability of the normal mode method to reproduce observed ground motion. To carry out these tasks a location must be selected where the earth's structure is known, and where strong ground motion recordings are available. The Imperial Valley in southern California meets these criteria, and is adopted as the study area in this work. This choice is particularly advantageous since other investigators have modeled earthquake strong ground motion in this region with different theoretical models, (Heaton and Helmberger, 1977, 1978; Swanger and Boore, 1978).

After selecting the Imperial Valley, results of the solution for the normal modes and dispersion curves are presented. To demonstrate the model in a general sense, examples of radiation pattern, directivity, dislocation rise time, and source depth effects are given. This will serve to demonstrate the features of the model, as well as to define the effect dynamic and geometric source characteristics have on ground motion. Two seismic events are then selected to demonstrate in more detail the normal mode technique, these are the 1968 Borrego Mountain earthquake and the 1976 Brawley earthquake. For each event the displacement waveforms are modeled. In addition, for the Borrego Mountain earthquake, synthetic acceleration time histories are compared to the accelerograph recording obtained at the El Centro station. The term synthetic refers to the waveform generated by the theoretical model. The synthetic Fourier amplitude spectra of acceleration are compared to the observed spectrum to assess the ability of the model to predict the

energy distribution as a function of frequency.

## IV.2 IMPERIAL VALLEY REGION

The Imperial Valley is an active seismic region in southern California which has experienced a number of moderate to large ($M_L$ greater than 5.5) earthquakes in the last 40 years. Figure IV.2.1 presents a map of the Imperial Valley and surrounding region, denoting

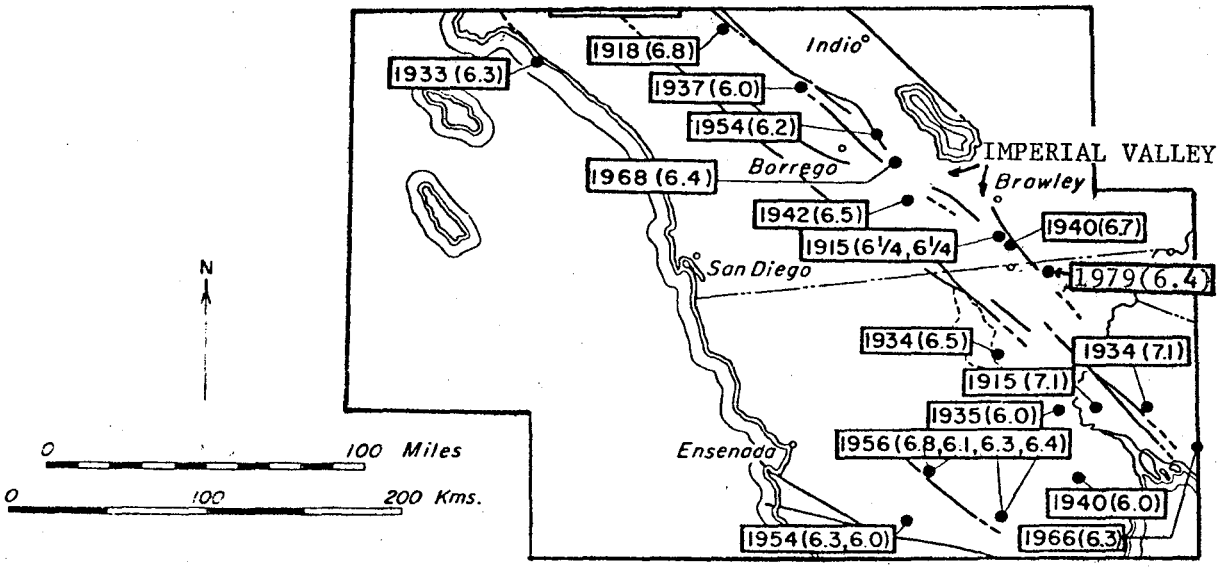


Figure IV.2.1 Earthquakes of magnitude 6.0 and greater in the southern California region, 1912 - 1972, (Hileman et al., 1973).

events of magnitude 6.0 and greater.

The 1940 Imperial Valley earthquake produced one of the most significant acceleration recordings of ground shaking ever obtained. Recently, the 1979 Imperial Valley earthquake produced a recording with the highest vertical acceleration ever, 1.74g, (USGS Open-File Report

79-1654, 1979). For reasons of seismicity alone, the Imperial Valley is an excellent region to consider for this study. In addition, and just as important, is the fact that the geologic structure in the Imperial Valley is well understood and in fact forms an ideal waveguide, (Biehler et al., 1964; Clayton and McMechan, 1980). The events to be studied in this work have been investigated by other researchers, (Heaton and Helmberger, 1977, 1978; Swanger and Boore, 1978), employing the generalized ray technique and the modal superposition method for a flat earth, respectively. These works serve as a guide in the choice of fault models to be used in this study.

### IV.2.1 IMPERIAL VALLEY EARTH STRUCTURE

Biehler et al. (1964) carried out P-wave refraction studies in the Imperial Valley region. Their study provides the type of information necessary to apply models such as the normal mode method. Figure IV.2.2 shows the Imperial Valley area, and the locations of the seismic refraction profiles. Based in part on their results, Heaton and Helmberger (1977) used a layer over a half-space in modeling the 1968 Borrego Mountain earthquake. Swanger and Boore (1978) on the other hand used the more complicated structure given in Table IV.2.1. Their model was set up to take into account the variation in lateral thickness of the Imperial Valley that exists between the hypocentral area of the Borrego Mountain earthquake and the El Centro recording station. Their earth structure is adopted in this work to model the Borrego Mountain earthquake and the 1976 Brawley event, except that the model in this study uses linear gradients to describe the variation with depth of the earth's density and seismic velocities. The earth structure used in this

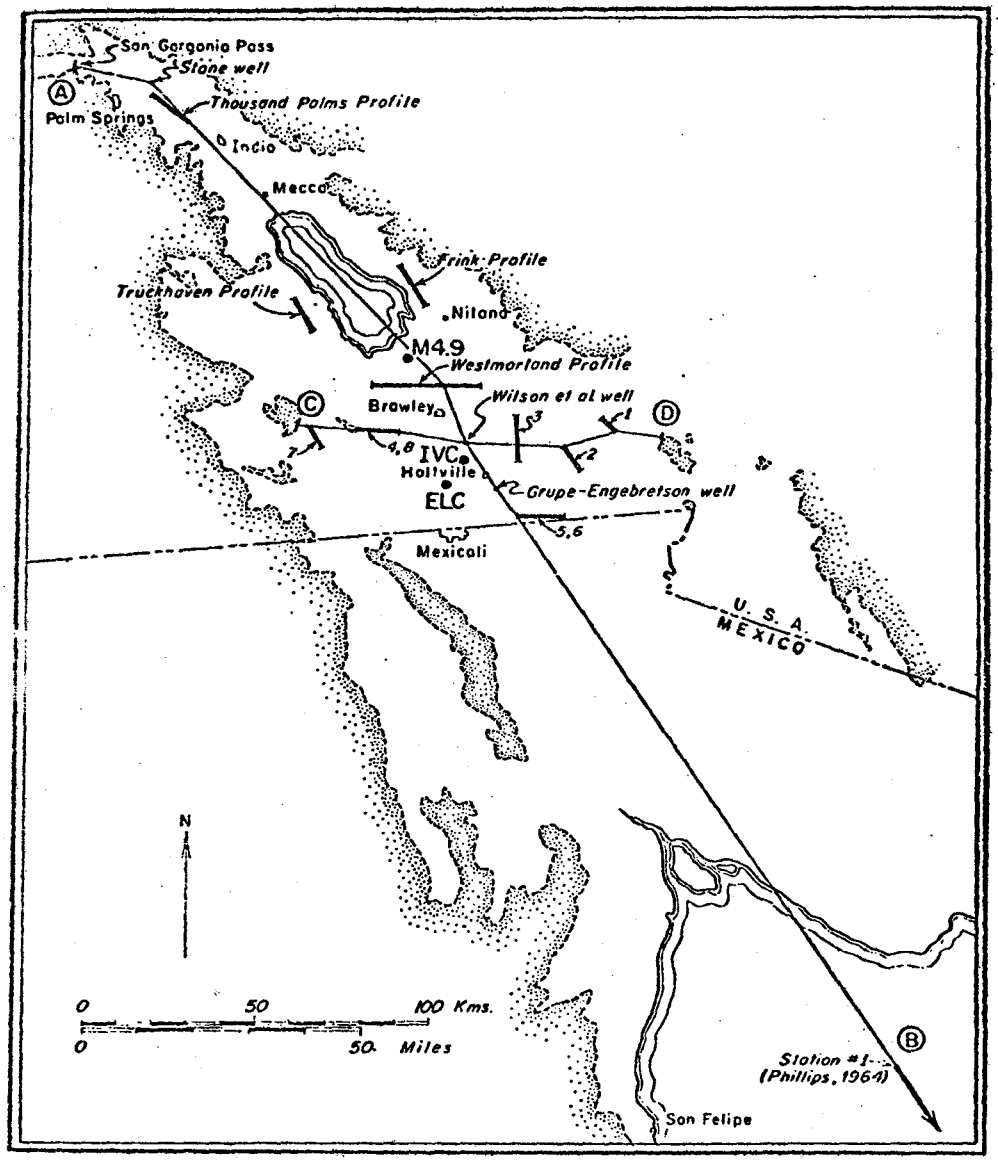


Figure IV.2.2 Map of Salton Trough showing locations of seismic refraction profiles and cross-section lines. Also shown are the long-period strong-motion stations, IVC and ELC, and the epicenter of the M4.9, November 4,1976 earthquake. Stippling indicates generalized outline of pre-Tertiary crystalline rocks bordering the Salton trough. This figure has been modified from Biehler et al. (1964).

work is shown in Figure IV.2.3 with the structure in Table IV.2.1. The

Table IV.2.1

STRUCTURE USED BY SWANGER AND BOORE (1978)

| Thickness (km) | P Velocity (km/sec.) | S Velocity (km/sec.) | Density ($gm/cm.^3$) |
|---|---|---|---|
| 0.25 | 1.7 | 1.0 | 2.0 |
| 0.30 | 2.1 | 1.2 | 2.2 |
| 1.35 | 2.4 | 1.4 | 2.2 |
| 0.95 | 3.3 | 1.9 | 2.4 |
| 1.65 | 4.3 | 2.5 | 2.5 |
| 7.0 | 6.2 | 3.6 | 2.9 |
| 8.5 | 7.1 | 4.1 | 3.0 |
| --- | 7.8 | 4.5 | 3.1 |

shear wave velocity and density are shown since the torsional modes are considered in this work. The linear gradient model is intuitively a realistic model of the earth's seismic profile but not one to which the Wiggins routine is restricted. In some cases, linear gradients within layers, and discontinuities at layer boundaries, may be the most suitable, and one which the present routine can handle. The effect of having discontinuities between layers is to insure sharp reflections, and to clearly define a waveguide. The desirability of this depends on the structure being considered. Recent studies of the Imperial Valley structure indicate that the use of linear gradients is a realistic representation of the seismic profile, (Clayton and McMechan, 1980).

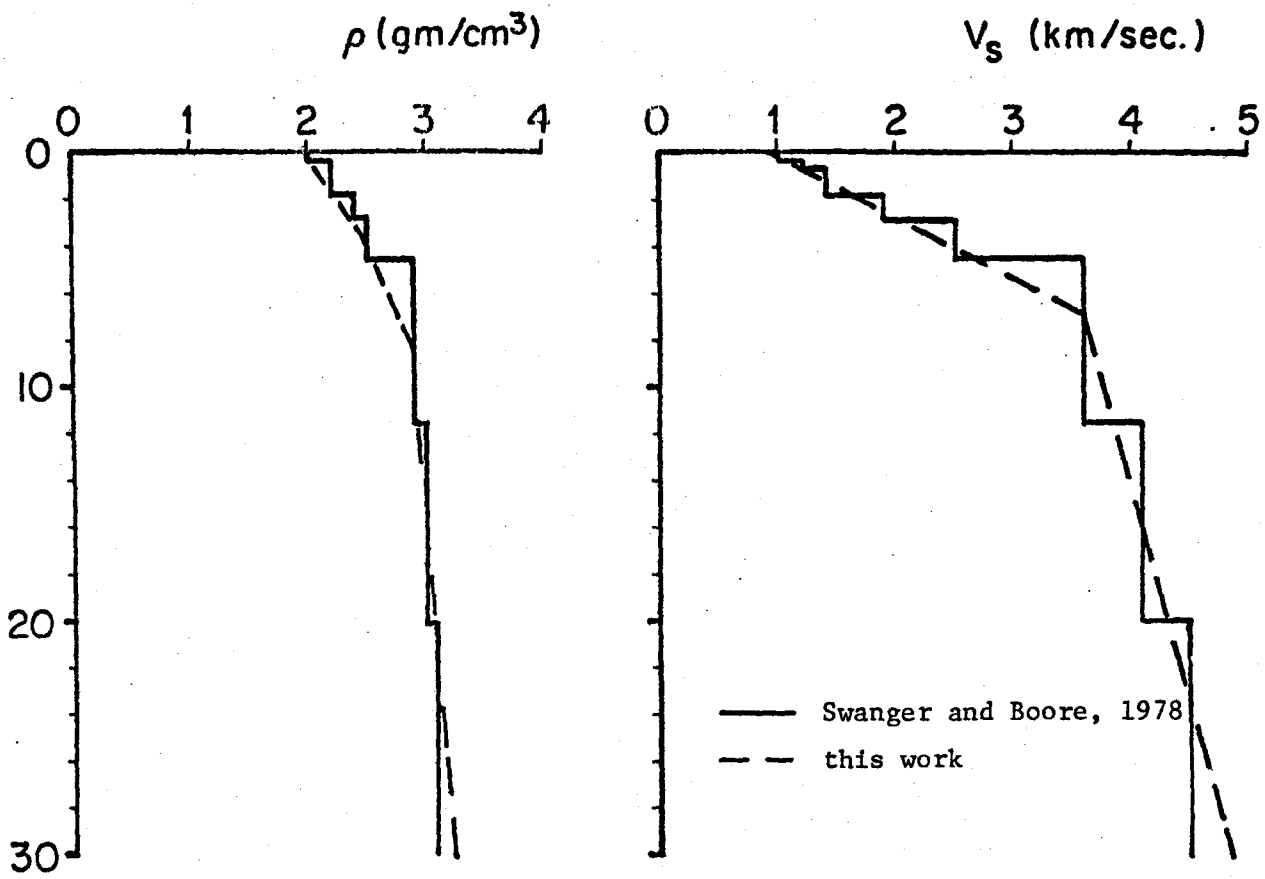


Figure IV.2.3 The earth structure used in the study shown with the model of Swanger and Boore (1978), which was used as a guide in setting up the linear gradient model.

## IV.2.2 RESULTS OF NORMAL MODE CALCULATIONS FOR THE IMPERIAL VALLEY EARTH STRUCTURE

For the Imperial Valley earth structure presented in the previous section, Wiggins' variational routine is used to generate the fundamental and seventeen higher torsional overtones (a total of 18 modes). The dispersion curves and eigenfunctions for each mode are calculated. The excitation coefficients are determined at nineteen depths, from 1 to 19 kilometers spaced at one kilometer increments. For the purpose of demonstrating the present probability model, eighteen modes provide frequency information up to approximately 5 hz., depending on the depth of the earthquake. There is no numerical reason why additional modes could not be determined and included in the solution. This section summarizes the results of the normal mode calculations.

Figure IV.2.4 gives the dispersion curves for the Imperial Valley structure in Figure IV.2.3. Figure IV.2.5 is an example of the depth dependent displacement eigenfunctions for three modes; the fundamental, the third overtone, and the seventh overtone. The mode shapes are shown for angular orders corresponding to frequencies of 1.0, 2.0, and 5.0 hz. Note that the higher overtones sample to a greater depth than the fundamental mode at a given frequency. As more overtones are included in the analysis, body waves are being modeled as opposed to surface waves when only the fundamental and first few overtones are considered. Since body wave amplitudes are of major importance in determining the strong motion, considering the higher overtones is essential.

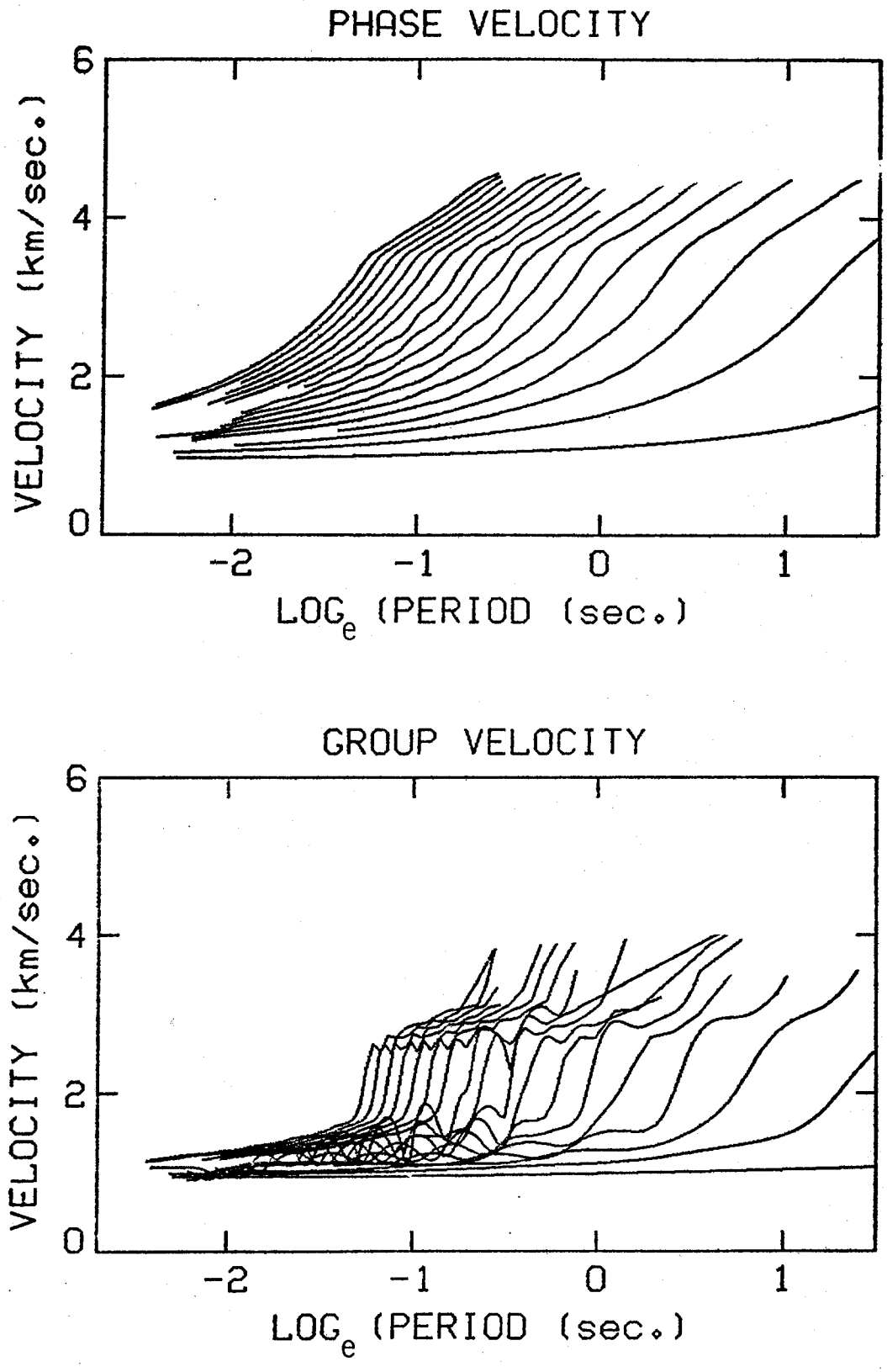


Figure IV.2.4 Dispersion Curves for the Imperial Valley structure.

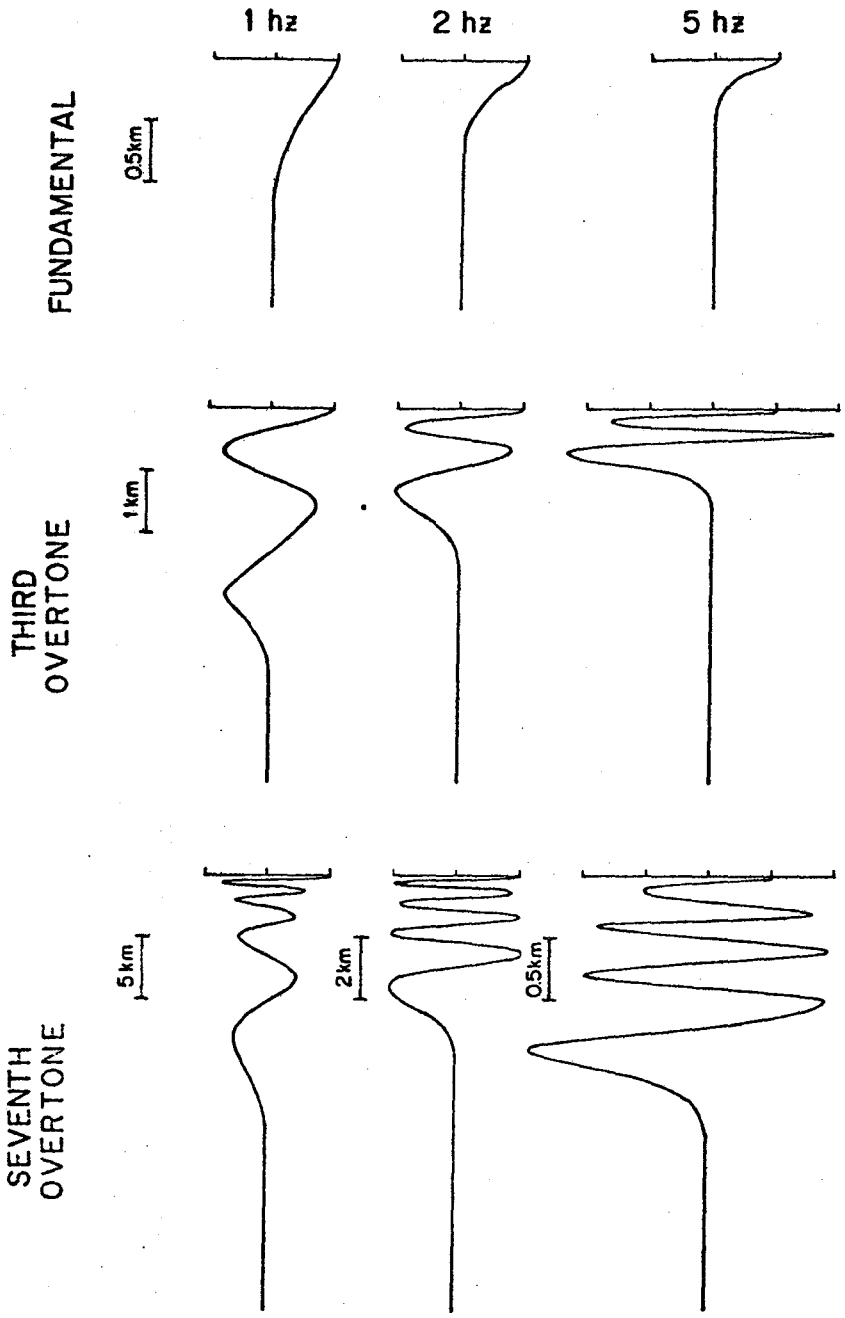


Figure IV.2.5 Examples of the depth dependent, displacement eigenfunctions for the fundamental mode, and the third and seventh overtones. The eigenfunctions are selected at angular orders corresponding to frequencies of 1, 2, and 5 hz. Note the difference in depth penetration at a given frequency.

## IV.3 EFFECT OF SOURCE PARAMETERS ON GROUND MOTION

This section demonstrates the effect different source properties have on ground motion. Examples are presented to illustrate the effects due to the radiation pattern of different source mechanisms, dislocation rise time, directivity, and source depth. The examples are presented by way of displacement time histories. Since displacement waveforms in general consist of the fundamental mode and 4 or 5 overtones, the time histories are low frequency and relatively narrowband. Consequently, phase and amplitude variations can be observed quite easily. The corresponding effect on the Fourier amplitude spectrum is easily understood, since the time domain effect will have a well known counterpart in the frequency domain, due to the linearity of the Fourier transform. Unless otherwise noted the displacement motion in the examples is for strike-slip motion on a vertical fault plane, ($\delta = 90^0$, $\lambda = 0^o$).

### IV.3.1 RADIATION PATTERN

The influence of fault geometry and radiation pattern for different earthquake source mechanisms is considered first. The fault and source-site geometric factors were presented in Chapter III. For easy reference, Figure III.5.1 is shown here.

The angles $\delta$ and $\lambda$ define the source geometry, and $\phi$ defines the source-site orientation. The following focal mechanisms are considered:

strike-slip: $\delta = 90^{o}$ , $\lambda = 0^{o}$

vertical dip slip: $\delta = 90^{o}$ , $\lambda = 90^{o}$

dipping thrust: $\delta = 45^{o}$ , $\lambda = 90^{o}$

dipping strike-slip: $\delta = 45^{o}$ , $\lambda = 0^{o}$

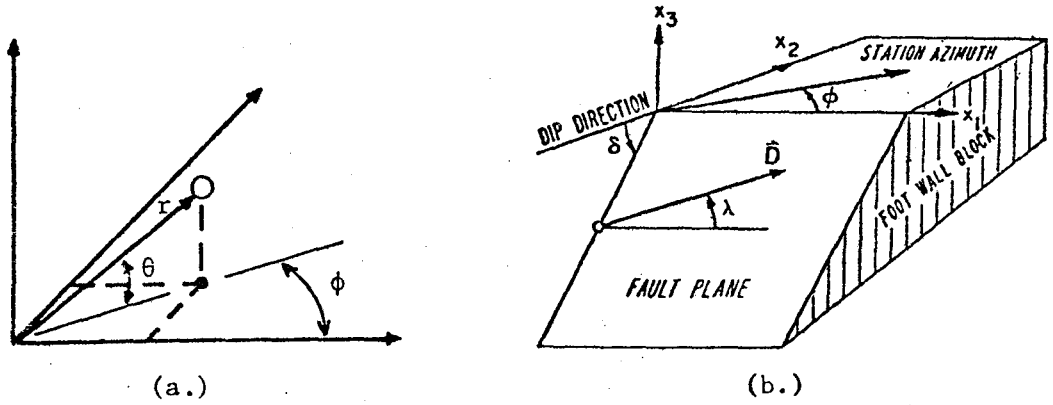


(a.) (b.)

Figure III.5.1 (repeated) (a.) Polar coordinate system with parameters, $r, \phi, \theta$ and (b.) fault representation defining the slip vector D and slip angle $\lambda$ which is measured counter clockwise from the $x_1$ axis and the dip angle $\delta$ measured from the negative $x_2$ axis.

The source is a point with a dislocation time function that is a ramp with a 1.25 second rise time. The time histories for each case are given in Figures IV.3.1 - IV.3.4. For each focal mechanism the azimuth is varied to demonstrate amplitude and polarity variation. Note the special case when the site lies on a radiation pattern node where no motion exists. See for example Figure IV.3.1 for a strike-slip event, ($\delta = 90^{o}$, $\lambda = 0^{o}$), at a $45^{o}$ azimuth. This phenomena does not occur during actual earthquakes since P and SV motion will be dominant at these azimuthal locations. Radiation pattern effects are a major component in the

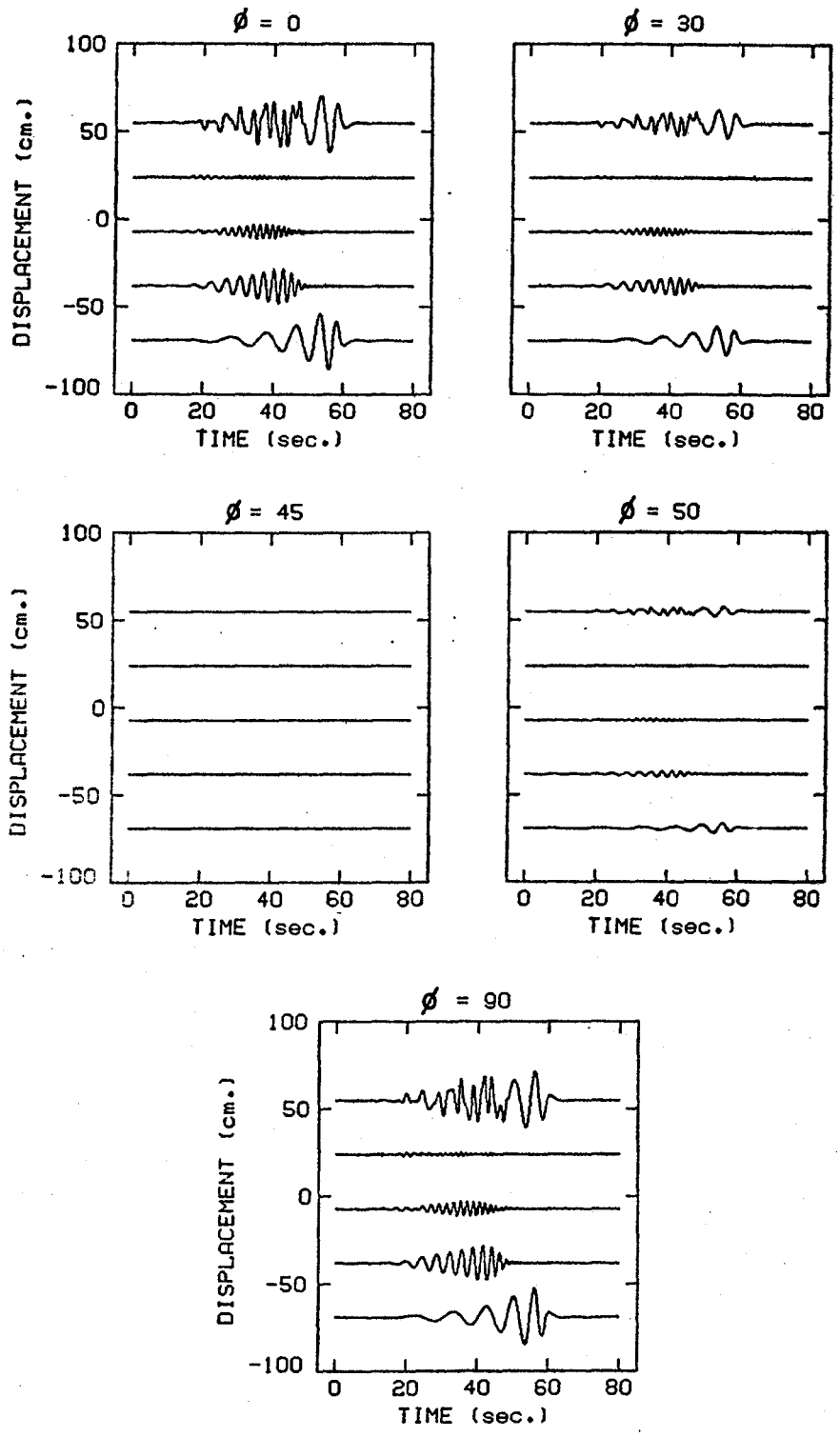


Figure IV.3.1 Displacement waveforms due to a strike-slip event, ($\delta = 90^{o}$, $\lambda = 0^{o}$), observed at different azimuths.

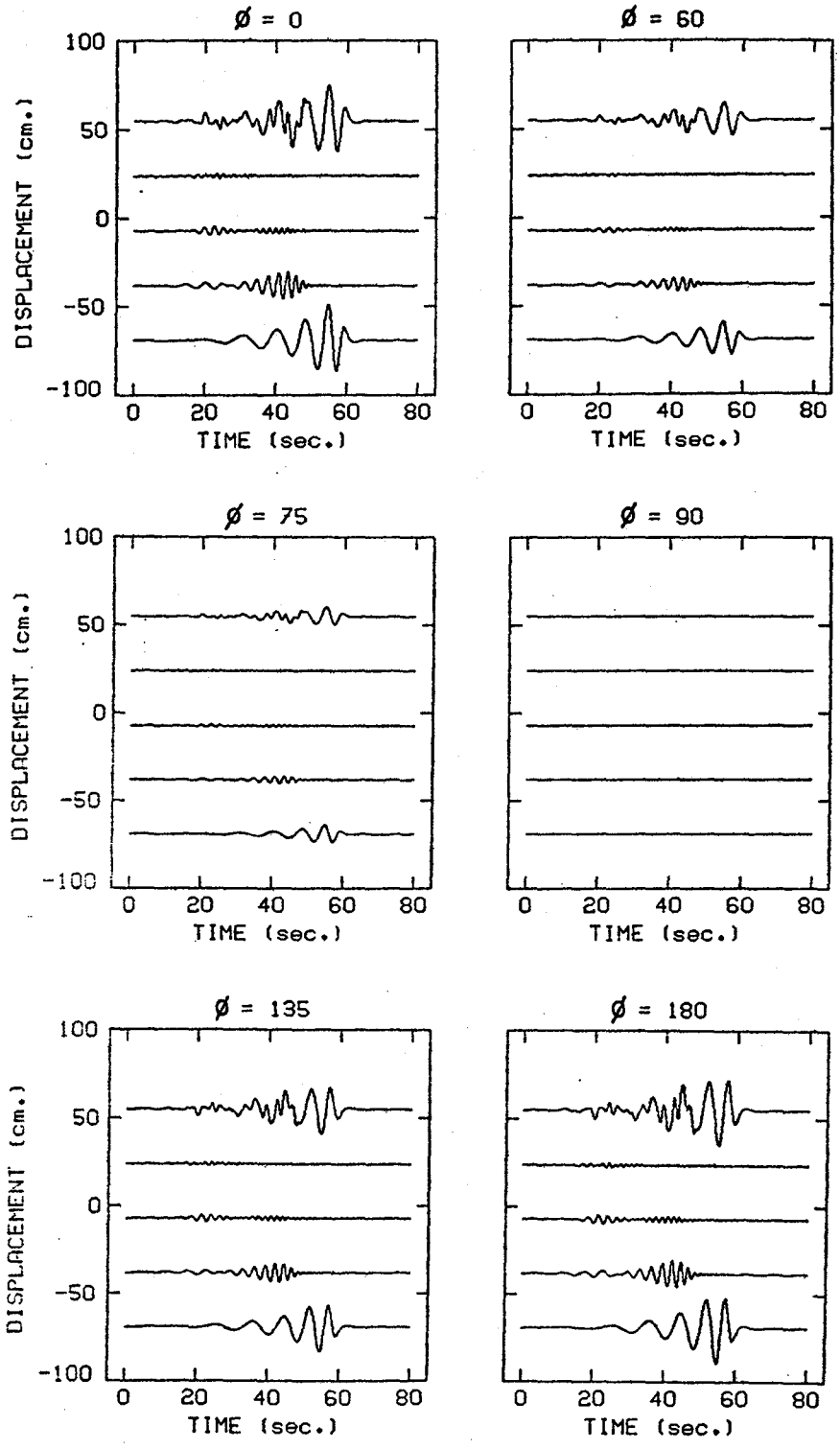


Figure IV.3.2 Displacement waveforms for a vertical dip slip fault, ($\delta = 90^{o}$, $\lambda = 90^{o}$), observed at different azimuths.

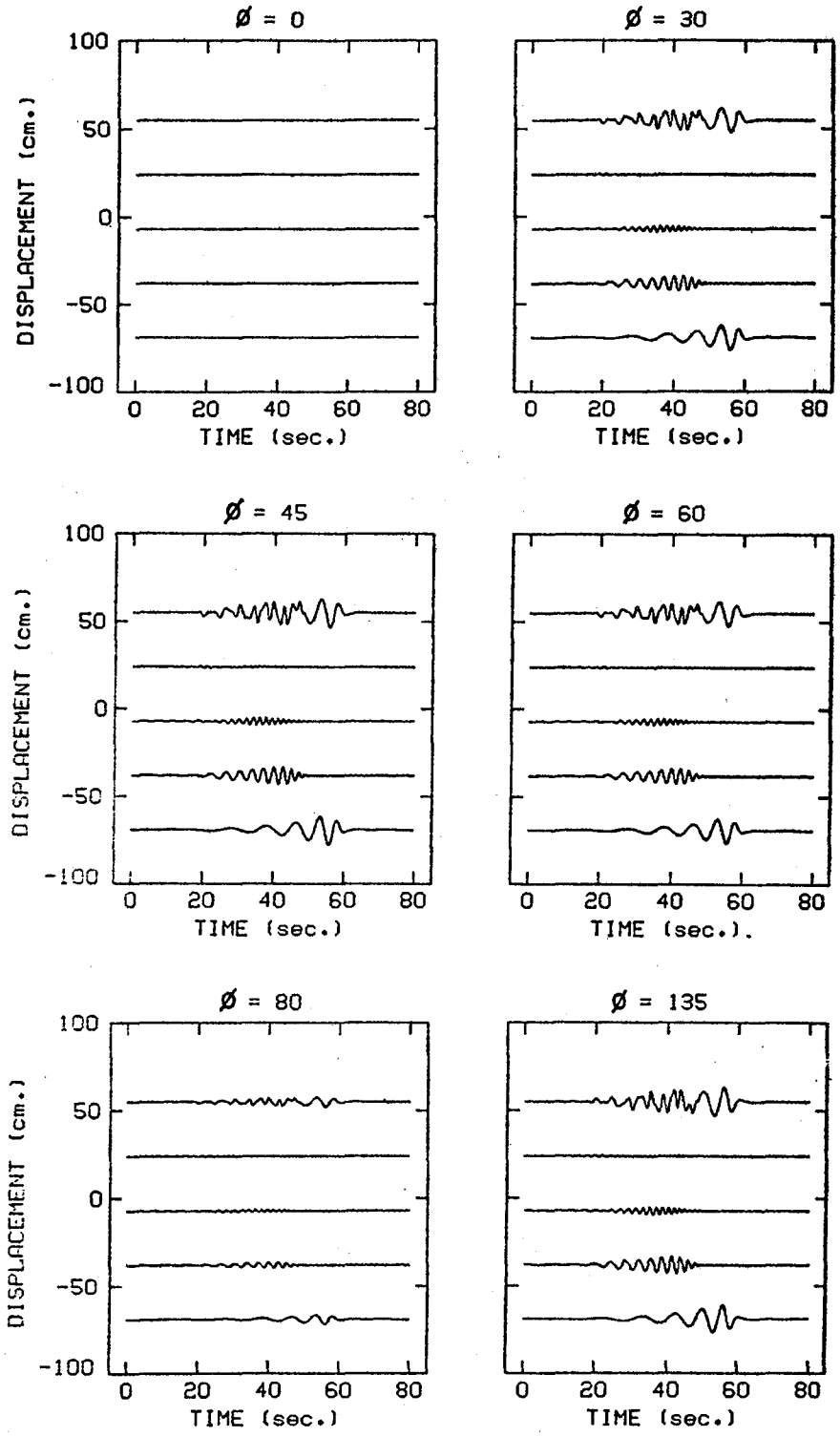


Figure IV.3.3 Displacement waveforms for a dipping thrust fault, ($\delta = 45^{o}$, $\lambda = 90^{o}$), observed at different azimuths.

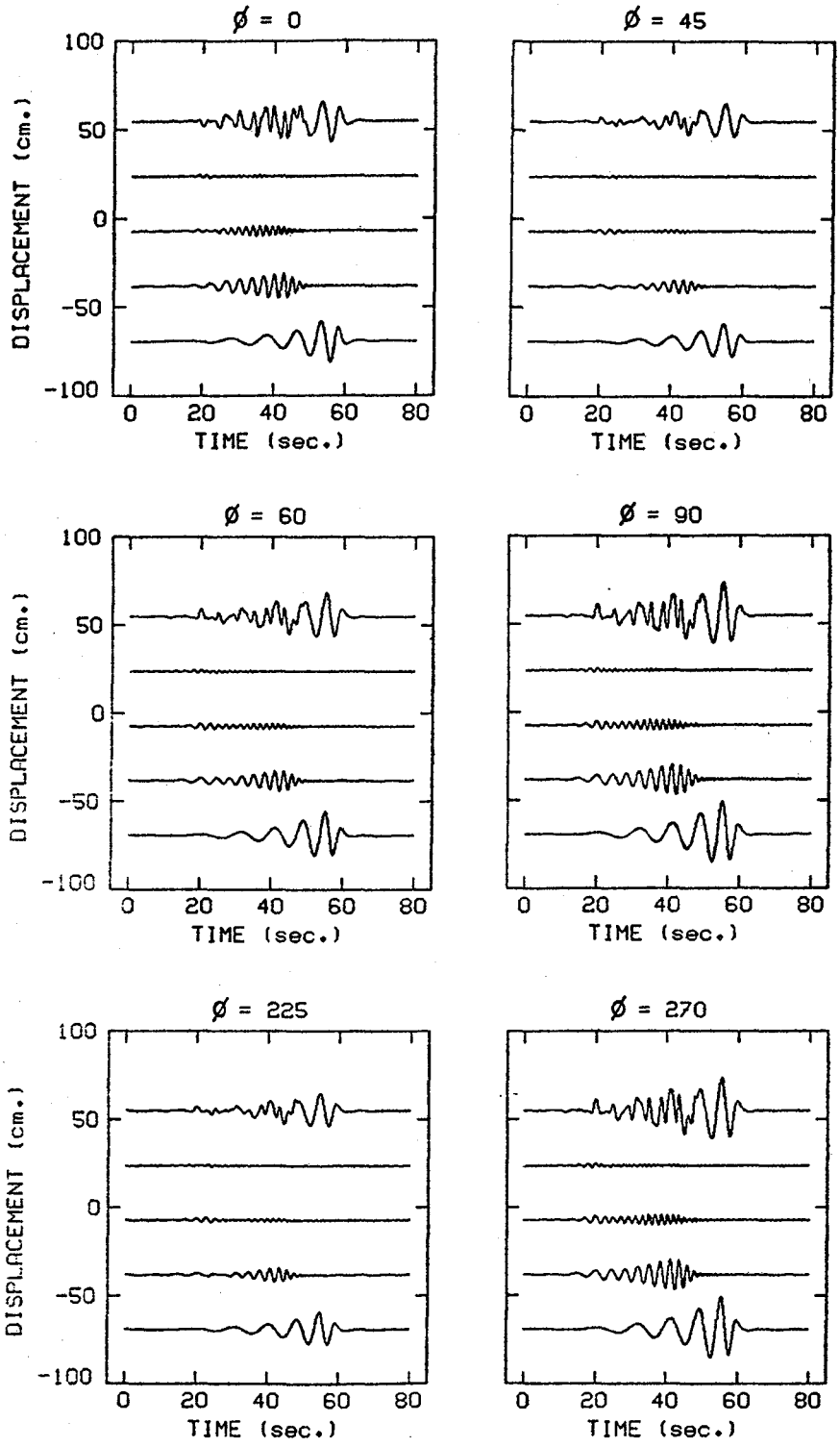


Figure IV.3.4 Displacement waveforms for a dipping, strike-slip fault, ($\delta = 45^{o}$, $\lambda = 0^{o}$), observed at different azimuths.

analysis to identify the focal mechanisms of earthquakes, (Bath, 1973). As an example of observed seismic wave radiation, the El Centro recording of the 1968 Borrego Mountain event lies almost exactly on a maxima of the radiation pattern for SH motion and therefore the recorded motion is predominantly transverse, (Heaton and Helmberger, 1977).

The radiation pattern and focal mechanism have first order significance on ground motion. This is predicted by theory, and is observed for every earthquake.

### IV.3.2 RISE TIME

As shown in Chapter III, a source dislocation function that varies as a ramp, modifies the time domain function by convolution with a box-car. This results in a smoothing of the time history to a degree that depends on the rise time duration and the frequencies of interest. Two examples of waveforms generated for a source with non-zero rise times are shown in Figure IV.3.5. Synthetics for rise times of 0.5 and 3.0 seconds are presented. The tremendous smoothing by a 3 second rise time is quite clear in Figure IV.3.5b. A nonzero rise time also results in a phase shift of $-\frac{\omega\tau}{2}$. The box car function which describes the particle velocity of a point on the fault is referred to as the far field source function. The use of a ramp dislocation is a common approach but not unique, (Aki and Richards, 1980).

### IV.3.3 SOURCE DIRECTIVITY

The third source factor to be considered is directivity. This is the term used to describe the influence of rupture propagation along a

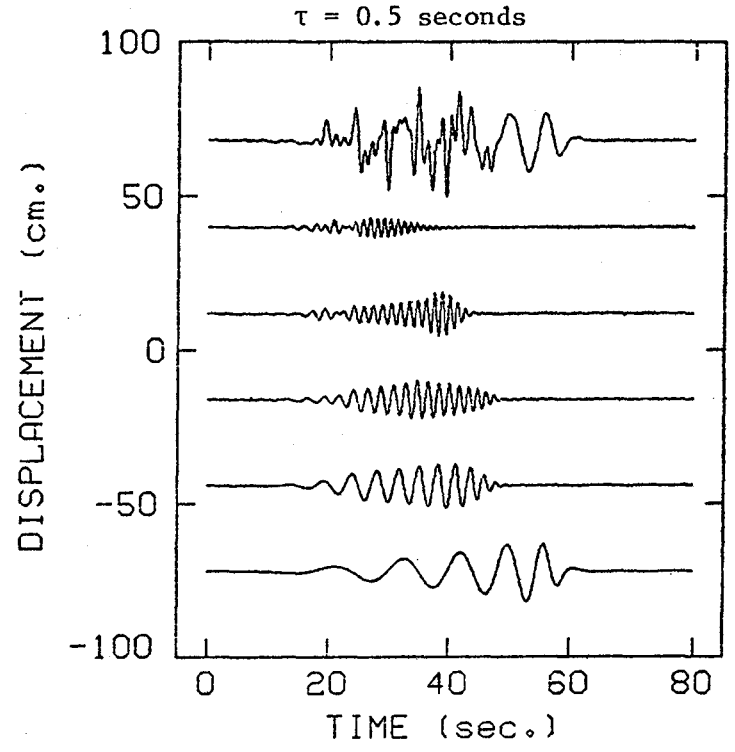


(a.)

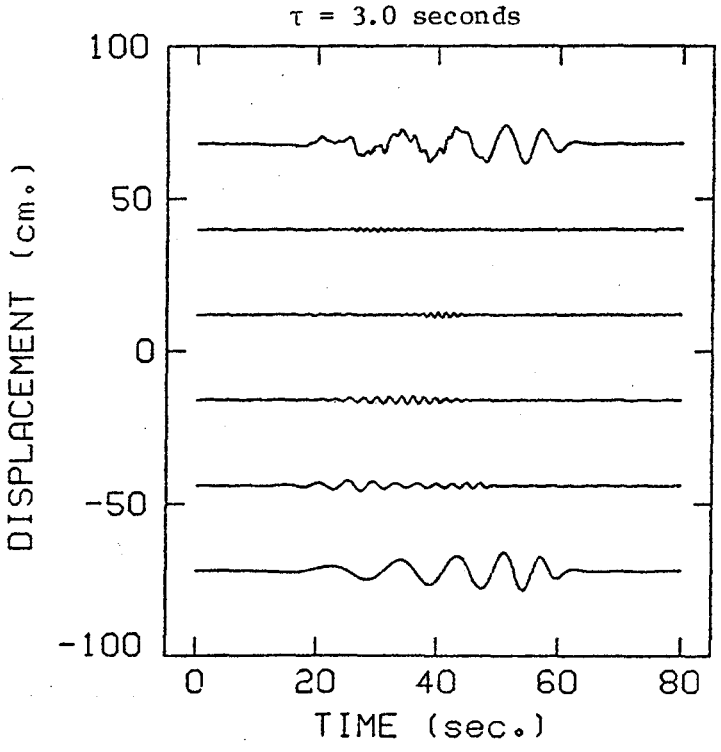


(b.)

Figure IV.3.5 Examples of the effect due to dislocation rise time, (a.) $\tau$ = 0.5 seconds and (b.) $\tau$ = 3.0 seconds.

source of finite length on the seismic radiation field. Waveform amplification occurs at forward azimuths due to constructive wave interference, contrasted by a deamplifying at back azimuths attributed to destructive wave interference. Ben-Menahem (1961) first studied the directivity function which has the form sin x/x, as given in Chapter III. Boore and Joyner (1978) have also studied directivity effects. The directivity function is repeated here for reference.

$$\frac{\sin(T_L\omega/2)}{T_L\omega/2}\, e^{-iT_L\omega/2} \qquad \text{(III.5.17)}$$

where $$T_L = \frac{L}{2}\left(\frac{1}{v_r} - \frac{\cos\phi}{c(\omega)}\right)$$

In Figure IV.3.6, taken from the paper by Boore and Joyner (1978), the dependence of the directivity factor $T_L$ on the ratio of the rupture velocity to the wave phase velocity and azimuth in a homogeneous whole space is shown.

The directivity effect on spectral amplitudes for forward azimuths is to increase the amplitudes of those frequencies above the corner frequency, $f_o$. Figure IV.3.7 presents a time domain example of the azimuthal effect on displacement waveforms. The fundamental mode and four overtones are used in the calculations with a 3.0 second duration far field source function that is a symmetric triangle. The radiation pattern and rise time contributions are constant in these examples.

There is approximately a factor of 5 difference in the motion at the forward azimuth, $\phi=0^{o}$, relative to the back azimuth, $\phi=180^{o}$.

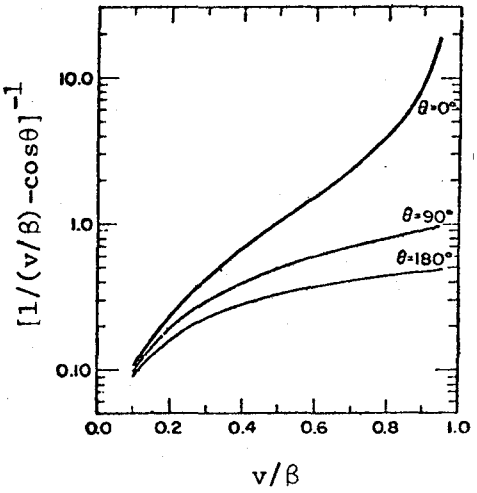


Figure IV.3.6 The dependence of the directivity on Mach number and azimuth. The peak motions are proportional to the ordinate. Note the disproportionate change going from azimuths of 0° to 90° compared to that from 90° to 180°. This figure is for a homogenous whole space and therefore does not hold for all frequencies in the present model (Boore and Joyner (1978)).

As observed by Swanger and Boore (1978), there is a complex interaction between the phase velocity, $c(\omega)$, and the rupture velocity. Figure IV.3.8 is an example in the time domain illustrating this point for the fundamental mode Love waves. This is similar to the frequency domain demonstration of Swanger and Boore. There is a factor of 7 difference between the case for a rupture velocity of 2.5 km./sec. and 1 km./sec.

Few cases have been observed where directivity has been accurately indentified as having played a major role. This is due in part to a lack of adequate multiple recordings for seismic events. One event for which directivity has been identified as having amplified the observed ground

motion is the 1979 Covote Lake earthquake, (Archuleta, 1979).

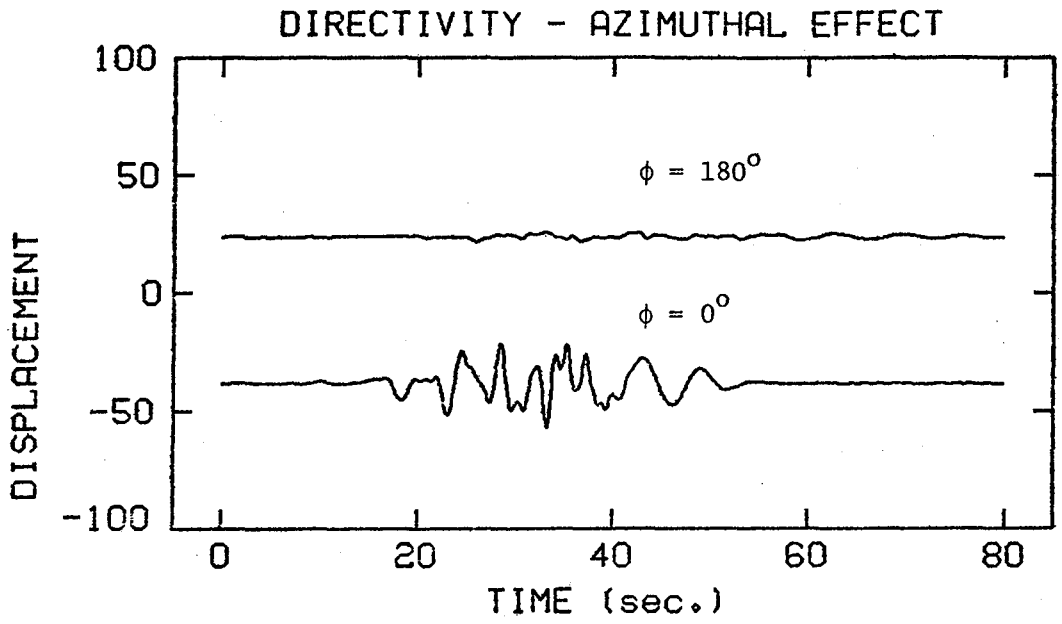


Figure IV.3.7 An example of the azimutal effect due to source directivity. The fault in this example was 11 km. long at 6 km. depth. The rupture propagated at a velocity of 2.5 km./sec. Results for the forward, $\phi = 0°$, and the back azimuth, $\phi = 180°$ are shown.

## IV.3.4 SOURCE DEPTH

The depth of the earthquake source which is modeled as a point or line source in this work, will have a distinct effect on ground motion. How different depths actually effect the motion will depend a great deal on the earth structure. For example in cases similiar to the Imperial Valley where there is a well defined waveguide, the motion is significantly altered if the event occurs in the waveguide or in the region below. Considerable variation in amplitude, frequency content, and duration can result.

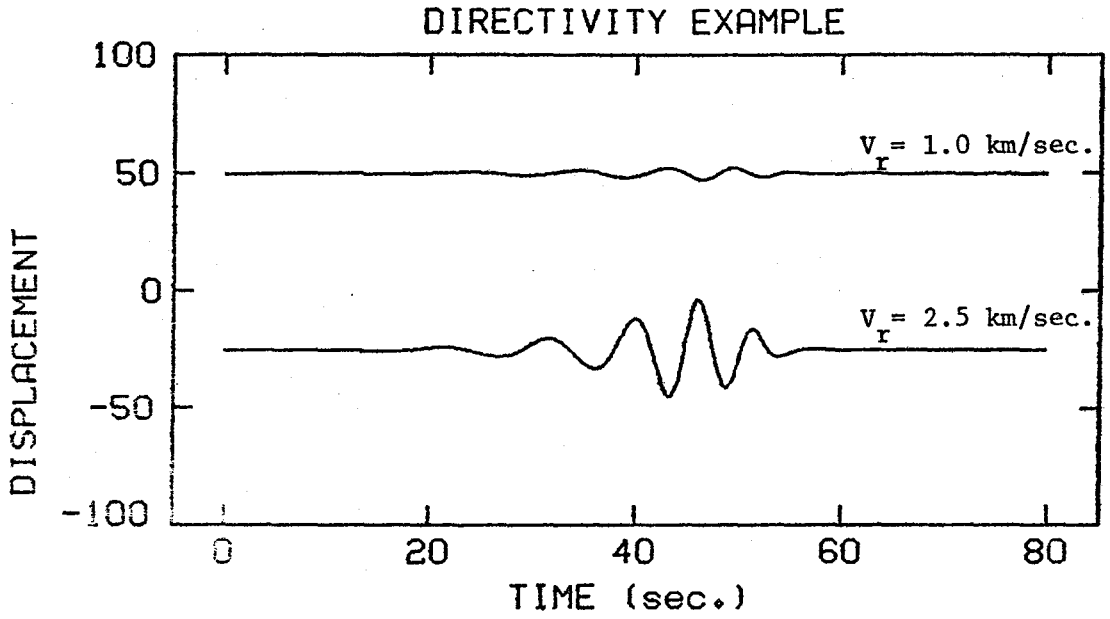


Figure IV.3.8 An example demonstrating the complex interaction between rupture velocity and phase velocity for the fundamental mode. The fault is 11 km. long, and rupture propagates toward the site with the velocities shown.

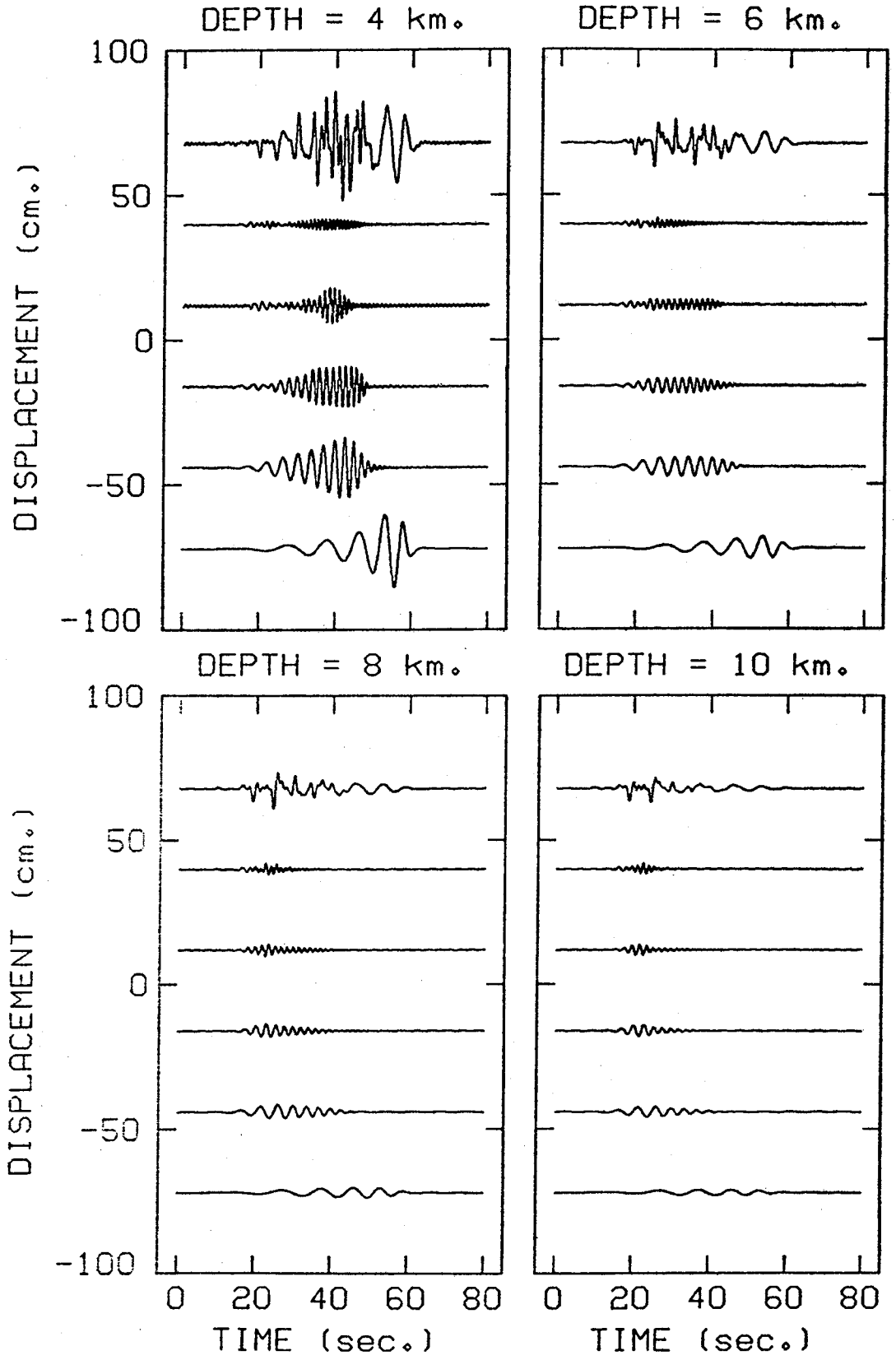


Figure IV.3.9 Synthetic waveforms generated for a point source at depths of 4, 6, 8, and 10 km. Note the extreme variation in amplitude between the event of 4 km. and the others. Also, note the large Love wave oscillations for the shallow (4 km.) event.

An example of waveform variation due to source depth is given in Figure IV.3.9 for depths of 4, 6, 8 and 10 km. The fundamental mode and four overtones are used in the calculations. In this case the source time function is a symmetric triangle of duration 0.75 seconds. There is a pronounced amplitude difference between the source at 4 km. and the others. A difference in the amplitude of the Love wave oscillations (the long period motion at the end of the time history) can also be observed. The source at 4 km. is in the low velocity waveguide (see Figure IV.2.3), thus resulting in high surface wave amplitudes. As the source is buried below the low velocity layer the relative amplitude of the surface waves to body waves is reduced.

## IV.4 BRAWLEY EARTHQUAKE OF 1976

The 1976 Brawley event occurred on November 4 and had a local Richter magnitude of 4.9. This was the largest event of a swarm that occurred in early November. The event triggered two displacement meters, the first at Imperial Valley College (IVC) and the second in El Centro (ELC). This event has been studied by Heaton and Helmberger (1978) using the Cagniard-deHoop technique, and by Swanger and Boore (1978) employing the modal superposition routines of Harkrider (1964). Both methods met with reasonable success in modeling the transverse motion. In this section the tangential motion at both stations is modeled and the seismic moment and far field source time function is estimated. The specific attenuation factor Q, is set to 200 throughout this study.

### IV.4.1 MODELING GROUND DISPLACEMENTS

Heaton and Helmberger (1978) presented a focal mechanism solution

determined from the Caltech-USGS network in southern California. Their findings indicate the fault dislocation was predominantly strike-slip on a near vertical plane, ($\delta = 90^{o}$, $\lambda = 0^{o}$). Station IVC lies almost exactly on a P-SV radiation pattern node, thus the motion recorded was predominantly transverse. Station ELC lies just $13^{o}$ off the P-SV node and therefore it also recorded a major portion of the SH motion, (Heaton and Helmberger, 1978). Figure IV.2.2 showed the earthquake epicenter and station locations for this earthquake. Station IVC is 33 km. from the epicenter, and station ELC is 36 km. away. From the results of Heaton and Helmberger (1978) the source is put at a depth of 7 kilometers on a vertical strike-slip fault. The earth structure is the one presented in section IV.2.

Figure IV.4.1 presents the step function response at each station of the fundamental mode and four overtones. The observed transverse displacement is shown at the top of each figure. Note the similarity in the observed waveforms, and in the synthetics for both stations. This is expected due to the proximity of the stations to one another and the finiteness of the source with respect to the source-site distances. The arrival time of the direct ray is shown on each figure thus allowing an accurate alignment of the synthetics with the observed record. This procedure is used throughout this study.

Figure IV.4.2 shows the result of applying a far field source function that is a symmetric triangle of 1.50 seconds duration. The observed displacements are given at the top of each figure. The synthetics quite clearly reproduce the overall character of the observed waveforms at both sites. Although some of the later peaks in the

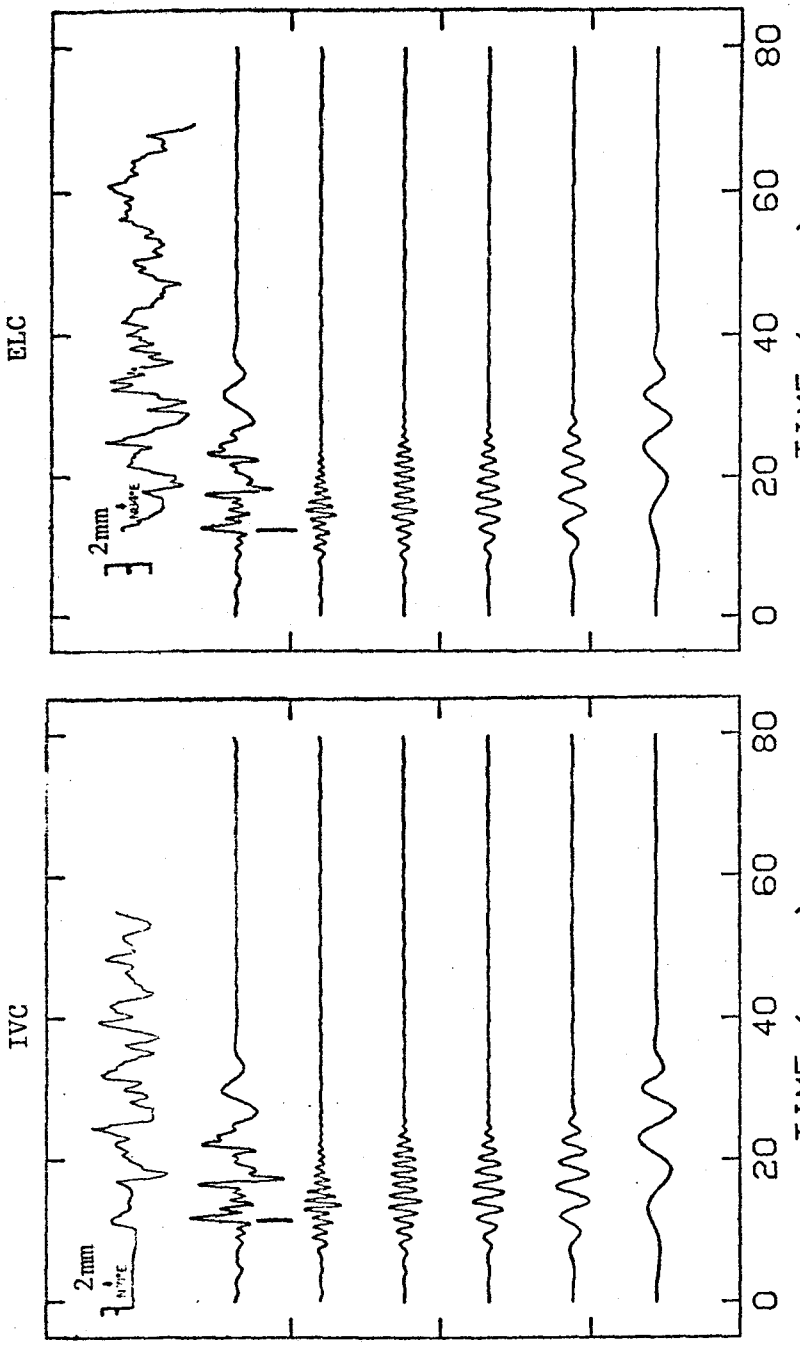


Figure IV.4.1 Displacement motion at stations (a.) IVC and (b.) ELC due to a point source with a step dislocation located at a depth of 7 km. The arrival time of the direct ray is noted by a vertical bar below the synthetic time history.

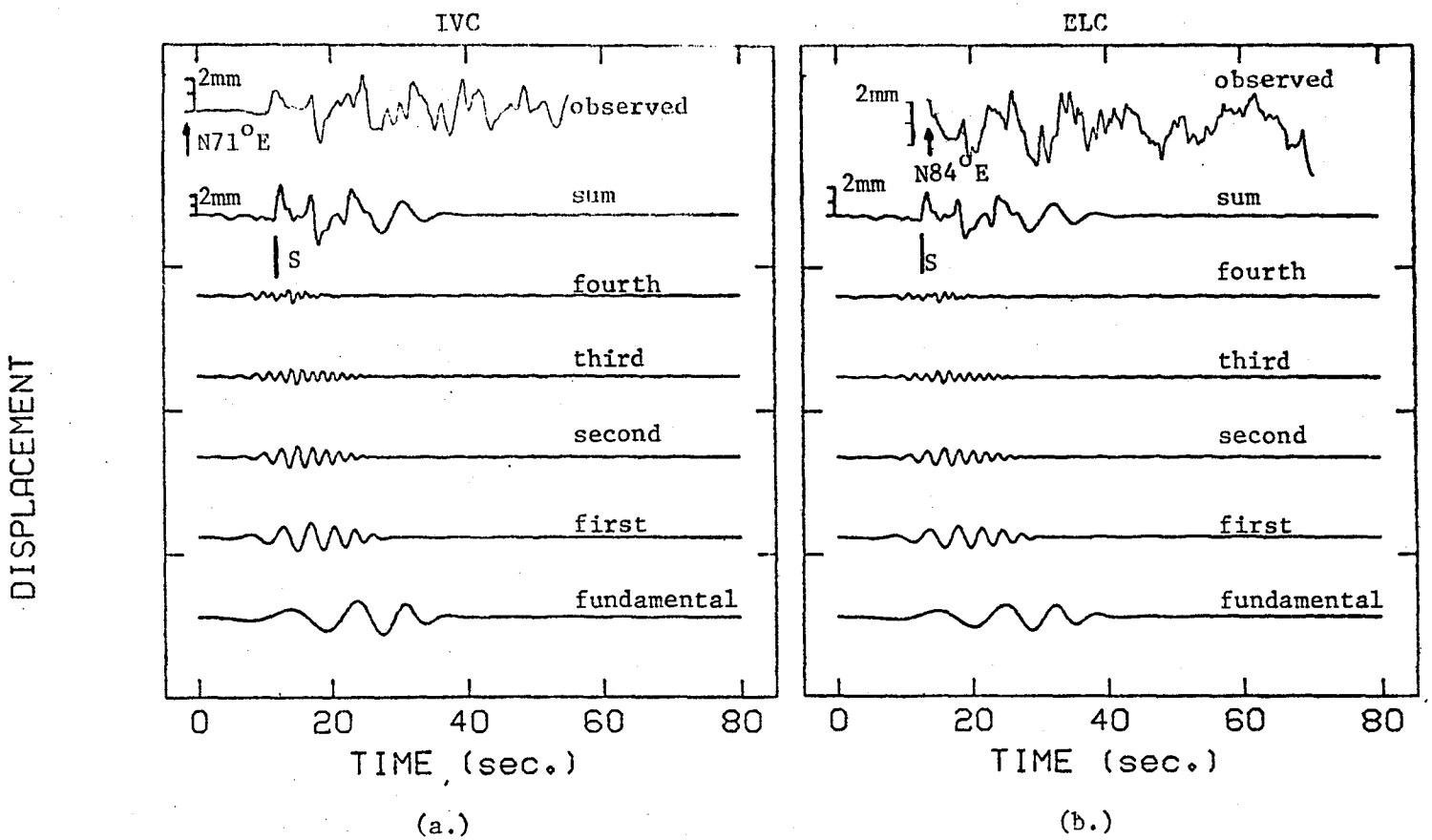


Figure IV.4.2 Comparison of the step function responses in Figure VII.4.1 convolved with a symmetric 1.5 second duration triangle, and the observed data, at stations (a.) IVC and (b.) ELC. The arrival time of the direct ray is noted by a vertical bar below the synthetic time history

synthetics have early arrival times which may be due in part to the earth structure used in these calculations, the waveform match is very good. Heaton and Helmberger (1978) in modeling the same event, have a first layer of approximately 1.0 km. thickness with a shear wave velocity of 0.88 km./sec. This is about 15% below the shear wave velocity in the present model. The seismic moment for the synthetics in Figure IV.4.2 was $4.65 \times 10^{23}$ dyne-cm which compares well with the value of $3.2 \times 10^{23}$ dyne-cm determined by Heaton and Helmberger (1978). Note that four overtones were required to reasonably reproduce the observed motion.

This exercise demonstrated the overall ability of the normal mode method to model strong motion displacements. It also served to illustrate the importance of the earth structure. For the frequencies modeled in the displacement waveforms, only a point source was required, thus the earth structure almost entirely determined the motion in this frequency band. The implications of this for modeling future strong ground motion in seismic hazard analysis are important and highlight the inadequacy of empirical attenuation models when these do not take into account the earth structure. The seismic moment estimate for this event was $4.65 \times 10^{23}$ dyne-cm, and the far field source function is estimated to be a symmetric triangle of 1.5 second duration.

## IV.5 BORREGO MOUNTAIN EARTHQUAKE

The Borrego Mountain earthquake of April 4, 1968 had a local Richter magnitude of 6.4. The event occurred on the Covote Creek fault with dislocation on the fault primarily right lateral. The displacement and

acceleration motion recorded in El Centro are modeled in this study. The results of Heaton and Helmberger (1977) and Swanger and Boore (1978) are used as a guide in the selection of source parameters. The intent in this study is not to present a complete seismological study of this event, but to demonstrate the general capability of the normal mode method to reproduce the observed ground shaking intensity at the recording site. The displacement recording is considered first, after which the acceleration record and the Fourier amplitude spectrum of acceleration are studied.

Figure IV.5.1 shows the epicenter and aftershock zone of the Borrego Mountain event and the El Centro recording station. As shown in the figure, the recording station has an azimuth of, $8^{o}$, and therefore lies very close to a maxima of the SH radiation pattern. The motion at El Centro was therefore predominantly transverse, as shown in Figure IV.5.2 where the observed radial, transverse, and vertical components of displacement as deconvolved from the Carder displacement meter are presented. The El Centro station is 60 km. from the earthquake epicenter. The specific attenuation factor, Q, is assigned a value of 200 throughout this study.

## IV.5.1 MODELING GROUND DISPLACEMENTS

The event is modeled first as a point source at a depth of 6 km. with a source dislocation function that varies stepwise. This result is shown in Figure IV.5.3 where the contribution of the first six modes are given with the sum. The step function response is convolved with two different far field source functions. The results of each convolution

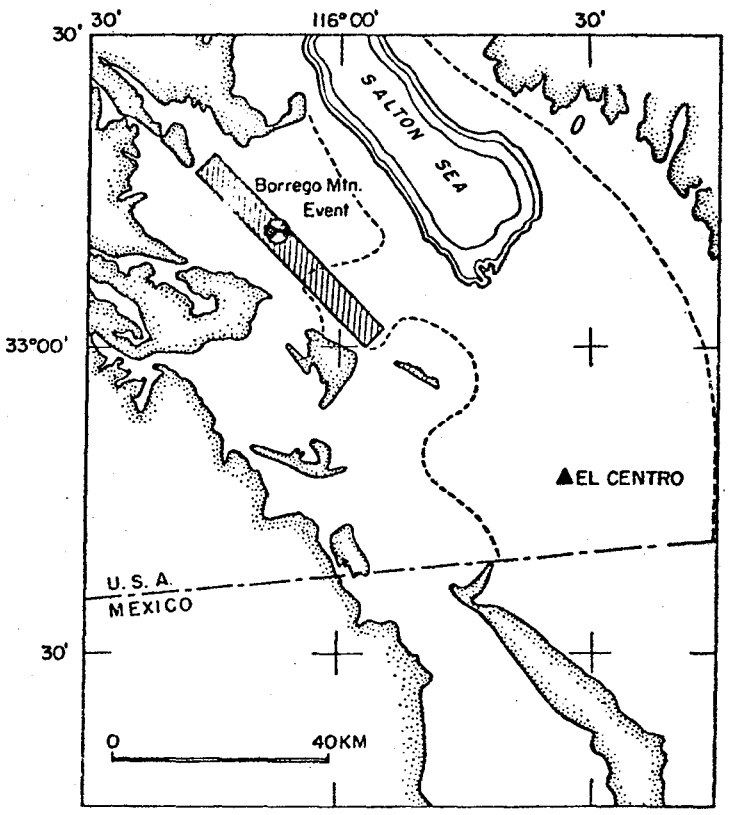


Figure IV.5.1 Map of the Imperial Valley area showing the epicenter of the 1968 Borrego Mountain earthquake and location of the El Centro recording site. The hatched rectangular area denotes where most of the aftershocks occurred, (Map modified from Swanger and Boore, 1978).

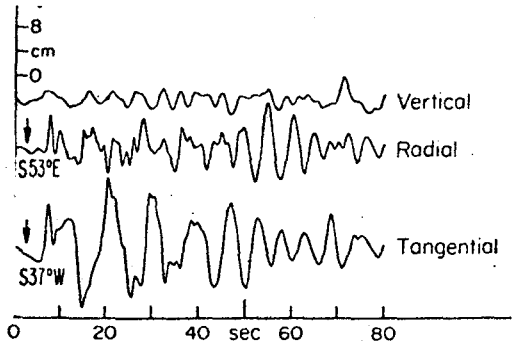


Figure IV.5.2 Observed ground motion displacements at the El Centro Station rotated into vertical, radial and tangential components.

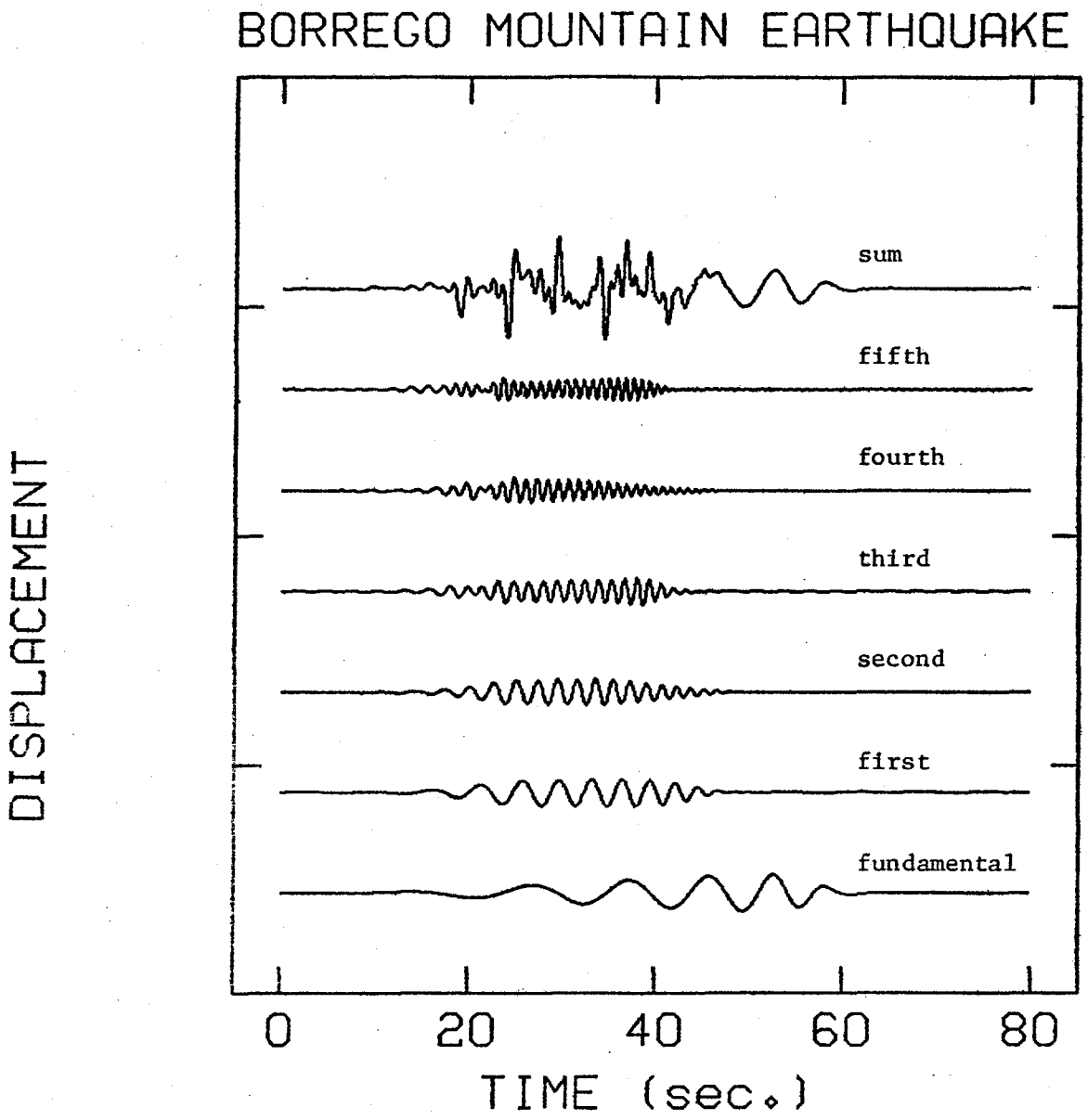


Figure IV.5.3 Transverse step function response due to a point source at 6 km. depth. The source is a vertical plane, with strike slip dislocation.

are given in Figure IV.5.4, with the observed displacement record. The seismic moment estimate and the arrival time of the direct ray are shown on each figure.

The synthetic waveforms reproduce the overall character of nearly 40 seconds of motion. In both examples the relative amplitudes of the peaks are not the same as in the observed record. Swanger and Boore (1978) point out the effect of the depth of focus on the relative amplitudes and suggest a focus depth of 8-9 km. for a point source would give better results.

The source is modeled next as a propagating line with two segments. In the first example the line source is at 6 km. depth and the rupture propagates with a velocity of 2.4 km./sec. for a step function disclocation in both segments. The segment lengths are 22 and 11 km. with the longer segment rupturing toward the recording site. Six modes are included in the solution for each segment and are shown in Figure IV.5.5 with the sum and the observed record. The first 6 waveforms are the contribution of the segment rupturing away from the site, the next 6 are for the segment rupturing toward El Centro. Note the contrast in the contributions to the total motion of the two segments. This is due to the directivity effect demonstrated earlier, and to the fact that the segment rupturing toward the site contributes 2/3 of the total seismic moment for an assumed distribution of the moment based on source length. Note that the later oscillations have been lost. Figure IV.5.6 presents the result of convolving the stepfunction response with a symmetric triangle of 3 second duration as the far field source time function. The match is improved over that of the stepfunction.

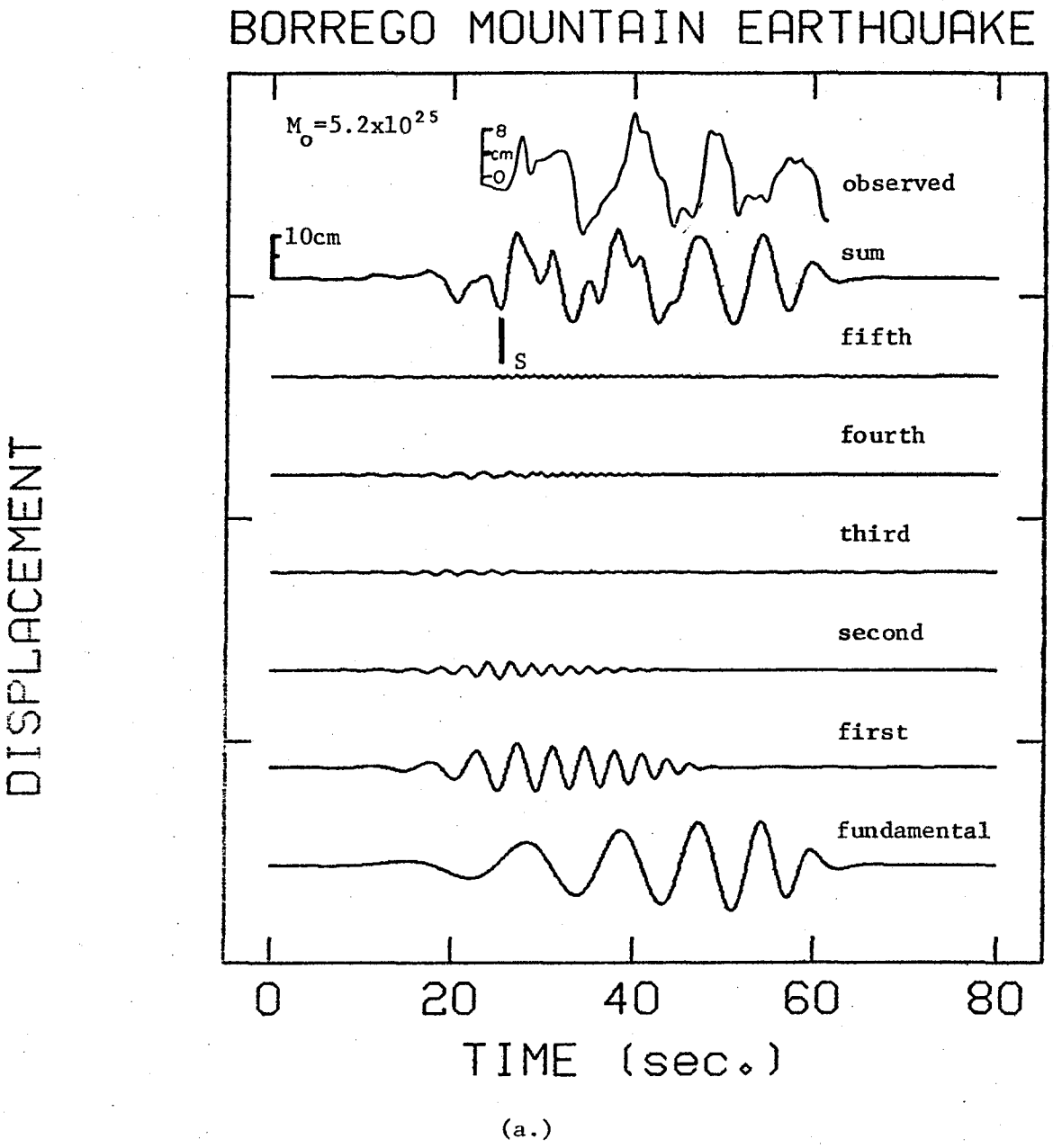


(a.)

Figure IV.5.4(a.) Comparison of the observed transverse component and the synthetic for the step function response in Figure VII.5.3 for a far field source function that is a symmetric triangle of 3 second duration. The moment estimate is in dyne-cms. The arrival time of the direct ray is shown.

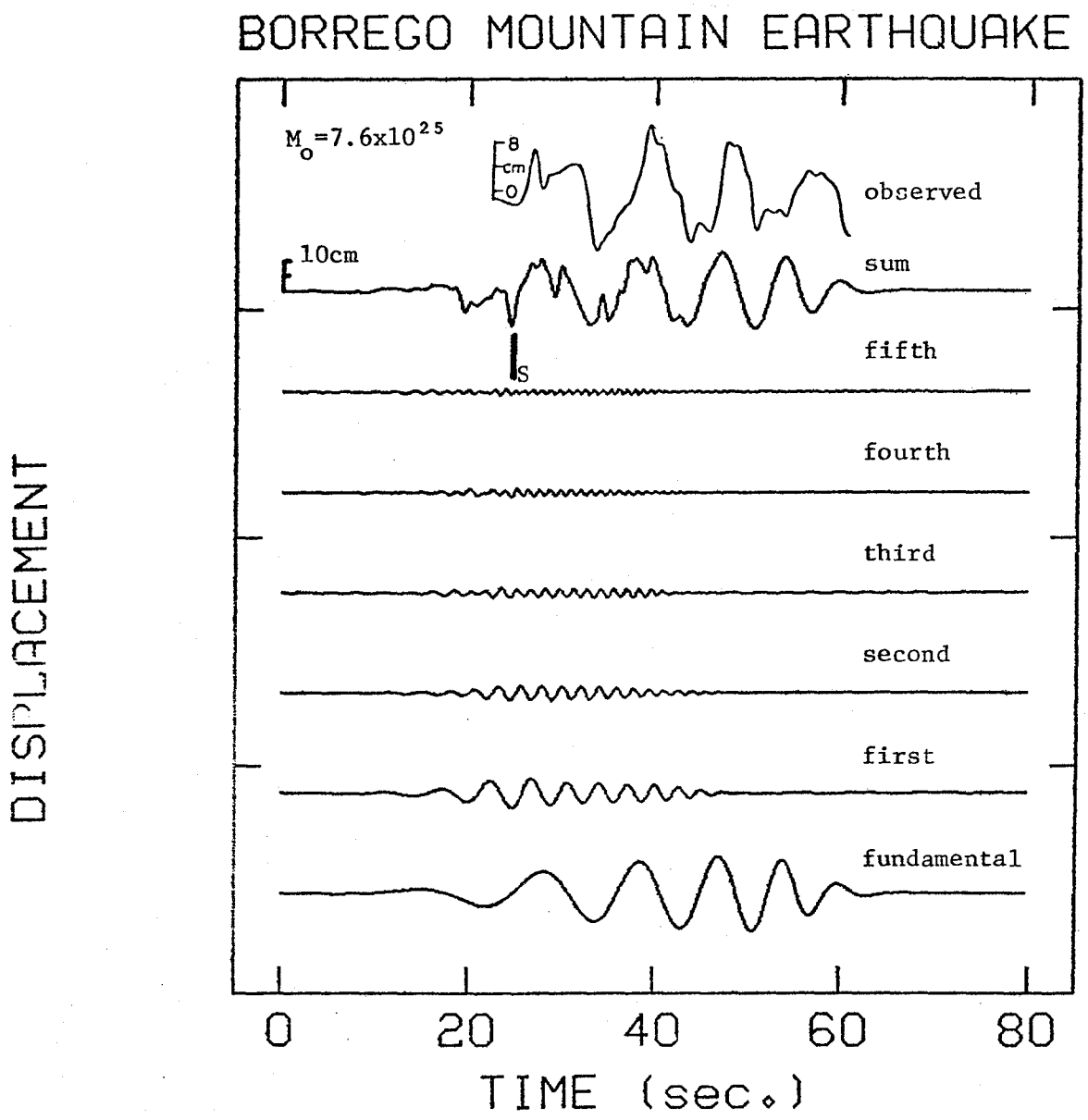


(b.)

Figure IV.5.4(b.) Comparison of the observed transverse component and the synthetic for the step function response in Figure VII.5.3 for a far field source function that is an inverted triangle of 4 second duration. The moment is in units of dyne-cms. The arrival time of the direct ray is shown.

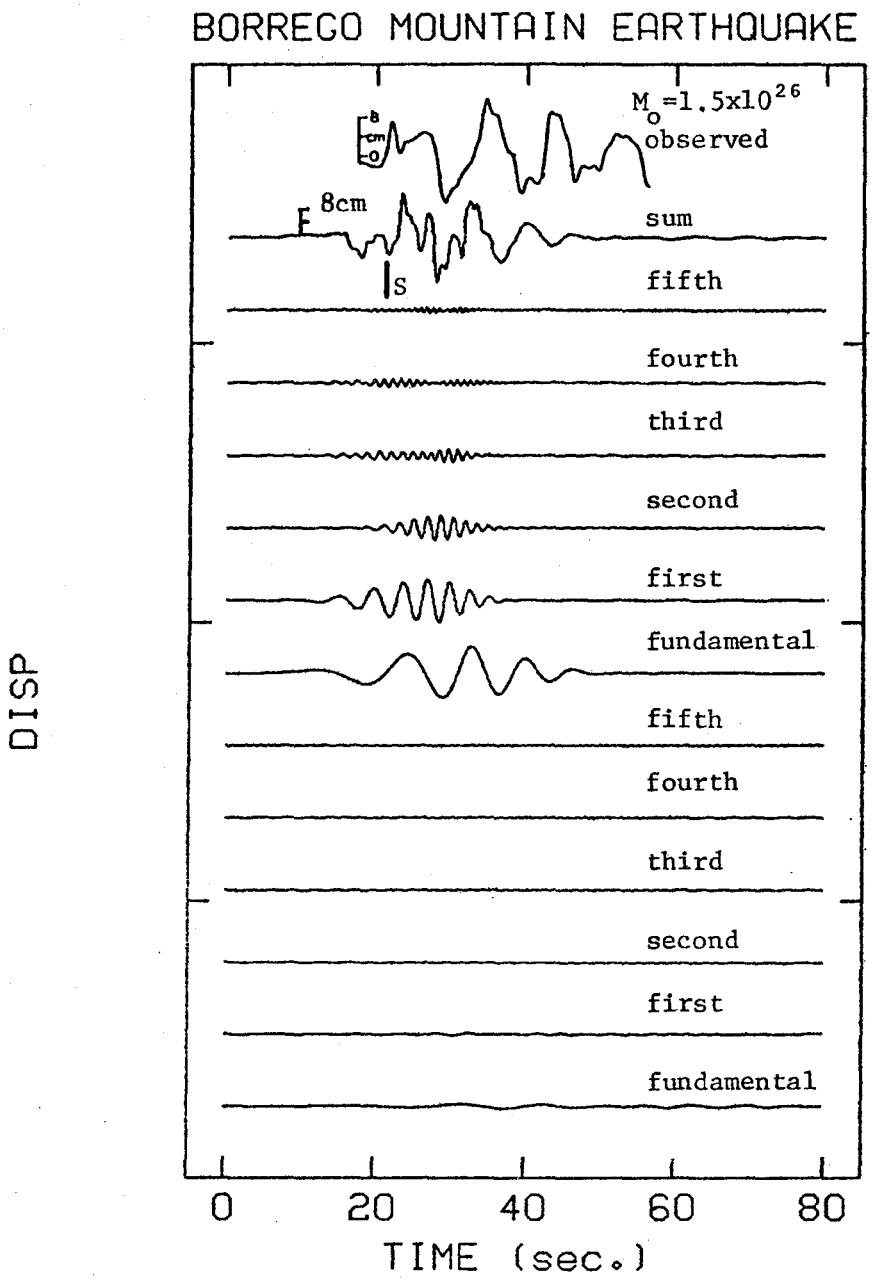


Figure IV.5.5 A comparison of the synthetic step function response for a fault 33 km. long with bilateral rupture and the observed displacement. The fault was modelled with 2 segments 22 and 11 km. in length. Rupture in the longer segment propagated at a velocity of 2.4 km./sec. towards El Centro. The rupture velocity in the shorter segment was the same. The arrival time of the direct ray is shown.

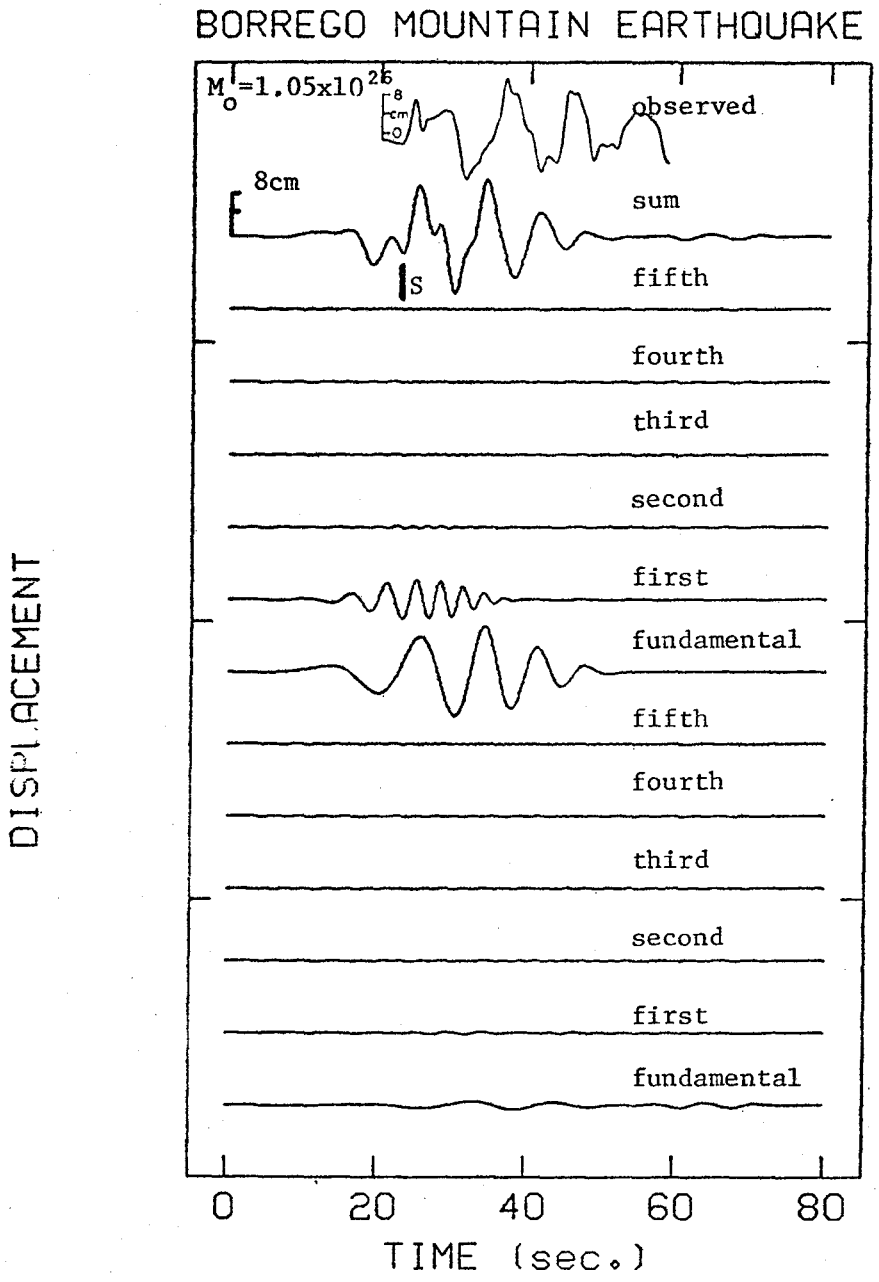


Figure IV.5.6 A comparison of the step function response in Figure VII.5.5 convolved with a symmetric triangle far field source function that has a duration of 3 seconds. Note the later Love wave oscillations are lost. The arrival time of the direct ray is shown.

Figure IV.5.7 presents the stepfunction response for a much shorter fault that ruptures bilaterally 5 km. toward El Centro and 4 km. away. Figure IV.5.8 shows the stepfunction response convolved with various far field source time functions. On each figure the observed record is given along with the seismic moment estimate. Both cases reproduce the general character of the observed record. Note that in the examples presented, the motion is modeled adequately by three or four modes.

The results of modeling the strong motion displacements show no clear constraints on the source dimensions. A point source seems to model the El Centro recording as well as an extended source. The 9 km. length fault and the point source appear to match the observed motion equally well. On the basis of these preliminary observations the suggestion by Burdick and Mellman (1976) that the Borrego Mountain earthquake was due to a massive rupture on a small rupture plane cannot be disputed. Their estimate of a circular rupture area, had an 8 km. radius and a stress drop of 96 bars.

The average seismic moment estimated from the results in Figures IV.5.4 and IV.5.8 is $9.3 \times 10^{25}$ dyne-cm. As pointed out by Swanger and Boore (1978) the Carder Displacement readings are less than those obtained from the doubly integrated accelerogram. Therefore the seismic moment based on comparisons with these displacements will be underestimated by approximately 20%, (Swanger and Boore, 1978). On this basis the seismic moment is increased to $1.12 \times 10^{26}$ dyne-cm. This compares well with the results of Burdick and Mellman (1976) who estimated the moment to be $1.10 \times 10^{26}$ dyne-cm., and Swanger and Boore (1978) who found an average moment of $1.2 \times 10^{26}$ dyne-cm.

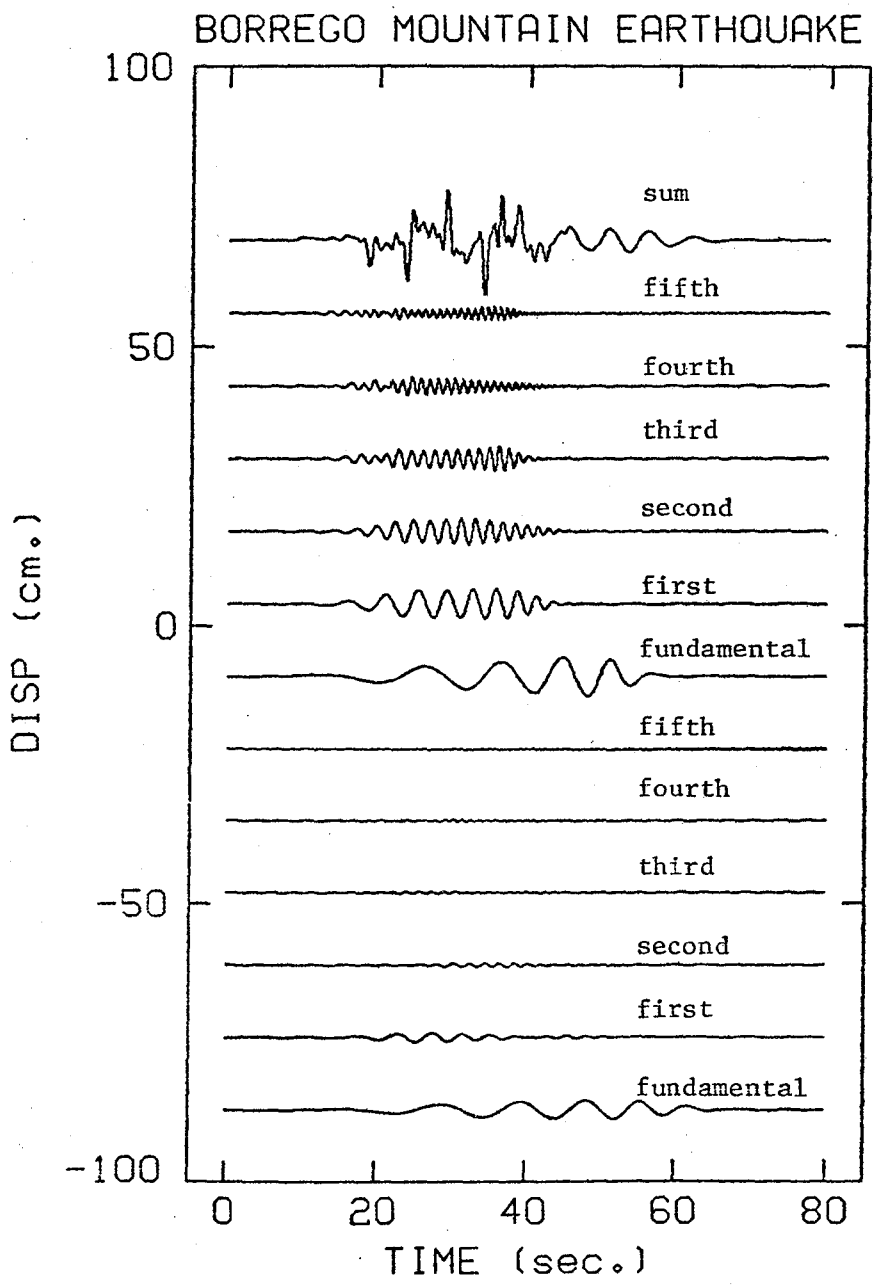


Figure IV.5.7 Step function response for a bilateral fault rupture, modeled with 2 segments, 4 and 5 km. in length. The contributions of the 4 km. segment which ruptures away from El Centro are the first six synthetics. The next 6 synthetics are the contributions of the 5 km. segment rupturing towards the site. The rupture velocity in both segments was 2.5 km./sec.

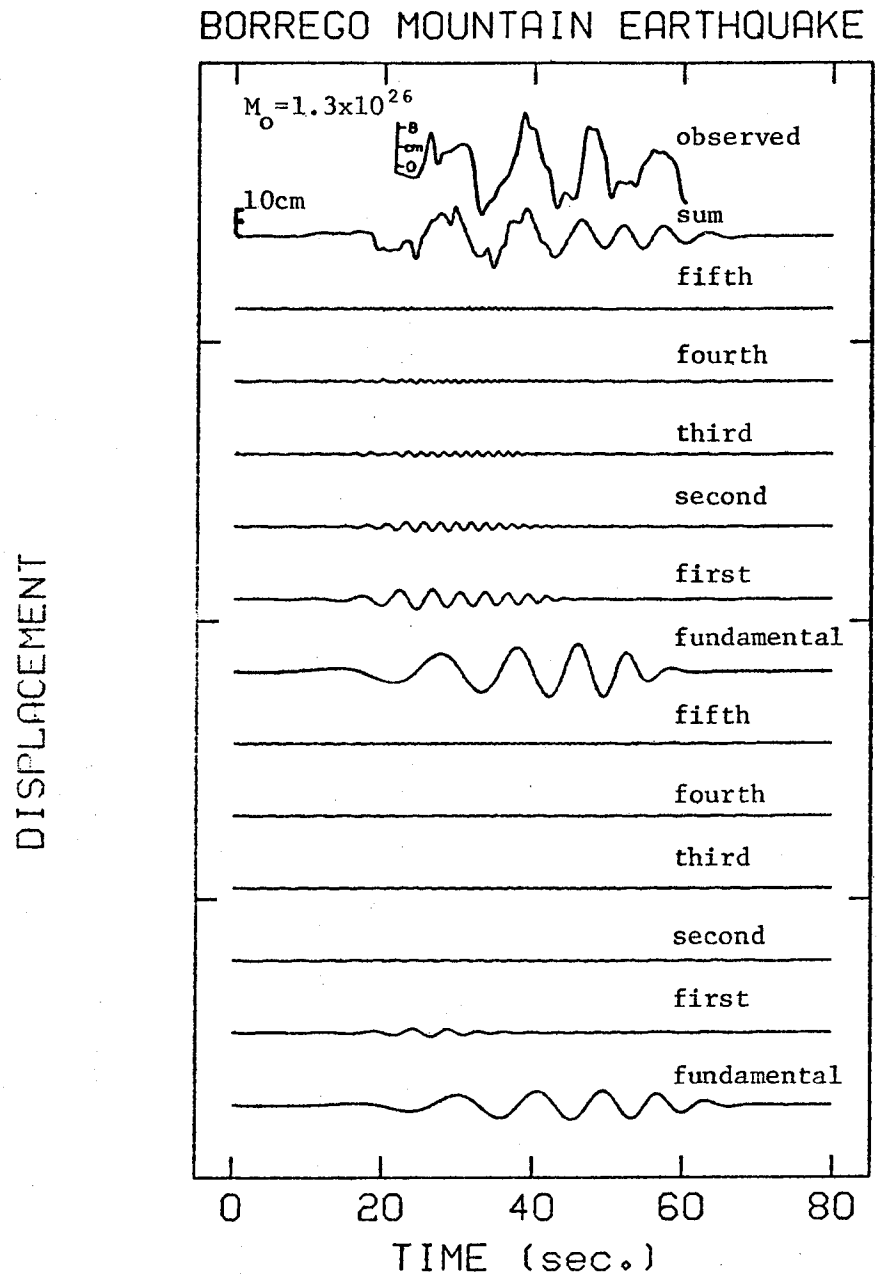


Figure IV.5.8(a.) Step function response of Figure VII.5.7 convolved with a reversed ramp far field source function of 4 second duration, compared with the observed displacements.

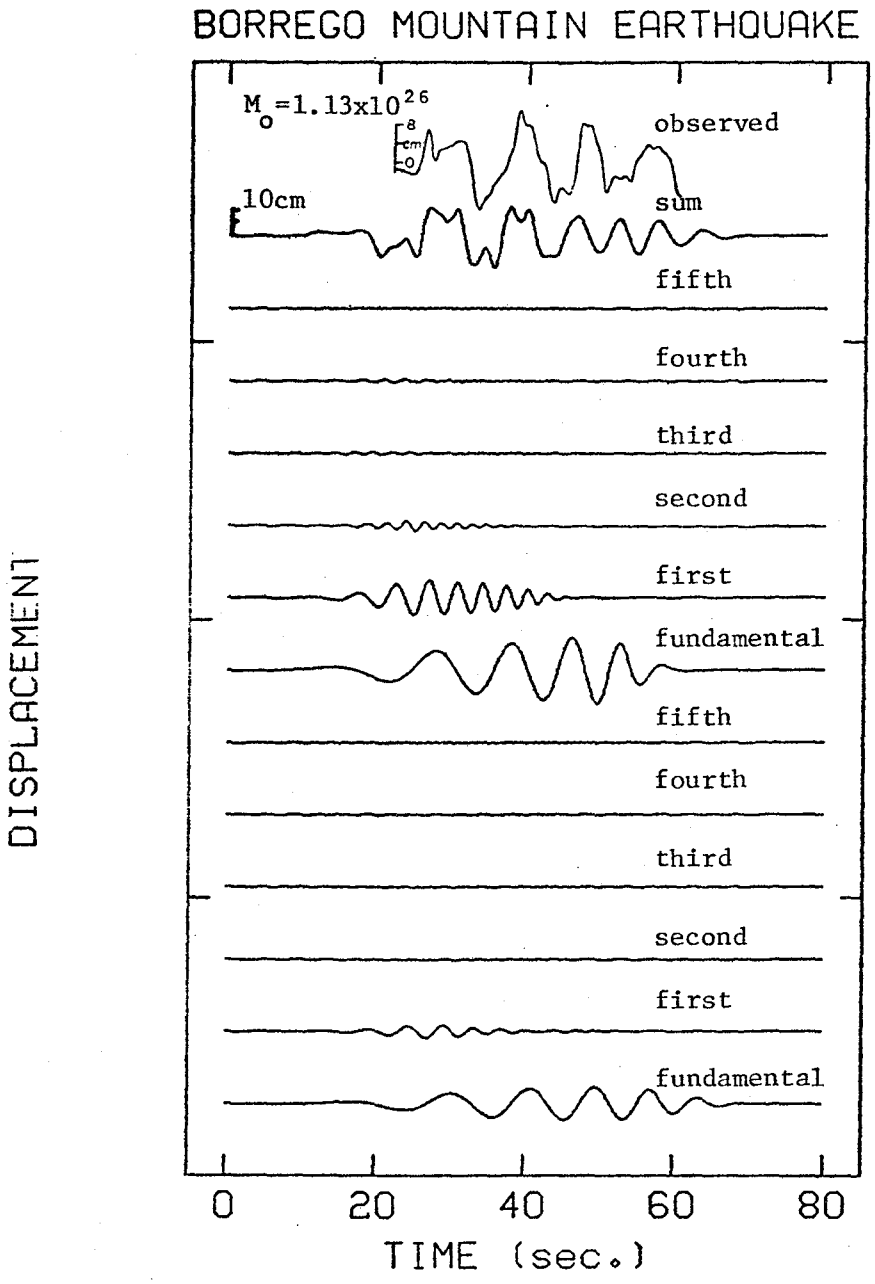


Figure IV.5.8(b.) A comparison of the step function response of Figure VII.5.7 convolved with a symmetric triangle far field source function of 3 second duration, and the observed transverse component.

## IV.5.2 MODELING STRONG MOTION ACCELERATION

Also recorded during the Borrego Mountain earthquake was an accelerogram obtained at the same recording station. The acceleration recording was processed by the Earthquake Engineering Research Laboratory at Caltech, (Trifunac and Lee, 1973). Synthetic acceleration time histories are generated for various sources and compared to the observed motion. The Fourier amplitude spectra are also compared to determine whether the energy has been accurately distributed over the frequency band being modeled.

In modeling the ground accelerations at El Centro the following approach is taken. Based on this work and that of Burdick and Mellman (1976), Heaton and Helmberger (1977), and Swanger and Boore (1978), the seismic moment is assumed known and equal to $1.0 \times 10^{26}$ dyne-cm. The fault rupture is then modeled to obtain synthetic acceleration time histories. These time histories are compared to the observed data for phase and amplitude correlation.

The first source considered is a point at 6 km. depth with a dislocation rise time of 0.75 seconds. Figure IV.5.9 shows the complete synthetic and the eighteen contributing overtones. Note for this case that all modes contribute about equally to the total motion, with the exception of the fundamental and the first overtone. The observed acceleration record is shown at the top of the figure which has been low pass filtered with a 3.5 hz. cutoff frequency to allow for a better comparison. There is a distinct similarity in the major arrivals of the

synthetic and the observed record. The amplitude of the synthetic acceleration is approximately an order of magnitude greater than the actual record. This is due to the large stress drop associated with the point source. Comparing the Fourier amplitude spectra of the observed and synthetic, it can be seen that the shape of the generated spectrum does not compare well with the observed. This is shown in Figure IV.5.10.

Figures IV.5.11 and IV.5.12 present the synthetic acceleration time histories for an extended source of 5 km. length at a depth of 6 km. In both cases a rise time of 0.75 seconds is used and the rupture propagates unilaterally toward El Centro for the entire fault length. In Figure IV.5.11 the rupture velocity is 1.5 km./sec. and in Figure IV.5.12 it is 2.5 km./sec. The observed record is shown at the top of each figure. A number of observations can be made from these examples. The rupture velocity and phase velocity interaction is evident in the time history amplitudes. The higher rupture velocity produces amplitudes about 3 times those in the lower rupture velocity case. A comparison of the synthetic waveforms with the observed reveals that for a slow rupture velocity, the match with the recorded motion is not very good. The comparison is considerably better in the case of a 2.5 km./sec. rupture velocity. The major wave arrivals of the synthetic align extremely well with those in the observed motion. The relative amplitudes of the major peaks compare favorably to their counterpart in the observed, however the amplitudes of the synthetics are still an order of magnitude greater than the observed motion.

Figure IV.5.13 compares the Fourier amplitude spectra of the

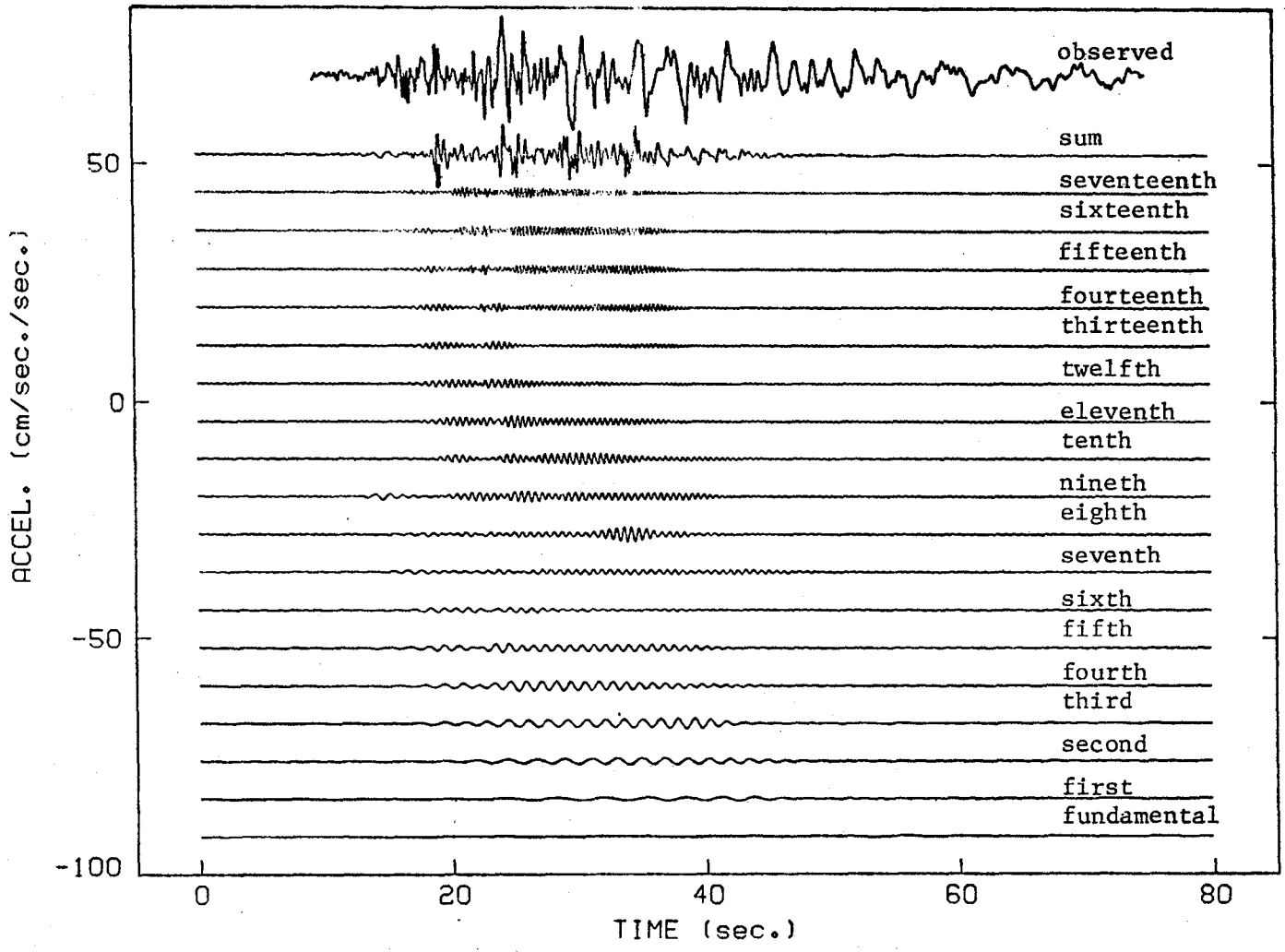


Figure IV.5.9 Acceleration response due to a point source buried at 6km. depth. The dislocation rise time was 0.75 seconds. The fundamental mode and 17 overtones are shown with the sum and the observed acceleration. The vertical scale is arbitrary. The arrival time of the direct ray is shown.

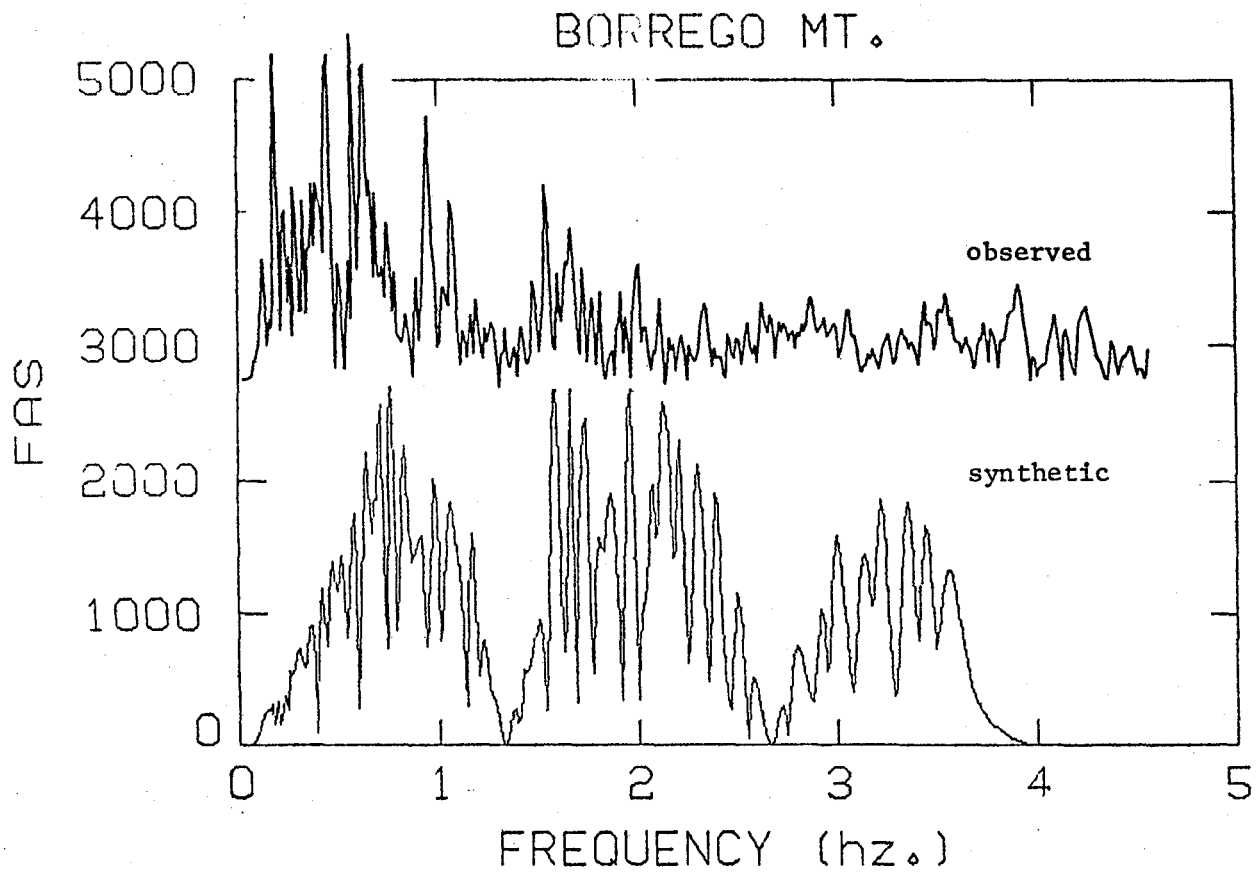


Figure IV.5.10 A comparison of the Fourier amplitude spectra of the observed ground motion and the synthetic motion due to a point source with a 0.75 second rise time. The seismic moment for this event was $1.0 \times 10^{26}$ dyne-cm. The vertical scale is arbitrary.

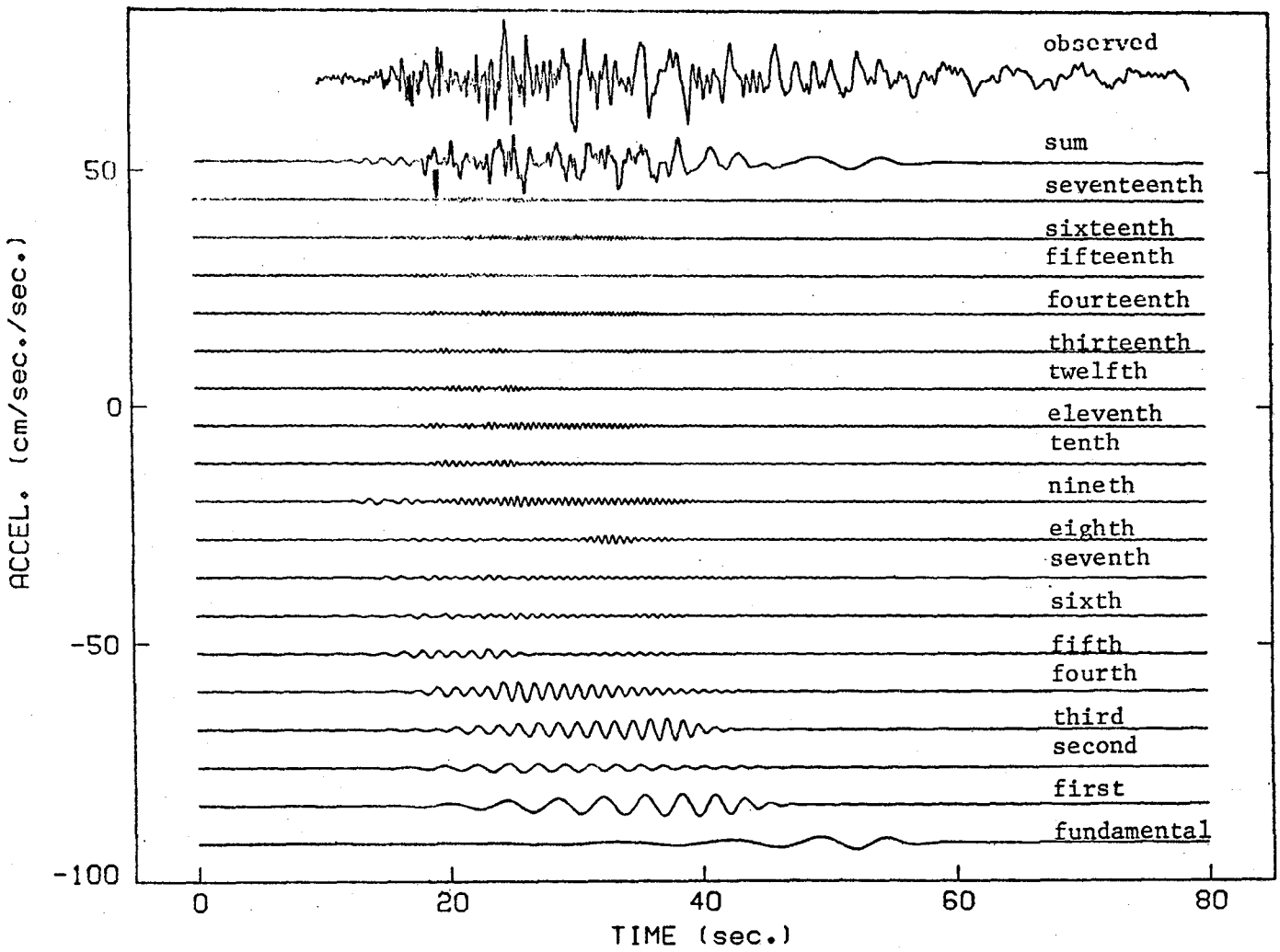


Figure IV.5.11 Comparison of the observed acceleration record and the synthetic for a fault 5 km. in length that ruptures towards El Centro at a velocity of 1.5 km./sec. The rise time was 0.75 seconds. The vertical scale is arbitrary. The arrival time of the direct ray is shown.

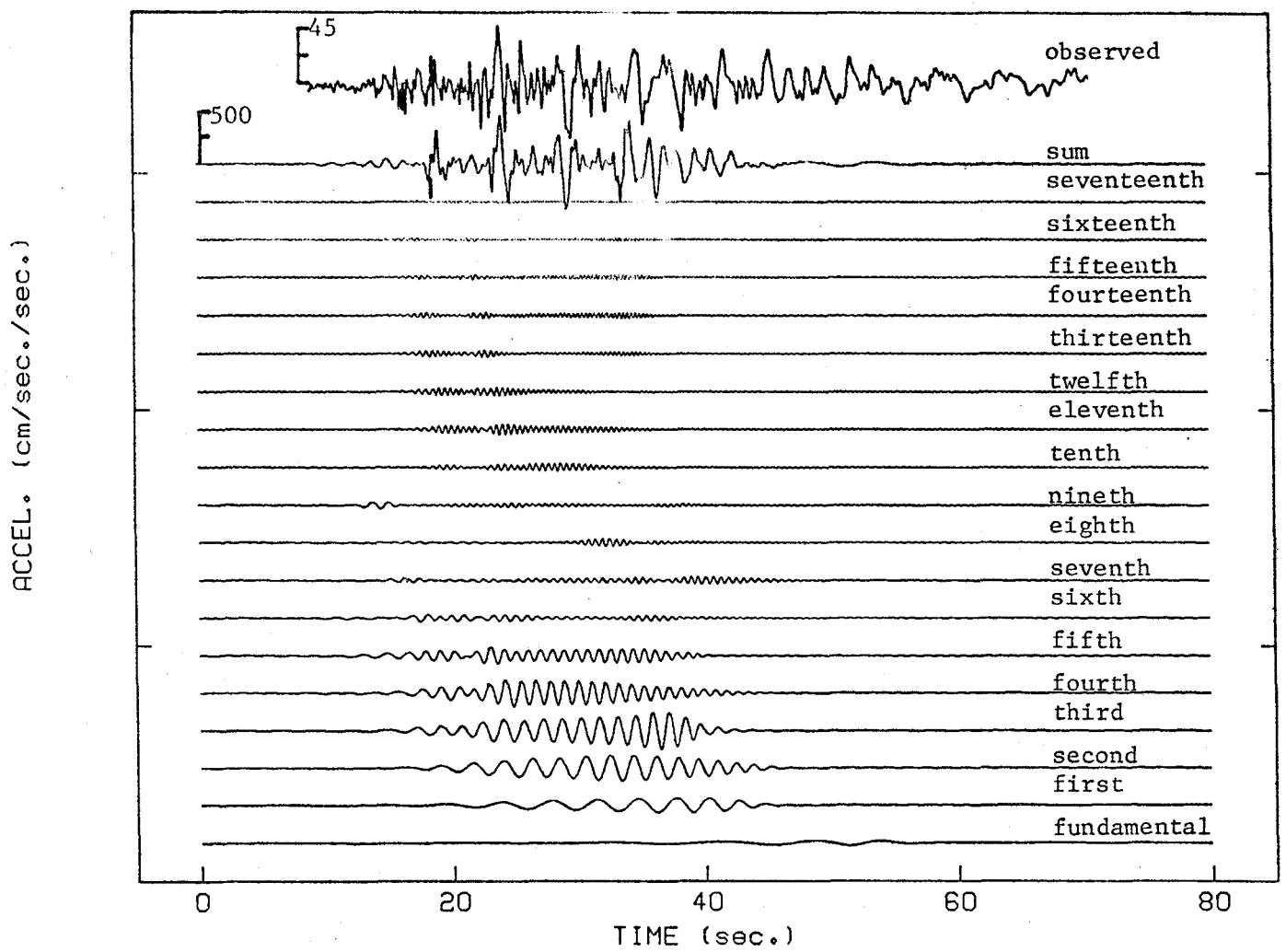


Figure IV.5.12 Comparison of the observed acceleration record and the synthetic for a fault 5 km. in length that ruptures towards El Centro at a velocity of 2.5 km./sec. The rise time was 0.75 seconds. The arrival time of the direct ray is shown.

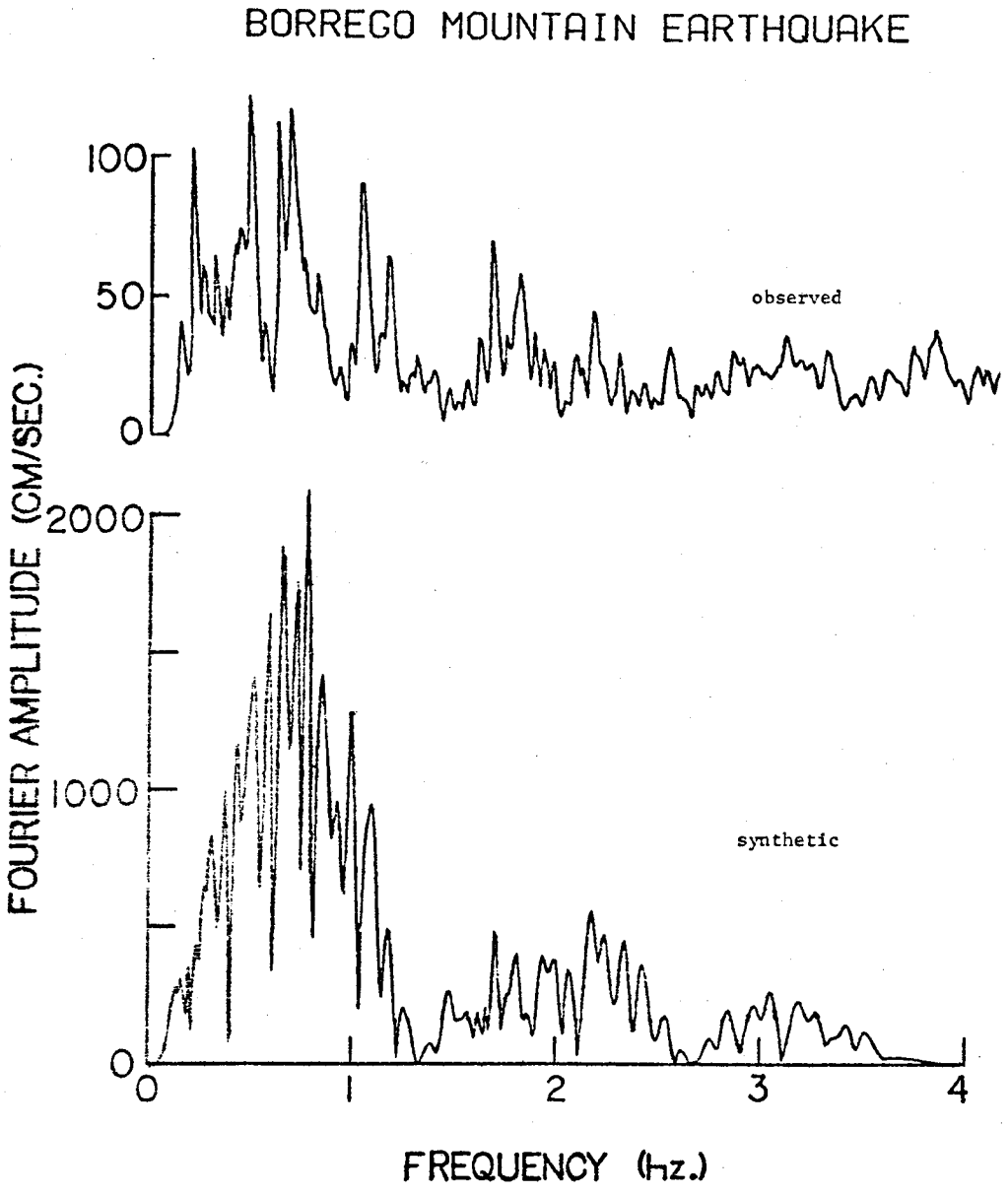


Figure IV.5.13 A comparison of the observed Fourier amplitude spectrum and the synthetic spectrum produced by a fault of 5 km. length that ruptures unilaterally toward El Centro. The rupture velocity is 2.50 km./sec. and the rise time is 0.75 sec.

synthetic in Figure IV.5.12 and the observed record. The spectral shape has been improved considerably over the stepfunction response with the introduction of a propagating source, but the amplitudes are significantly higher than for the observed. This is due to the high stress drop corresponding to the event. If the source is rectangular, and the length is assumed twice the width, (Geller, 1976), the average stress drop would be about 1280 bars. This is an unrealistically high value for the average stress drop, (Kanamori and Anderson, 1975), as the acceleration motion reflects.

The next source investigated consists of a bilateral rupture which ruptures 5 km. toward and 4 km. away from the recording station. The rupture velocity was 2.5 km./sec. with a rise time of 0.75 seconds in both segments. The waveform is shown in Figure IV.5.14 with the observed acceleration. The comparison is again very good. The major wave arrivals are matched well for approximately twenty seconds. Comparing the synthetics in Figure IV.5.12 and IV.5.14, it is noticed that there is very little difference between these results. This indicates the strong directivity effect leading to the domination of the motion by the segment rupturing toward the recording station. Figure IV.5.15 compares the Fourier amplitude spectra of the synthetic and the recorded waveform. The spectral amplitudes are still significantly larger than those for the observed record. The average stress drop associated with this event is 219 bars.

It is apparent from the synthetics generated to this point, that the motion is governed to a considerable degree by the earth structure. This appears to be the case, since for nearly every source modeled there are

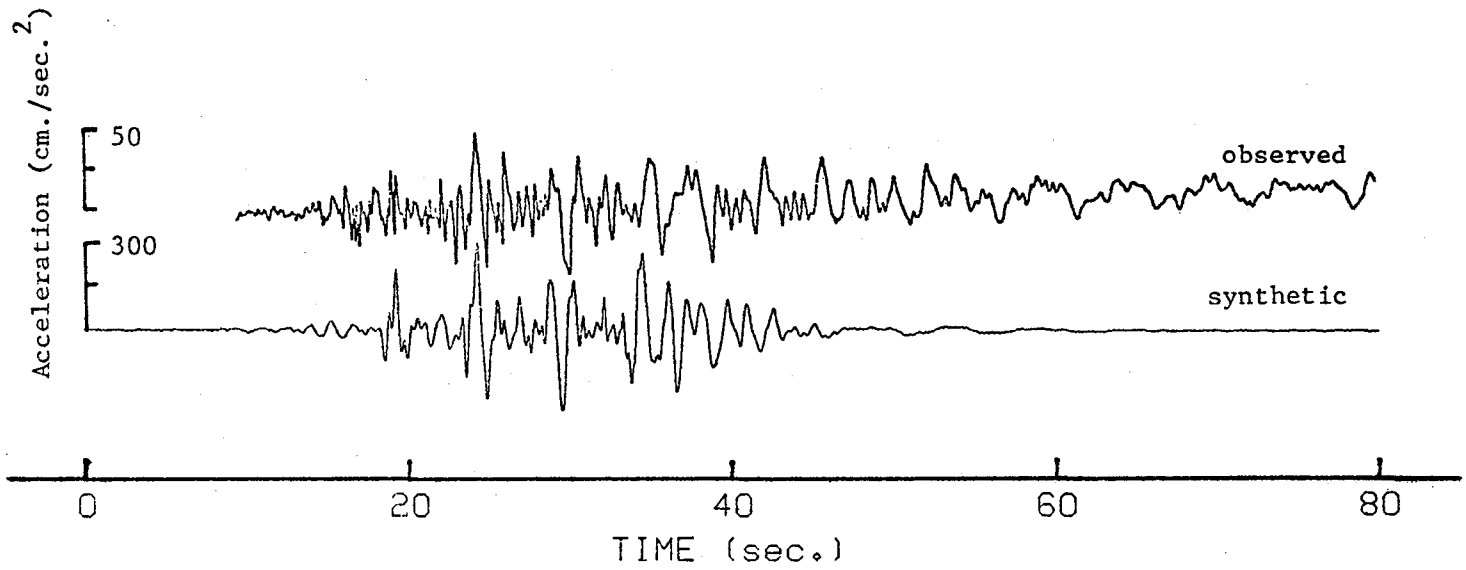


Figure IV.5.14 Synthetic acceleration record shown for a fault 9 km. in length that ruptured bilaterally, 5 km. toward the recording station and 4 km. away. The rupture velocity and rise time are 2.5 km./sec. and 0.75 sec. respectively in both segments.

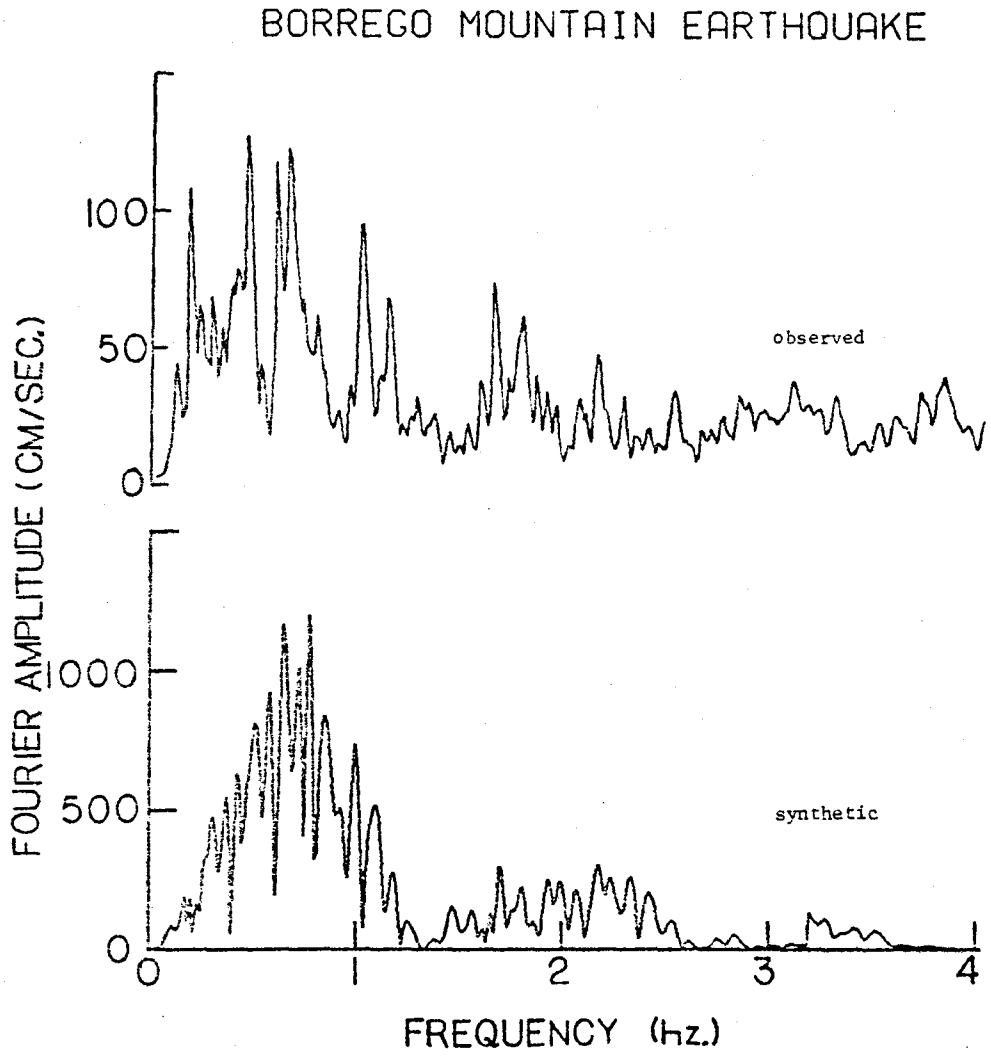


Figure IV.5.15 A comparison of the observed Fourier amplitude spectrum and the synthetic spectrum for a fault with bilateral rupture. Two segments of 4 and 5 km. rupture away and toward the site respectively. The rupture velocity is 2.50 km./sec. and the rise time is 0.75 in both segments.

distinct arrivals of certain phases. This was true for the point source as well as the extended sources. The directivity effect is very evident in the examples for an extended source. The difficulty in obtaining a solution rests in the ability to resolve the source characteristics, namely, the source dimensions, rupture velocity, rise time, and depth. For a single station, located at almost a zero azimuth, this task is particularly difficult. Since the stress drop is proportional to acceleration, the acceleration amplitudes can be reduced by a corresponding decrease in the average stress drop. For a given seismic moment, this is accomplished by increasing the dimensions of the rupture area. The examples to follow take this into account, along with the effect of source depth.

Figure IV.5.16 presents an example of four events with the same source characteristics but buried at depths from 6 to 9 km. The source is 13 km. long and is modeled with two segments. A 7 km. segment ruptures toward El Centro and a 6 km. segment ruptures away. The rupture velocity and rise time are 2.7 km./sec. and 0.75 seconds respectively in both segments. The increase in depth has the effect of reducing the amplitudes of all waves, in particular the later surface wave oscillations. However by increasing the fault dimensions, the waveform amplitudes have been reduced but are still quite a bit higher than those in the observed record.

Figure IV.5.17 presents two synthetics to test the effect of low rupture velocities for the segment rupturing toward El Centro. The rupture velocities are 1.90 and 2.1 km./sec. The first observation to be made is that the slow rupture velocities result in a lengthening of the

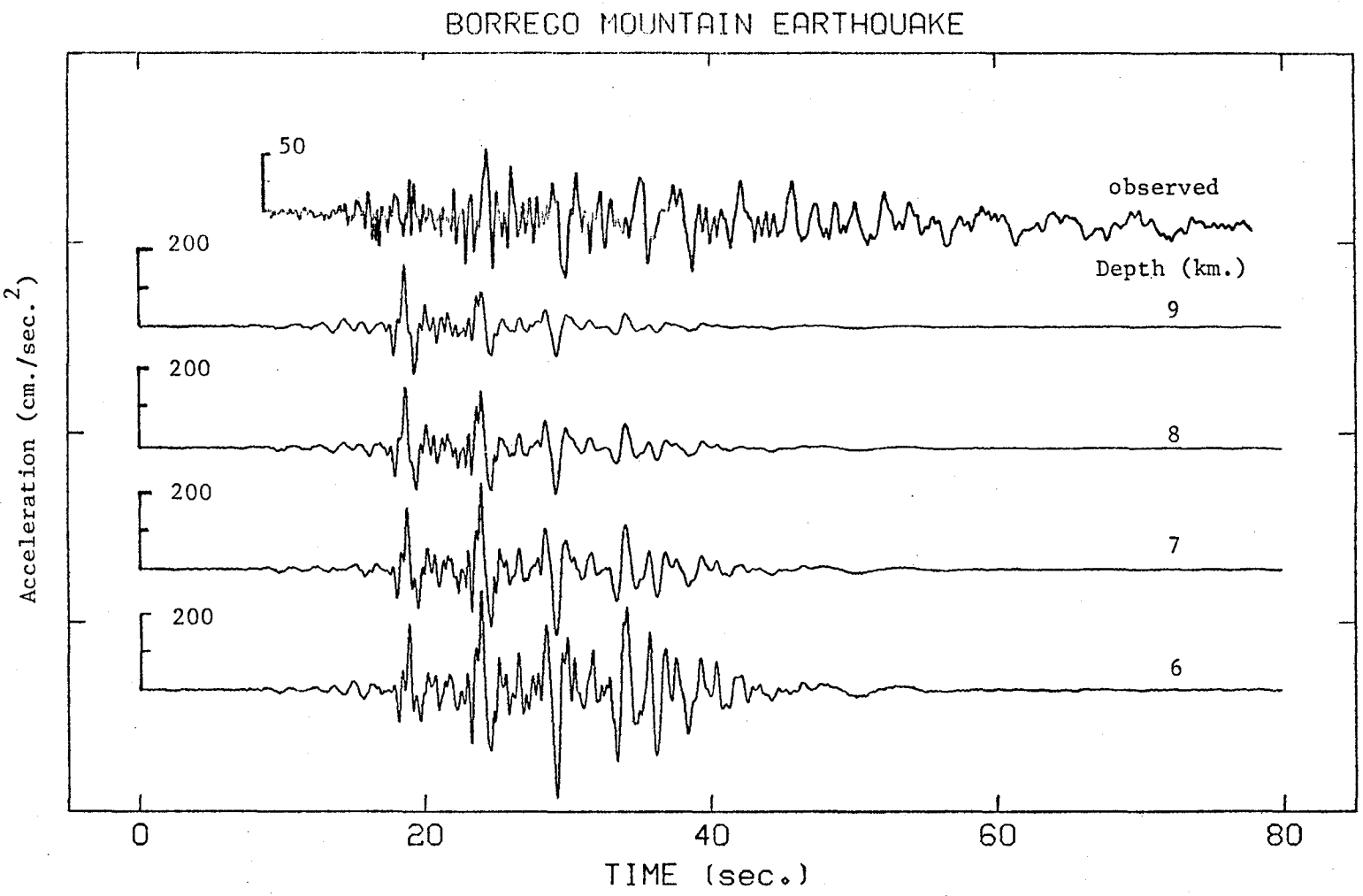


Figure IV.5.16 Examples to demonstrate the effect of source depth. The source is 13 km. long modeled with 2 segments; the 7 km. ruptures toward El Centro and the 6 km. segment ruptures away. The rupture velocity and rise time are 2.7 km./sec. and 0.75 sec. respectively in both segments.

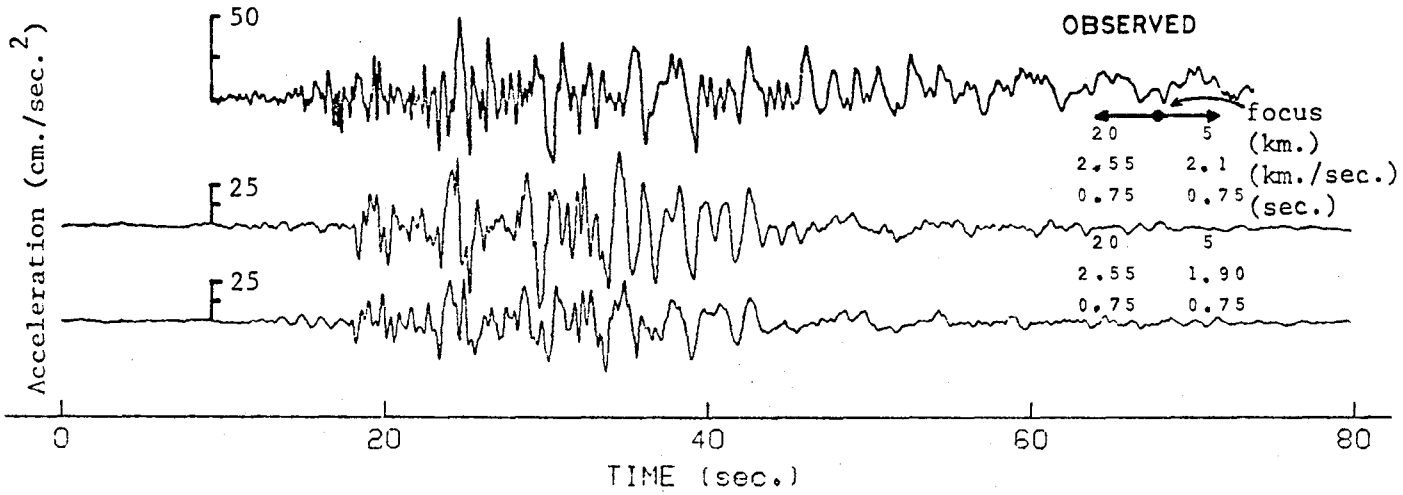


Figure IV.5.17 An example demonstrating the effect of slow rupture velocities for the segment rupturing toward El Centro. The source is at 6 km. depth.

major peaks, and a corresponding decrease in the wave amplitudes. Basically the slow rupture results in a loss in the character of the synthetic waveform. This suggests that for the segment rupturing toward El Centro, a rupture velocity greater than 2.1 km./sec. is indicated. This lower bound is similar to the value suggested by Swanger and Boore (1978) in their study of ground displacements.

The next group of synthetics considered are for faults of increasingly longer rupture lenghts. These examples are set up based on the previous results that seem to indicate that a single line source be placed at a depth of 6 - 7 km. and that a relatively short segement of about 5 km. length rupturing toward El Centro dominates the observed motion.

The results shown in Figure IV.5.18 attempt to obtain a reasonable amplitude match with the observed record. As the segment that ruptures away from El Centro is increased in length the amplitudes improve. Due to the destructive interference of the directivity effect, the changes in rupture velocity or length of the segment rupturing away does not effect the motion as recorded at El Centro. The best amplitude-phase match is for the case of a 55 km. fault where a 50 km. segment ruptures from the focus to the north.

A comparison of the Fourier amplitude spectrum of the observed record and the synthetic indicates that the shape and spectral values match reasonably well with the observed. This is shown in Figure IV.5.19.

The examples presented in this section demonstrate the strong

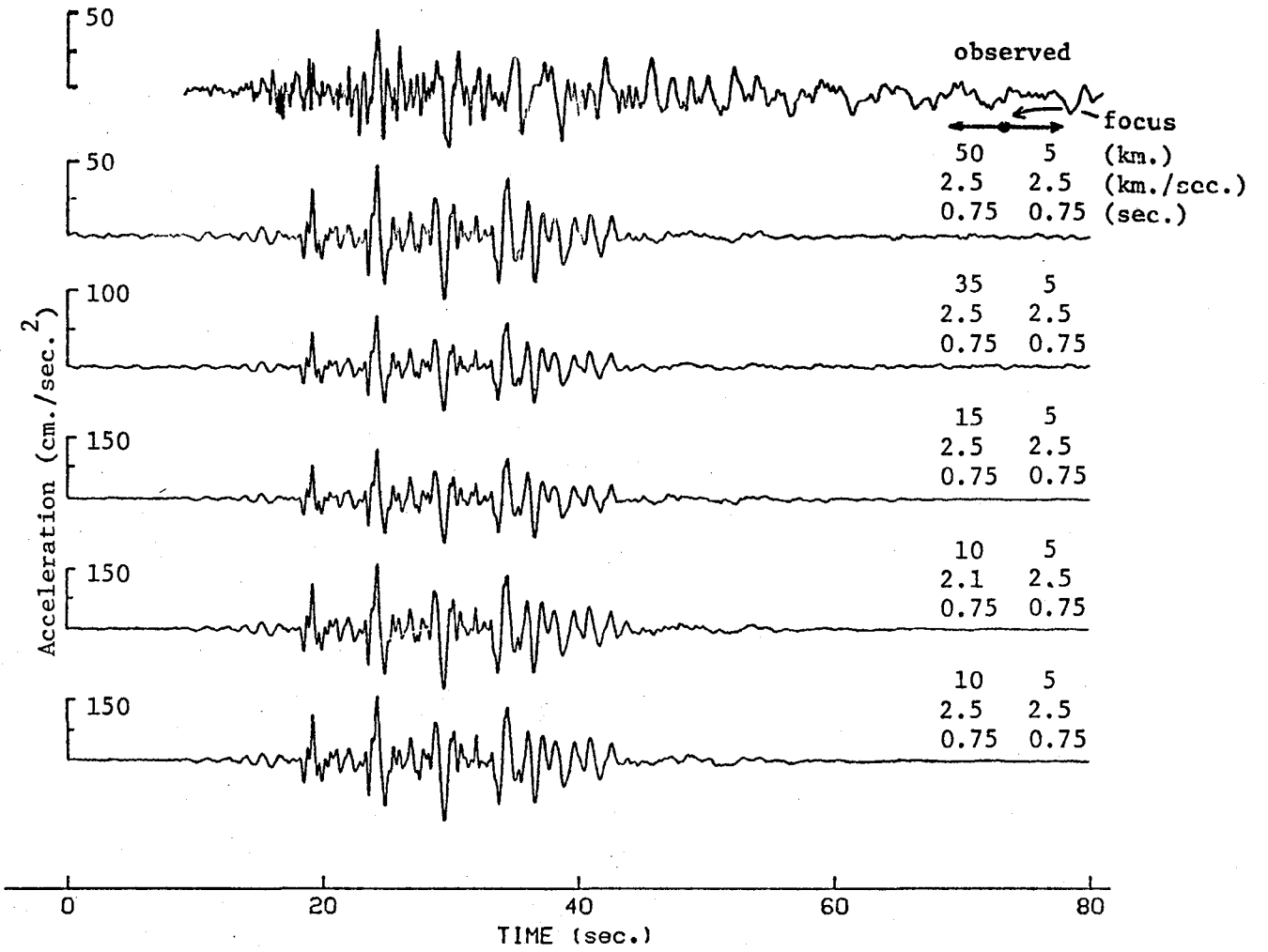


Figure IV.5.18 Synthetic acceleration records for faults of increasing rupture length. The effect of the segment rupturing away from El Centro is minimal. The fault parameters are given with synthetic.

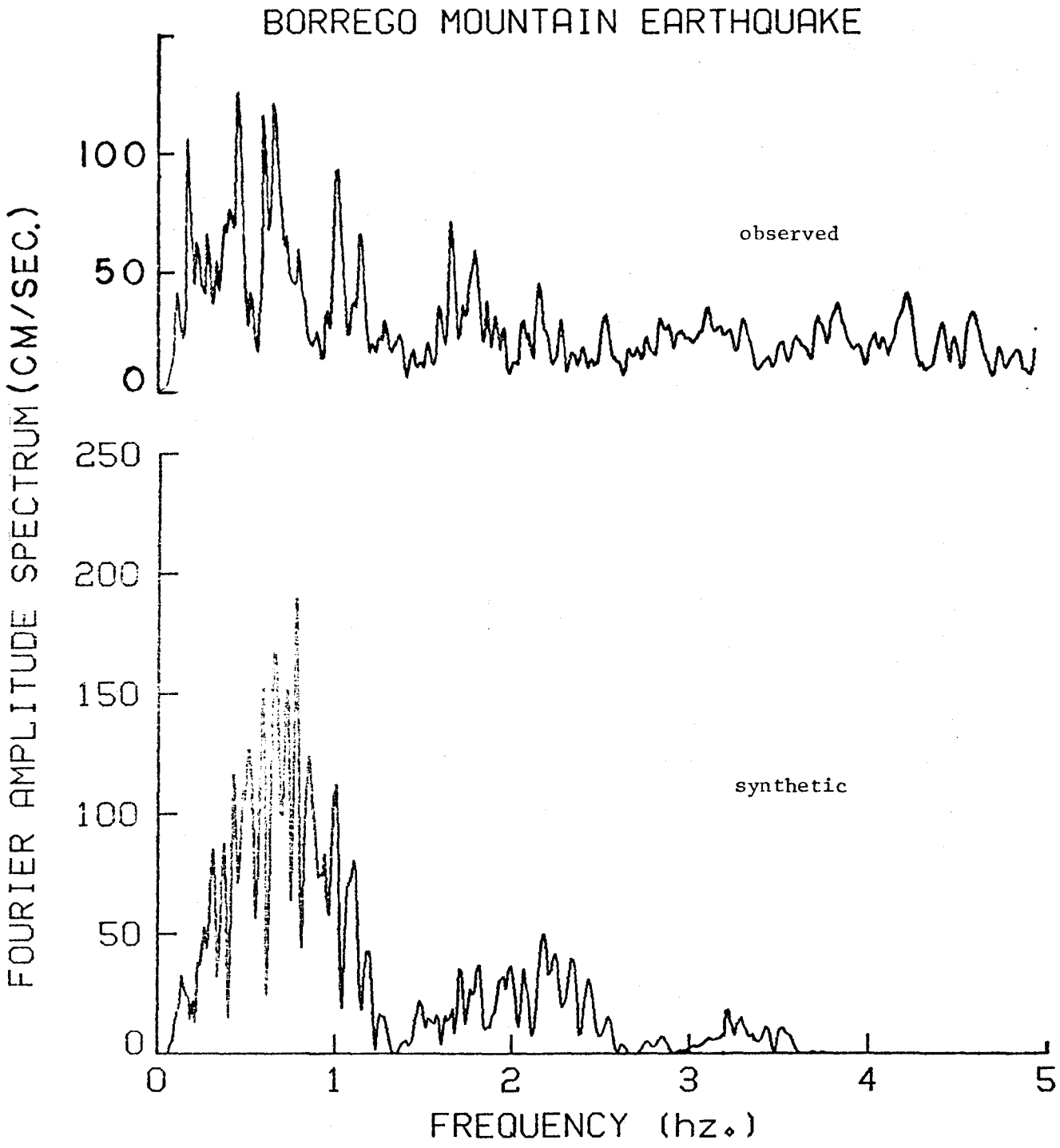


Figure IV.5.19 A comparison of the Fourier amplitude spectra of the observed record and the synthetic, for a fault that ruptures 5 km. toward El Centro and 50 km. away from the site. The rupture velocity and rise time are 2.5 km./sec. and 0.75 sec. respectively. The observed spectrum has been smoothed.

sensitivity of the acceleration motion to the details of the fault rupture. As expected, the rupture velocity, directivity, and the average stress drop are the dominant factors. Based on a single station recording, efforts to resolve these factors are quite constrained. Results based on acceleration amplitudes suggested that the fault ruptured for a length of 55 km., but are in no way conclusive.

The study presented was intended to demonstrate the ability of the normal mode method to model strong ground motion. The observations of previous investigators have been used throughout this study in selecting source parameters.

## IV.6 SUMMARY

This chapter presents results using the normal mode method described in Chapter III. The Imperial Valley structure was chosen as an appropriate region for this study due to the excellent information on the Imperial Valley structure and the availability of strong motion data. Effects on strong motion due to radiation pattern, focal mechanism, rise time, directivity, and source depth were given. These factors demonstrated the variation of ground displacements due to different properties of the seismic source and source-site geometry.

Two earthquakes were considered to show the capability of the normal mode method to model strong ground motion, these were the 1976 Brawley earthquake and the 1968 Borrego Mountain event. For both events the ground displacements were modeled, and for the Borrego Mountain earthquake ground acceleration was also considered. For the Brawley earthquake a point source was used to reproduce the overall character of

the observed displacements. The seismic moment estimated for this event was $4.6 \times 10^{25}$ dyne-cm. This event not only served to demonstrate the capability of the normal mode method to reproduce recorded strong motion displacements, but also clearly showed the importance of the earth structure.

The Borrego Mountain earthquake served to demonstrate the importance of the earth structure as well as the significance in being able to define the details of the source when modeling high frequency motion. This event provided an opportunity to model ground accelerations as well as displacements. A seismic moment of $1.12 \times 10^{26}$ dyne-cm is estimated from the displacement synthetics for this earthquake.

The results of modeling the acceleration motion indicate the extreme sensitivity of the waveform amplitudes to stress drop and rupture velocity. Source directivity played a major role in generating synthetic accelerograms having the proper phase and relative amplitude match. Modeling the acceleration motion made it possible to obtain an estimate of the spatial extent of the fault rupture which could not be accomplished in modeling the displacement motion. The preliminary results of this study suggest that the motion observed at El Centro was dominated by the rupture along a single fault segment that ruptured toward the recording station. This segment is estimated to be 5 km. long, and the rupture velocity is approximately 2.5 km./sec. A lower bound on the rupture velocity of 2.1 km./sec. is suggested for this segment. With data from just one recording station it becomes very difficult to resolve any details of the rupture as it propagates away from the site. As a result the solution presented is not very well

constrained. The excellent match of the waveform phases emphasizes the first order importance of the Imperial Valley structure on future efforts to predict strong ground motion and suggest that modeling ground accelerations may be well suited to resolve source dimensions and rupture characteristics.

# CHAPTER V - MONTE CARLO SIMULATION OF STRONG MOTION ACCELERATION

## V.1 INTRODUCTION

This chapter describes the Monte Carlo simulation employed to generate observations of the earthquake process discussed in Chapter II. This approach is similar to the one used by Boore and Joyner (1978), and Savy (1978), to generate realizations of a stochastic rupture process. Monte Carlo simulation is a realistic method to obtain numerically, a statistical sample from a probabilistic model that may be extremely complex or impossible to solve analytically. Simulation may in some cases be the only means to obtain a solution. The other topics to be addressed in this chapter are the description of the random variables of the process, the statistical information available about these variables and their assumed probability distributions.

The simulation presented in this study can be used for a number of applications other than the one discussed in Chapter II. For example, the ability to generate an ensemble of realistic acceleration time histories at a site due to a maximum credible event, would be one such application. This capability may be particularly advantageous for special structures such as nuclear power plants, LNG facilities, etc.

## V.2 MONTE CARLO SIMULATION

The problem of interest in this work is to determine the derived distribution of a variable(s) which is a function of a number of random variables. Monte Carlo simulation is an alternative solution technique

that can be used to "solve" such problems. The cost effectiveness of modern computers makes simulation a reasonable and practical alternative in many applications.

The concept of simulation is one of sampling a sufficiently large number of times from the probability distributions of the functionally independent variables to obtain observations of the dependent variable, given their functional relationship. The term sufficiently large theoretically means infinity, but in practical applications the number of similations is usually chosen based on the degree of accuracy needed. A simulation therefore constitutes a set of experiments, which if repeated an infinite number of times would produce a histogram that is exactly the probability distribution of the dependent variable.

During the experiment a random sample is obtained from the probability distribution of each independent variable. Sampling from a probability distribution is carried out by obtaining a set of random numbers that are mapped through the cumulative distribution function of the random variable of interest. This is usually done by choosing random numbers from a table, (Abramowitz and Stegun, 1972), or as generated from a computer algorithm, that are equally likely (Uniformly distributed). The Uniform random variable is then related, or mapped by a mathematical function, into the random variable of interest.

Mathematically, for continuous variables, sampling from the probability distribution of a random variable x, can be defined as follows. Let,

$$F_X(x_o) = P\,[X \leq x_o]$$

and (V.2.1)

$$f_Y(y_o) = 1 \qquad o \leq y_o \leq 1$$

Since samples of y are Uniformly distributed, the problem is that of a derived distribution to map y into x. What is required, therefore, is a function, g(y), such that,

$$x = g(y)$$

$$F_X(x_o) = F_Y(g^{-1}(y)) \qquad \text{(V.2.2)}$$

where the function g(y) represents the one to one transformation or mapping of y into x.

To summarize, sampling from the probability distribution of a random variable requires the ability to generate or obtain samples of a Uniformly distributed random variable and a functional relationship describing the mapping to the random variable of interest.

## V.3 STOCHASTIC FAULTING PROCESS

Seismic occurrence models, such as Poisson or Markov models describe the distribution of seismic events in time. The method presented here is conditional on the occurrence of an event, therefore the size of the earthquake is assumed known. The extension of the model to the total seismic hazard simply involves including the event size as a random variable, (Savy, 1978). This discussion is also limited to a single seismic source. Once again considering more than one source in the hazard model involves a summation of the hazard due to each source, (Shah

et al., 1975). With this introduction, the Monte Carlo simulation begins with the following known information: the seismic source and all information needed to define it geometrically, the seismic moment, and the site location. Figure V.3.1 presents graphically the input just described.

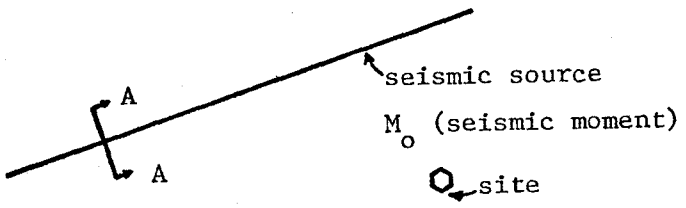


(a.) plan view

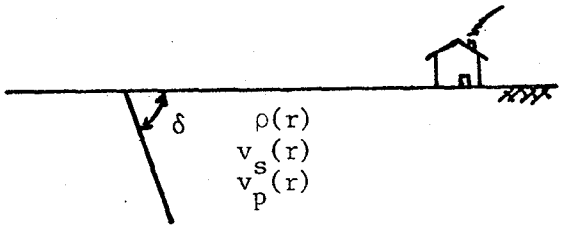


(b.) cross-section A-A

Figure V.3.1 A view of the problem input as considered in this work, (a.) plan view defining the seismic source, event size and site location, and (b.) a crossection defining the fault geometry, and earth structure.

## V.3.1 RANDOM FAULT SEGMENTS

Chapter III presented the method for determining the Fourier

transform of acceleration due to a single fault segment rupturing along a line source. The form of the solution due to the complete fault rupture is the sum of the individual segment contributions, where the fault is modeled as a series of line segments at constant depth. These segments are called coherent segments, (Boore and Joyner, 1978; Savy, 1978), meaning along their length, the random variables of the fault rupture are constant.

The concept of introducing randomness into the description of the fault or rupture process is not new, (Haskell, 1966; Boore and Joyner, 1978; Kanamori, 1979). The basic theme is to take into account in dislocation models, the roughness or spatial variation of frictional resistance along the fault, Nur (1978).

Before the fault segments can be described, the region on the fault plane that ruptures must be identified. The fault has been modeled as a dipping plane described by the location of its surface strike, and dip angle. In seismic hazard analysis it is generally assumed that the occurrence of an event is equally likely at any point on the fault. If different parts of a fault exhibit varying levels of seismicity, the fault is often divided into separate seismic sources. The assumption of equally likely occurrence is also made here, therefore the center of the fault area to rupture is assumed to be Uniformly distributed along the fault length.

Kanamori and Anderson (1975) have looked at data relating seismic moment and average stress drop to the area of rupture. For a constant stress drop, log (S) $\sim$ 2/3 log $M_o$, where S is the rupture area and $M_o$ is

the seismic moment. In their study, events were grouped according to whether they occurred on faults that are inter-plate faults, that is they are boundaries between major tectonic plates or intra-plate, meaning the fault lies within a plate. They found that events occurring on inter-plate faults have average stress drops of about 30 bars. Similarly intra-plate events had an average stress drop of around 100 bars. For those events not belonging to either group, an average stress drop of 60 bars was suggested. For an assumed stress drop and seismic moment, an estimate of the rupture area is obtained from the relation derived by Kanamori and Anderson (1975). The rupture area is estimated according to,

$$\log (S) = \frac{2}{3} [\log (M_o) - \log (c\Delta\sigma)] \qquad (V.3.1)$$

where $\Delta\sigma$ is the average stress drop and c is a geometric factor depending on the shape of the rupture area. In this work strike-slip events are considered, therefore equation (V.3.1) becomes,

$$\log (S) = \frac{2}{3} [\log (M_o) - \log (\frac{\pi}{2} \Delta\sigma A_r)] \qquad (V.3.2)$$

where $A_r$ is the aspect ratio of rupture width to length. Geller (1976) has shown empirically, with considerable scatter, that the aspect ratio has a mean value of 1/2. Since, as Geller points out, no distinction can be made between inter and intra plate events, the aspect ratio is considered random, and Uniformly distributed between 1/3 and 2/3 with a

mean of 1/2. For a realization of the aspect ratio, the rupture area is determined, since, $M_o$, and $\Delta\sigma$ are both known.

From the location of the center of the rupture zone on the fault, and the rupture area, the bounds on the region of fault dislocation is defined. From this point the fault segments can be generated. After Boore and Joyner (1978), the coherence length of a segment is taken to follow the exponential probability law with parameter $\lambda_\ell$. The exponential probability density function is given as,

$$f_{X_\ell}(x_\ell) = \lambda_\ell \, e^{-\lambda_\ell x_\ell} \qquad (V.3.3)$$

$$x_\ell \geq 0$$

The mean coherence length is $1/\lambda_\ell$. A maximum value of the segment length is set, thus truncating the above distribution. Beginning at one end of the fault, segments are generated and their corresponding widths determined from the aspect ratio.

The moment corresponding to each fault segment is proportional to its area such that,

$$M_o = \sum_{i=1}^{\text{all segments}} M_{o_i} \qquad (V.3.4)$$

$$M_{o_i} = \frac{S_i}{S} M_o$$

The result of this part of the simulation is shown in Figure V.3.2.

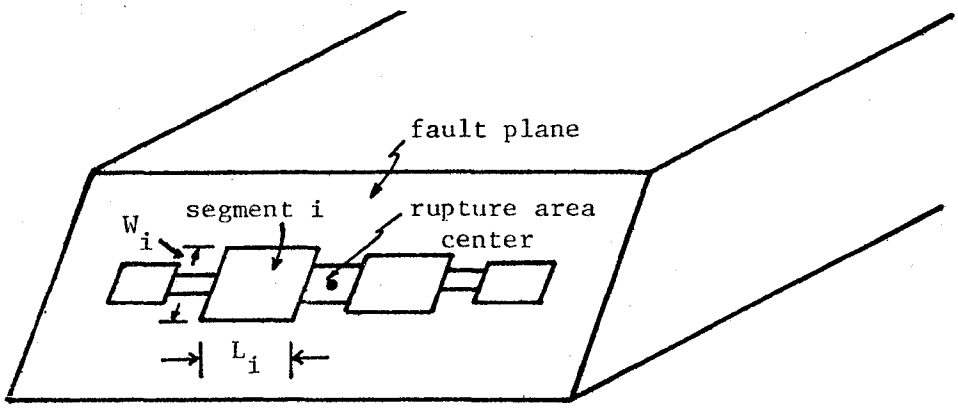


Figure V.3.2 A view of the fault plane divided into a series of random fault segments. For each segment the rupture velocity and dislocation rise time is also generated.

## V.3.2 RUPTURE VELOCITY AND RISE TIME

Geller (1976) has carried out an empirical study of a number of moderate and large earthquakes. From that study an average value of the rupture velocity of $0.72\beta$ was found, where $\beta$ is the shear wave velocity. There is considerable variation in observed rupture velocities with no significant trends offered. Therefore the rupture velocity is assumed to be Uniformly distributed from $0.5\beta$ to $1.0\beta$.

Geller (1976) also studied the dislocation rise time, and based on certain assumptions related it to the rupture area of the fault. This scaling law relationship is given as,

$$\bar{\tau} = \frac{16 \cdot S^{1/2}}{7^{3/2} \cdot \beta} \qquad (V.3.5)$$

where S is again the rupture area and $\beta$ the shear wave velocity at the source, and $\bar{\tau}$ is the mean rise time, of a Uniform distribution. For each fault segment a value of the rupture velocity and rise time are selected.

## V.4 EARTHQUAKE FOCUS

The point of rupture initiation or focus of the earthquake is assumed to occur with equal likelihood at any point along the length of rupture. The depth of the focus is somewhat more constrained in that shallow strike slip events are modeled in this work, and to ensure reasonable frequency information for the 18 modes generated in Chapter IV. The depth of focus is also Uniformly distributed, from 4 to 8 kilometers. This is an assumption of this work, but one which could be relaxed by including higher modes.

## V.5 DISCUSSION

The probability distributions on the random variables described in the previous sections have been developed based on readily available published results or standard assumptions used in seismic hazard analysis. Specifically, the works of Geller (1976) and Kanamori and Anderson (1975) have been used to estimate source properties. This information is quite general in that no specific fault or tectonic region was considered. This section discusses briefly more refined aspects of defining information about the faulting process.

The probability distributions employed in the present model were based on generalized results or scaling laws, and common assumptions based on little or no information. However, for particular regions or

for a particular fault, there may in fact be considerable information available. This statement is particularly true for variables such as the location of the rupture zone, focus location, state of stress on the fault, etc., (Seih, 1979). The methods to obtain and refine this type of information have increased significantly in recent years, particularly with the interest in earthquake prediction. Similarly, as the number of recorded strong motion events increases, for a particular fault or fault system, the possibility of refined, source specific information on dynamic fault properties is quite possible. With improved information more realistic probability density functions will be derived.

This state of affairs may require a more detailed development of the probability distributions on the random variables of the earthquake. The use of Bayesian analysis to sort and combine the many possible sources of information may be a possibility in the future.

## V.6 TOTAL MOTION DUE TO A FAULT RUPTURE

The motion at the site is the superposition of the effects due to individual fault segments. The total motion is then a double summation over the number of modes, and segments. Recall there is an implied summation over angular order as discussed in Chapter III. From eq. (III.5.18) this is,

$$A(\omega) = \sum_{k=1}^{nseg} \sum_{j=1}^{modes} -\omega^2 \, C_j(\omega) \, \frac{(\sin(\tau_k \omega /2))}{(\tau_k \omega /2)} \qquad \text{(V.6.1)}$$

$$\frac{(\sin(T_{L_k} \omega /2))}{(T_{L_k} \omega /2)} \exp(-i\omega(t_{r_k} + \frac{\tau_k}{2} + \frac{T_{L_k}}{2}) \exp(-\frac{\omega r_k}{Qu(\omega)})$$

where: $C_j(\omega) = \frac{1}{\sqrt{\sin\theta_k}} (p_k P_j^1(\omega) + iq_k Q_j^1(\omega))$

$$\exp(-i\frac{\pi}{4}) \exp(-i\omega a\theta_k / c_j(\omega)) \qquad \omega \geq 0$$

$C_j(-\omega) = C_j^*(\omega) \qquad \omega < 0$

$vr_k$ = rupture velocity (km/sec.) in the $k^{th}$ segment

$c_j(\omega)$ = phase velocity (km/sec.) of the frequency $\omega$

$u_j(\omega)$ = group velocity (km/sec.) of the frequency $\omega$

$p_k, q_k$ = geometric factor for the $k^{th}$ segment

$P_j^1(\omega)$, $Q_j^1(\omega)$ = excitation coefficients corresponding to the $j^{th}$ mode

$T_{L_k}$ = directivity factor for the $k^{th}$ segment

$$= \frac{L_k}{2.0} \left( \frac{1}{vr_k} - \frac{\cos\phi_k}{c_j(\omega)} \right)$$

$\tau_k$ = rise time for $k^{th}$ segment

$t_{r_k}$ = trigger time for $k^{th}$ segment

$r_k$ = distance(km.) from the source to the $k^{th}$ segment

$\theta_k$ = distance(radians) from the source to the $k^{th}$ segment

$Q$ = specific attenuation factor

$L_k$ = length of the $k^{th}$ segment in km.

$a$ = radius of the earth

$\phi_k$ = source-site azimuth (radians) for the $k^{th}$ segment

Note that the earth's damping has been included in eq. (V.6.1). For each simulated event eq. (V.6.1) is applied, generating a realization of the Fourier transform of acceleration.

## V.7 SUMMARY

To summarize the simulation process, Figure V.7.1 is a flow chart indicating the steps followed. The result, as described in Chapter II, is the likelihood function on rms acceleration at the site, and an ensemble of spectral shape functions from which the probability distribution on spectral amplitude is derived.

Monte Carlo Simulation

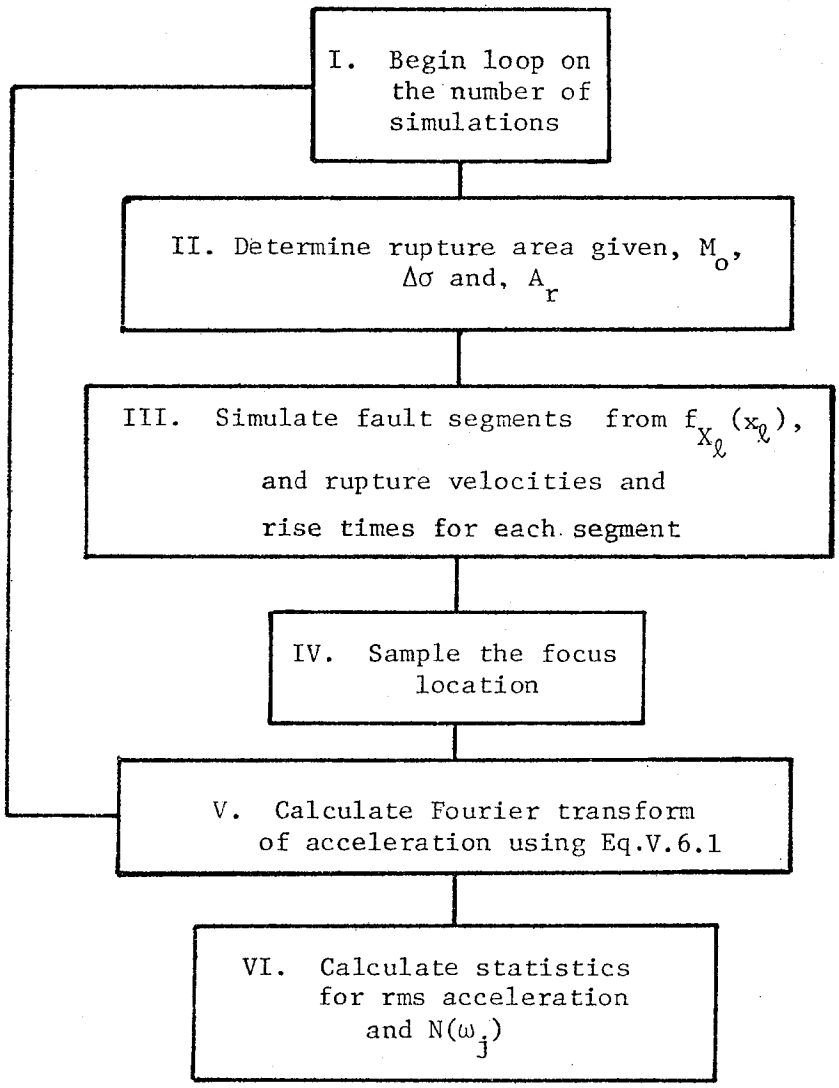


Figure V.7.1 A flowchart indicating the Monte Carlo simulation procedure.

# CHAPTER VI - PROBABILISTIC APPLICATIONS

## VI.1 INTRODUCTION

This chapter presents numerical results for the probability model presented in Chapter II. Results are also presented from a sensitivity study that identifies, in a stochastic setting, the dependence of the rms acceleration, frequency content, and time histories on the source parameters. An example applying the Bayesian model is presented first, followed by the results of the sensitivity study.

## VI.2 BAYESIAN PROBABILITY MODEL

In Chapter II the problem of interest was defined according to knowledge of the seismic source, the seismic moment of the event, and the site where the ground shaking hazard was to be determined. An example is presented based on input of this form to demonstrate the use of the Bayesian model.

Figure VI.2.1 presents the source-site geometry and earth structure for the event to be modeled. The parameters of the event are summarized in Table VI.2.1 along with the variables to be used in the Monte Carlo simulation.

The Bayesian analysis proceeds in the following way. The stage I analysis provides a posterior estimate of the mean rms acceleration based on the strong motion data. This probability density function was denoted, $f_1''(\mu)$. Proceeding with the stage II analysis, the stage I posterior represents the prior information and is denoted, $f_2'(\mu)$.

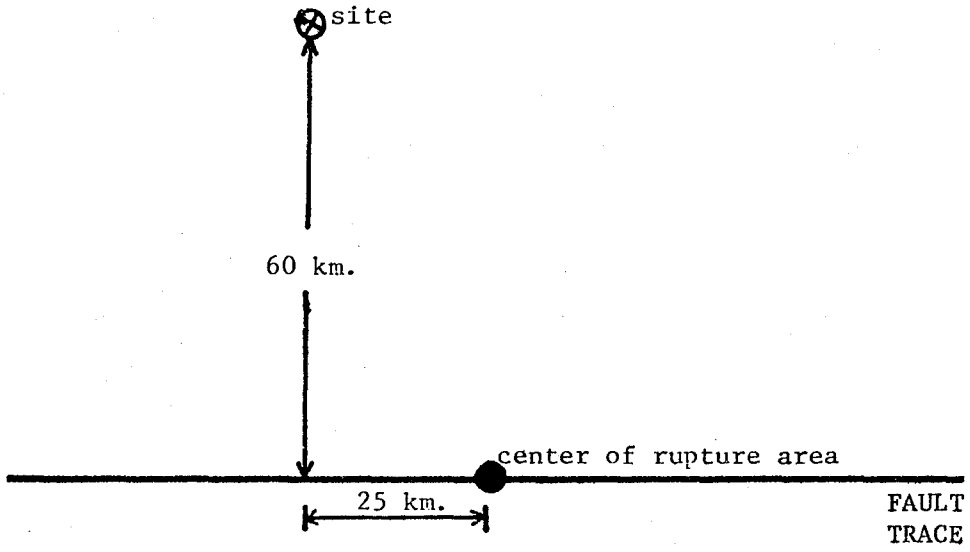


(a.) plan view

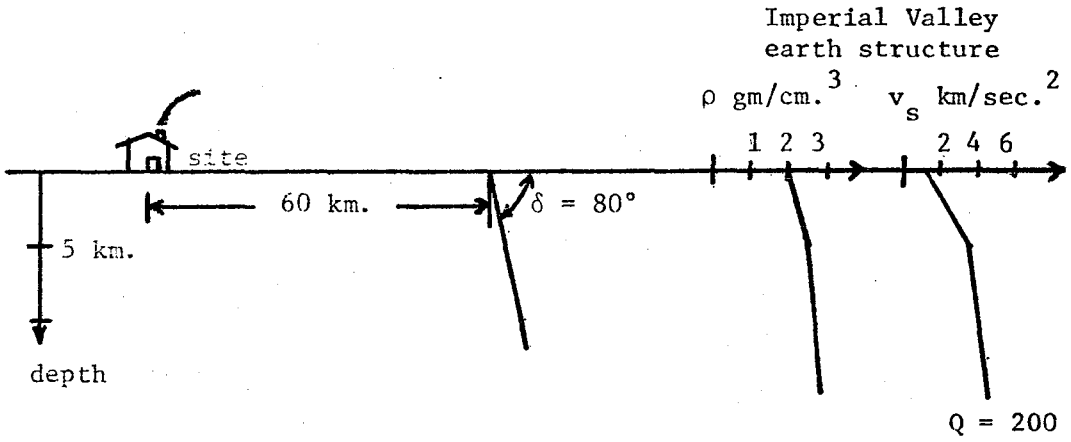


(b.) crossection view

Figure VI.2.1 Geometric and earth structure input for an example of the Bayesian probability model.

Therefore the stage II prior information on the mean rms for an event of this size, is given by an attenuation curve similar to that presented by McCann (1980) for events with a seismic moment on the order of $10^{26}$ dyne-cm. The prior input is summarized in Table VI.2.2. Recall that the prior distribution on the mean rms is approximated by a Normal distribution, therefore the prior probability density function in the stage II analysis, $f_2'(\mu)$, is N(24.66, 5.29).

Table VI.2.1

Parameters of the Example Problem

| | |
|---|---|
| Seismic Moment: | $5.0 \times 10^{26}$ dyne-cm. |
| Source-site distance: | 60 km. |
| Fault Type: | inter-plate, $\Delta\sigma$ = 15 bars |
| Fault dip: | $80^{o}$ |

Variables Used in the Monte Carlo Simulation

| | Mean | Range |
|---|---|---|
| Focus depth (km.) | 6.5 | 5 - 8 |
| Rupture velocity (fract. of the shear wave velocity) | 0.75 | 0.5 - 1.00 |
| Aspect ratio (width/length) | 0.5 | 0.4 - 0.60 |
| Coherence length (km.) | 5.0 | 0.0 - 10.0 |
| Maximum number of fault segments | 10 | |

Table VI.2.2

Summary of Prior Information

| | | |
|---|---|---|
| $E[\ell n(rms)]$ | = | $\alpha + \beta\, \ell n(dist)$ |
| $\alpha$ | = | 6.804 |
| $\beta$ | = | -0.928 |
| n | = | 14 |
| $\sigma^2_{y\|x=60}$ | = | 0.625 |
| $\sigma^2_{E[y\|x=60]}$ | = | 0.045 |
| $E[rms_{60}]$ | = | 24.66 cm/sec.$^2$ |
| $\sigma[rms_{60}]$ | = | 17.01 cm/sec.$^2$ |
| $\sigma[\overline{rms}_{60}]$ | = | 5.29 cm/sec.$^2$ |

Table VI.2.3

Results of Monte Carlo Simulation

| | |
|---|---|
| no. of simulations: | 25 |
| $\overline{z}$: | 70.17 cm/sec.$^2$ |
| $\sigma_z$: | 34.55 cm/sec.$^2$ |

For the parameters in Table VI.2.1, a Monte Carlo simulation was performed to generate observations of ground motion due to a stochastic fault rupture. The results of the simulation are given in Table VI.2.3,

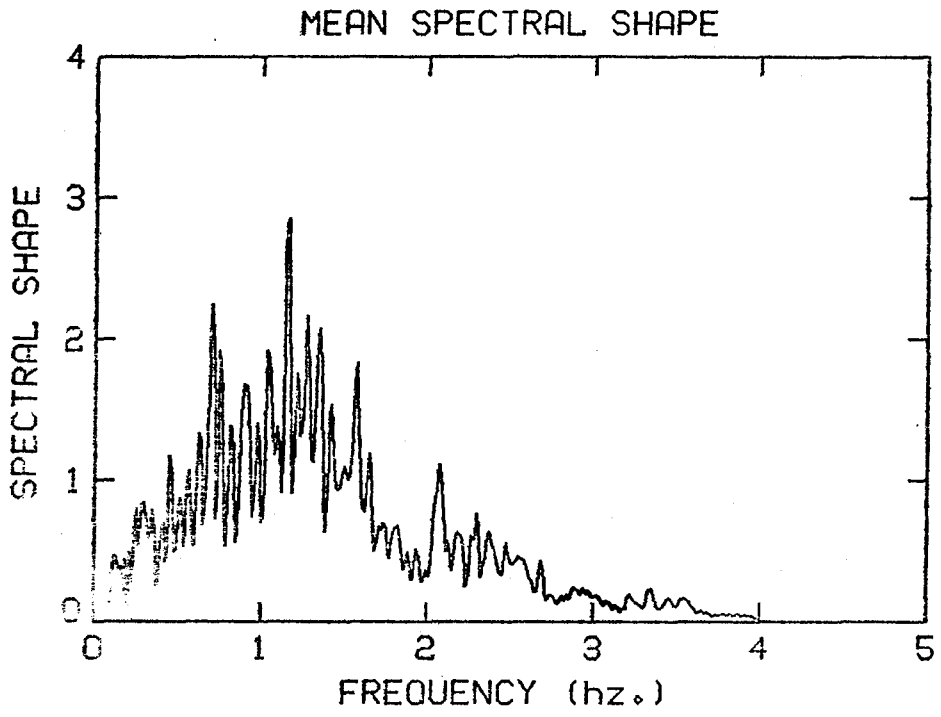


Figure VI.2.2 The mean power spectrum shape for the simulation parameters in Table IX.2.1.

and the mean power spectral density shape is given in Figure VI.2.2. The likelihood function, denoted $L(z|\mu)$, has a mean and standard deviation of 70.17 and 3.40 cm/sec.$^2$ respectively. Recall that the variance of the process was assumed known and equal to the variance derived from the stage I analysis. Thus the likelihood function, $L(z|\mu)$, is N(70.17, 3.40). The posterior distribution on the mean rms acceleration, which is also Normally distributed, is determined from Bayes theorem and

is found to be N(57.56, 2.86). Note the significant effect the additional observations have on the expected value of the rms. This new estimate is a weighted value based on the uncertainty in the mean value from each source of information. In this example the variation in the likelihood estimate of the mean is lower than its counterpart in the prior. As a result the updated estimate of the expected rms value is significantly influenced by the likelihood information. This is shown

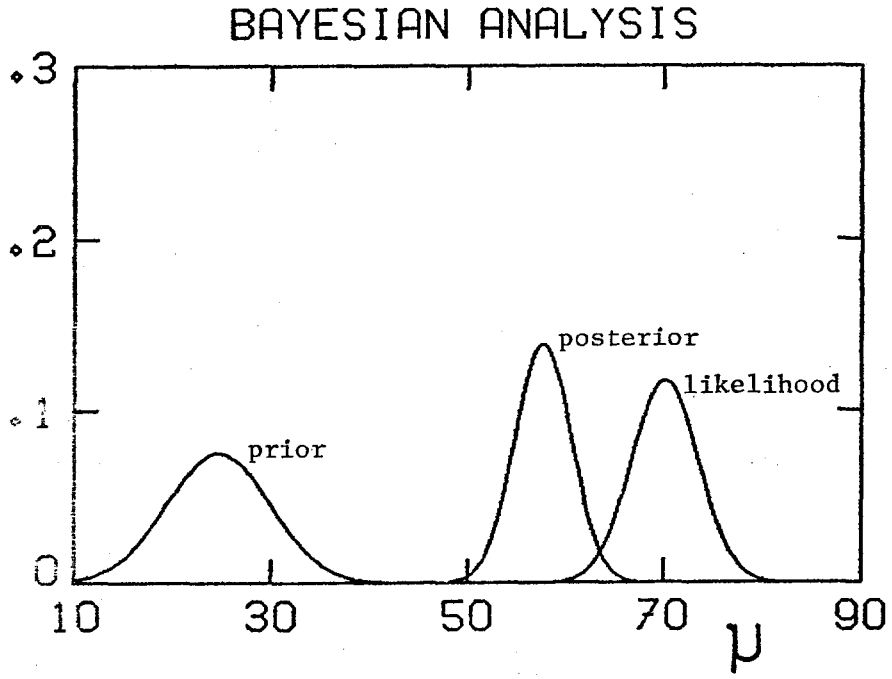


Figure VI.2.3 The Stage II Bayesian analysis for the example described in the text. Note the significant effect the likelihood function has on the posterior probability density function. This is an illustrative example and not meant to represent an actual case.

graphically in Figure VI.2.3.

The marginal distribution on the rms acceleration is determined using eq. (II.4.4). This distribution is also Normal with a mean of 57.56 and a standard deviation of 23.16, each in units of cm/sec.$^2$ The

final result derived from the probability model is the probabilistic power spectrum as defined by eq. (II.4.5). For assumed independence of the spectral shape and the rms acceleration, the expected value of the power spectral ordinates and their variance can be determined by the following relations,

$$E[S(\omega_j)] = E[rms^2]\ E[N(\omega_j)]$$

$$E[S^2(\omega_j)] = E[(rms^2)^2]\ E[N^2(\omega_j)]$$

$$\sigma^2(S(\omega_j)) = E[S^2(\omega_j)]\ E[S(\omega_j)] \qquad \text{(VI.2.1)}$$

The complete distribution, $f(S(\omega_j))$, is determined from a numerical integration of eq. (II.4.5).

## VI.3 SENSITIVITY STUDY

Of major importance in applying the model developed in this work is to understand the degree of sensitivity of the rms acceleration, duration, time histories, and spectral values on the input parameters. Examples are presented to consider the effect when the source parameters are varied. A standard case is defined, then each parameter is altered individually to identify that parameters relative effect. Examples of time history realizations and Fourier amplitude spectrum realizations are given.

The results of the simulation are provided in Table VI.3.1 where the source parameters are defined in terms of example number 1, the standard case. After the first case, the parameter list identifies the variable that has been changed from the standard. The nominal case is the one

Table VI.3.1

Results of the Sensitivity Study

| Simulation Number | Parameter | $\overline{rms}$ | $\sigma_{rms}$ | $T_{min}$ - $T_{max}$ | $\overline{N}$ (1.0 hz) | $\overline{N}$ (2.0 hz) |
|---|---|---|---|---|---|---|
| 1 | See Table IX.1.1 | 70.17 | 34.55 | 13.28 - 37.5 | 0.70 | 0.37 |
| 2 | $\Delta\sigma$ = 50 bars | 128.70 | 60.52 | 8.59 - 30.47 | 0.69 | 0.18 |
| 3 | $\Delta V_r$: 0.4 - 0.80$\beta$ | 64.66 | 37.34 | 9.38 - 35.94 | 0.80 | 0.22 |
| 4 | mean coherence length 3.0 (km)<br>maximum length 9.0 (km) | 115.0 | 50.65 | 8.59 - 39.84 | 2.15 | 0.36 |
| 5 | mean coherence length 7.0 (km)<br>maximum length 21.0 (km) | 66.34 | 41.42 | 7.81 - 34.38 | 0.82 | 0.24 |
| 6 | Q = 100 | 41.33 | 18.47 | 11.72 - 28.91 | 0.40 | 0.22 |
| 7 | $\phi \simeq 20^{o}$ | 251.4 | 195.4 | 8.59 - 25.78 | 0.65 | 0.22 |

shown in Figure VI.2.1 with the parameters listed in Table VI.2.1. The simulation results are summarized by the mean and standard deviation of the rms, the mean spectral value at frequencies of 1.0 and 2.0 hz., and the range of the strong motion duration as determined using the method developed by McCann (1980).

Figures VI.3.1 - VI.3.7 present time history realizations for each simulation case, and Figure VI.3.8 is the corresponding realization of Fourier amplitude spectra for the first case. The functions plotted in these figures have been normalized. The simulation results indicate the strong dependence of ground acceleration on the average stress drop, rupture velocity, and station azimuth. From these results and the example in the previous section it is recognized that the use of the model in applications will have to be studied in depth to calibrate its use for a given region.

## VI.4 DISCUSSION

As demonstrated in Chapter IV, and further recognized in the simulation results of this chapter, the waveform amplitudes are very sensitive to the details of the fault rupture. The rupture velocity, stress drop, and source directivity appear to have the greatest effect. The stress drop describes the source strength in the frequency range where accelerations are dominant. The effect of stress drop was recognized in Chapter IV in modeling the acceleration motion recorded at El Centro during the Borrego Mountain earthquake. Similarly, the significant effect of source-site azimuth and rupture velocity - phase velocity interaction were demonstrated. These factors can result

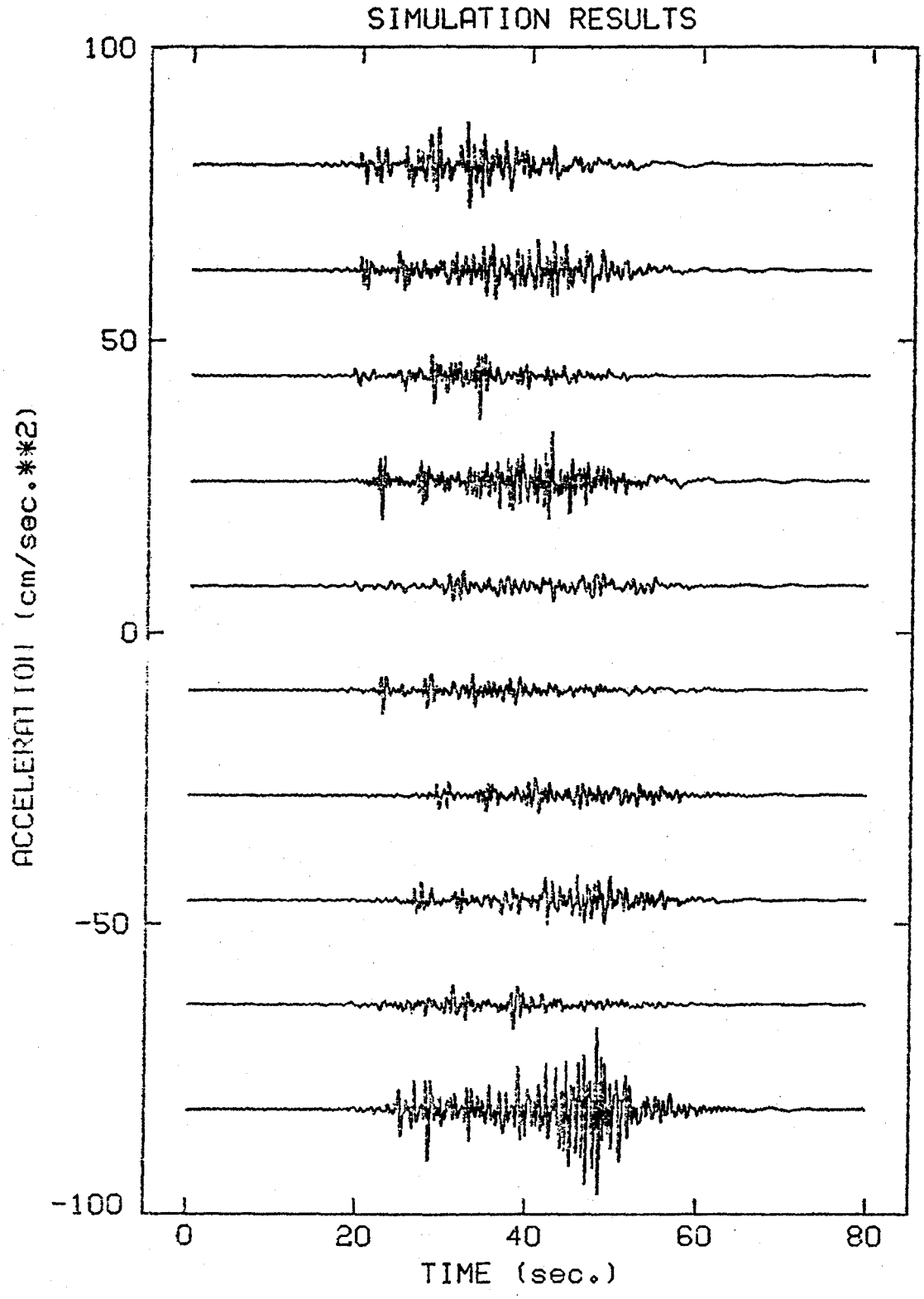


Figure VI.3.1 Time history realizations for simulation case 1. The vertical scale is arbitrary in Figures IX.3.1 - IX.3.7.

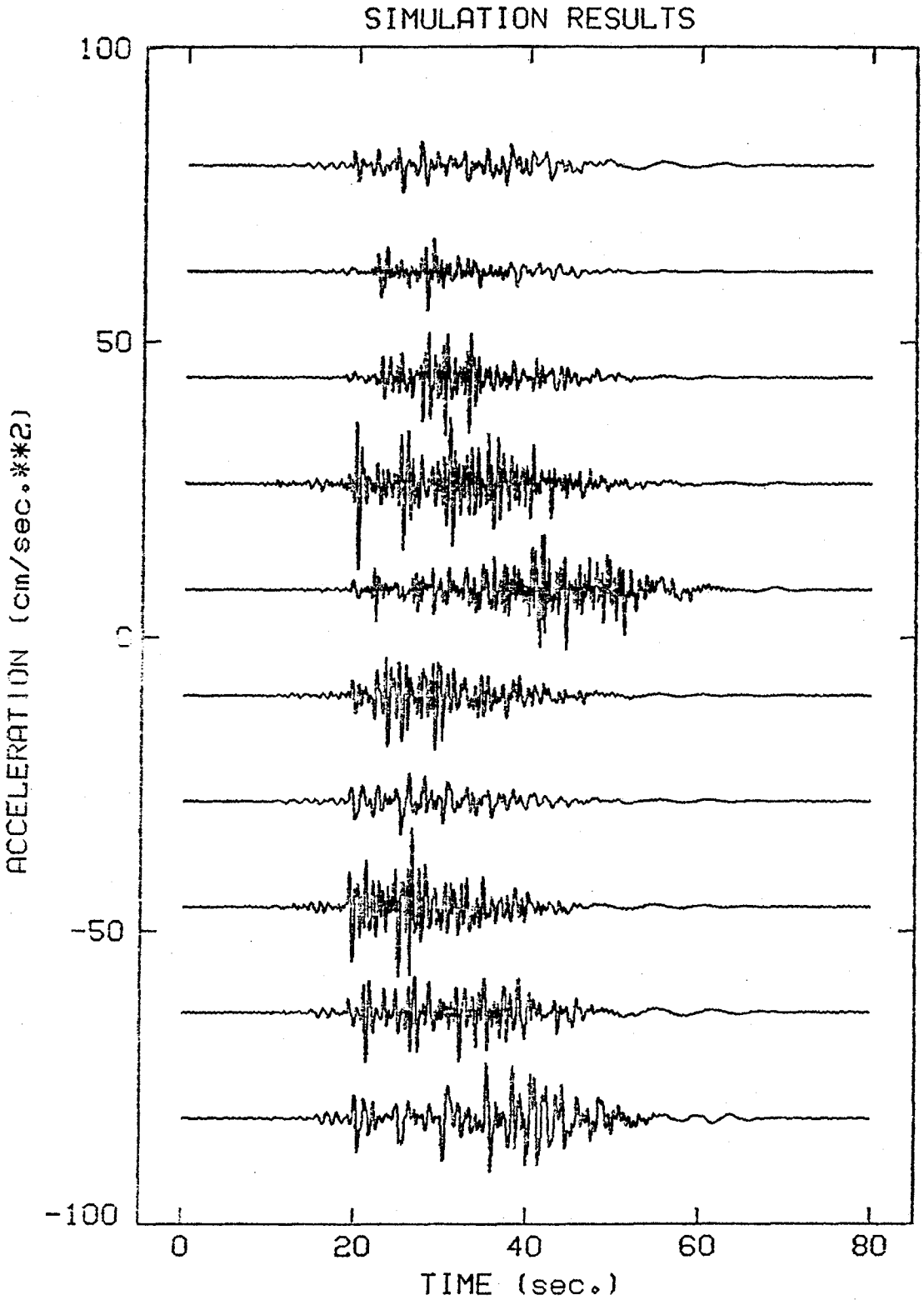


Figure VI.3.2 Time history realizations for simulation case 2.

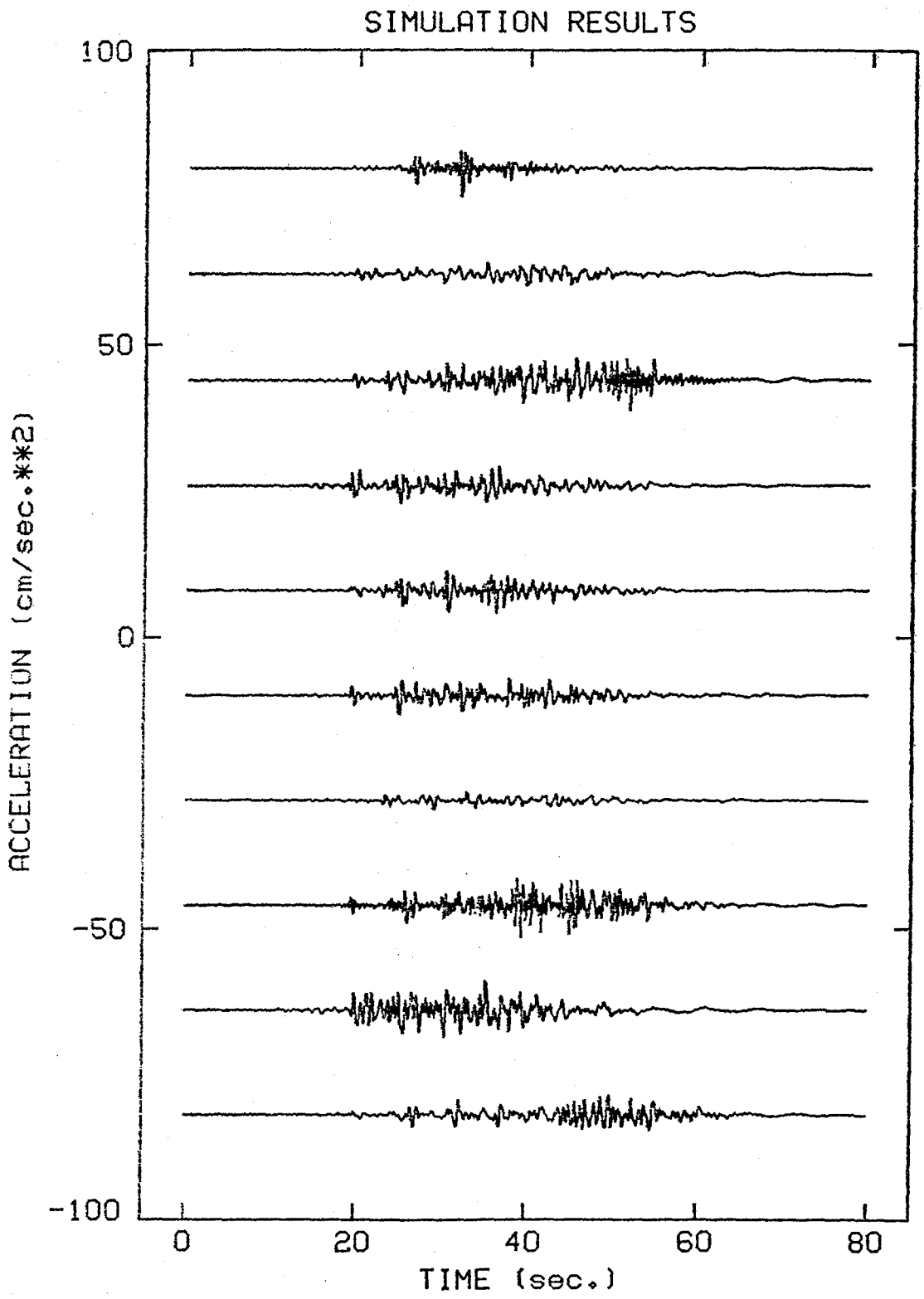


Figure VI.3.3 Time history realizations for simulation case 3.

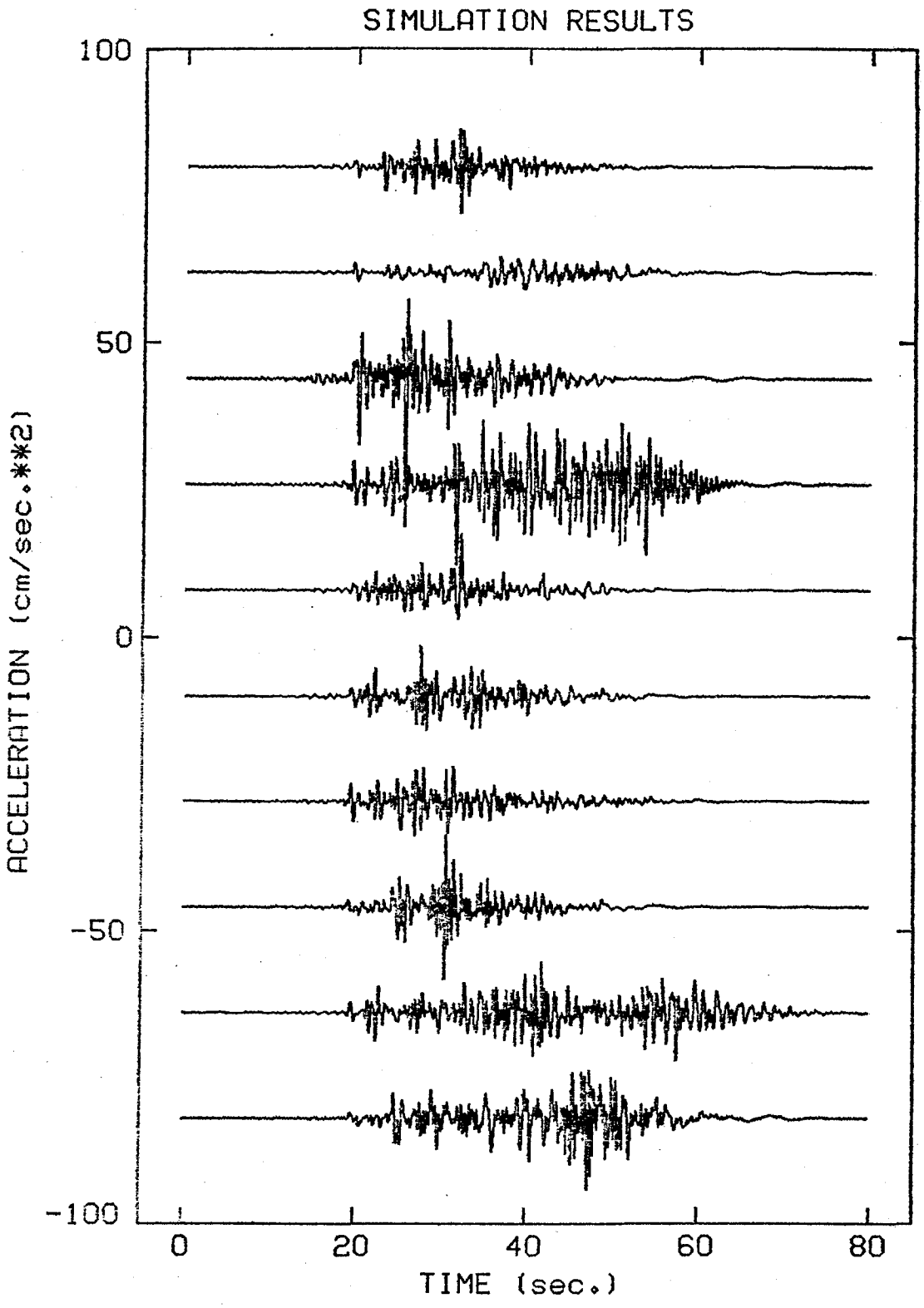


Figure VI.3.4 Time history realizations for simulation case 4.

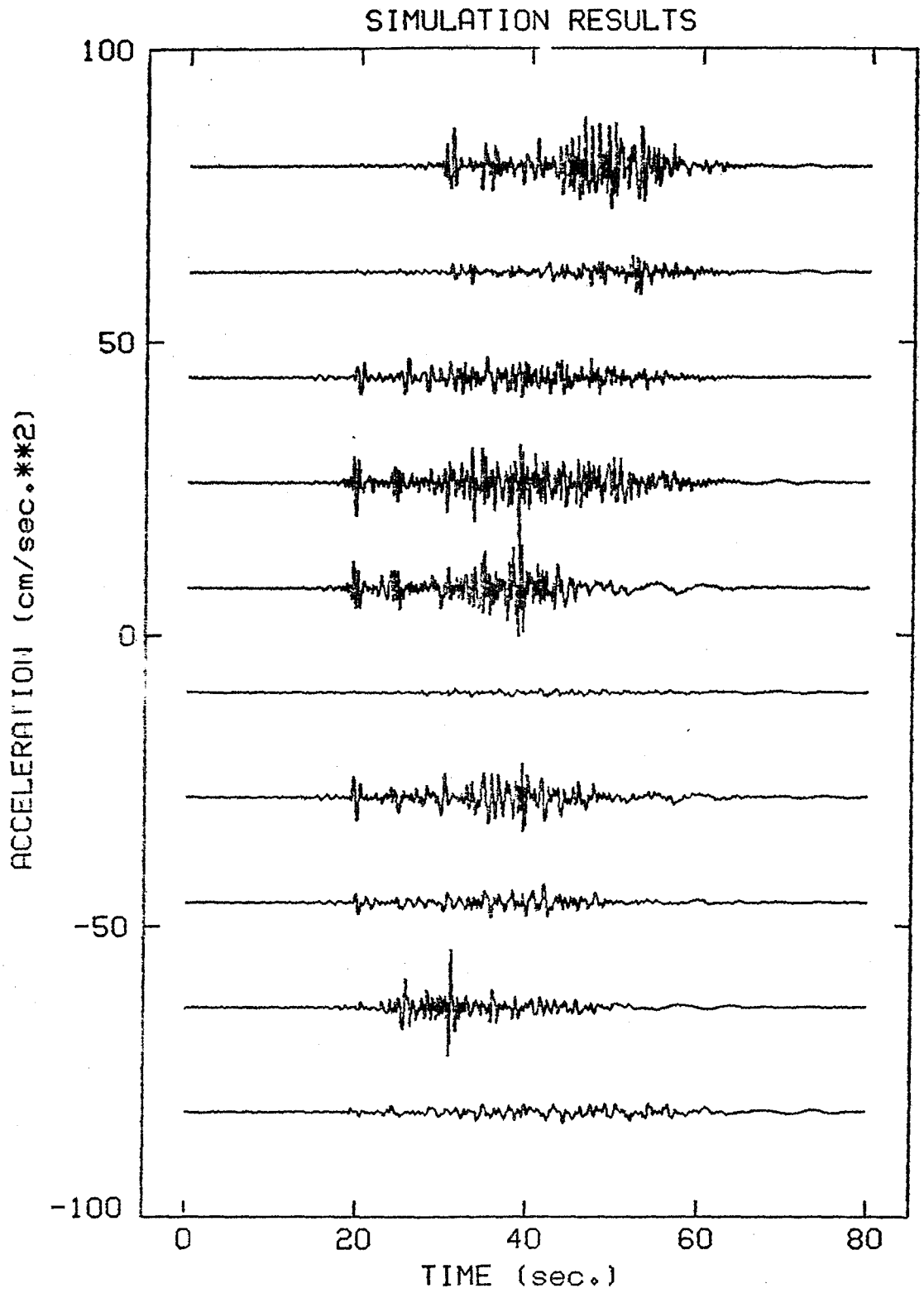


Figure VI.3.5 Time history realizations for simulation case 5.

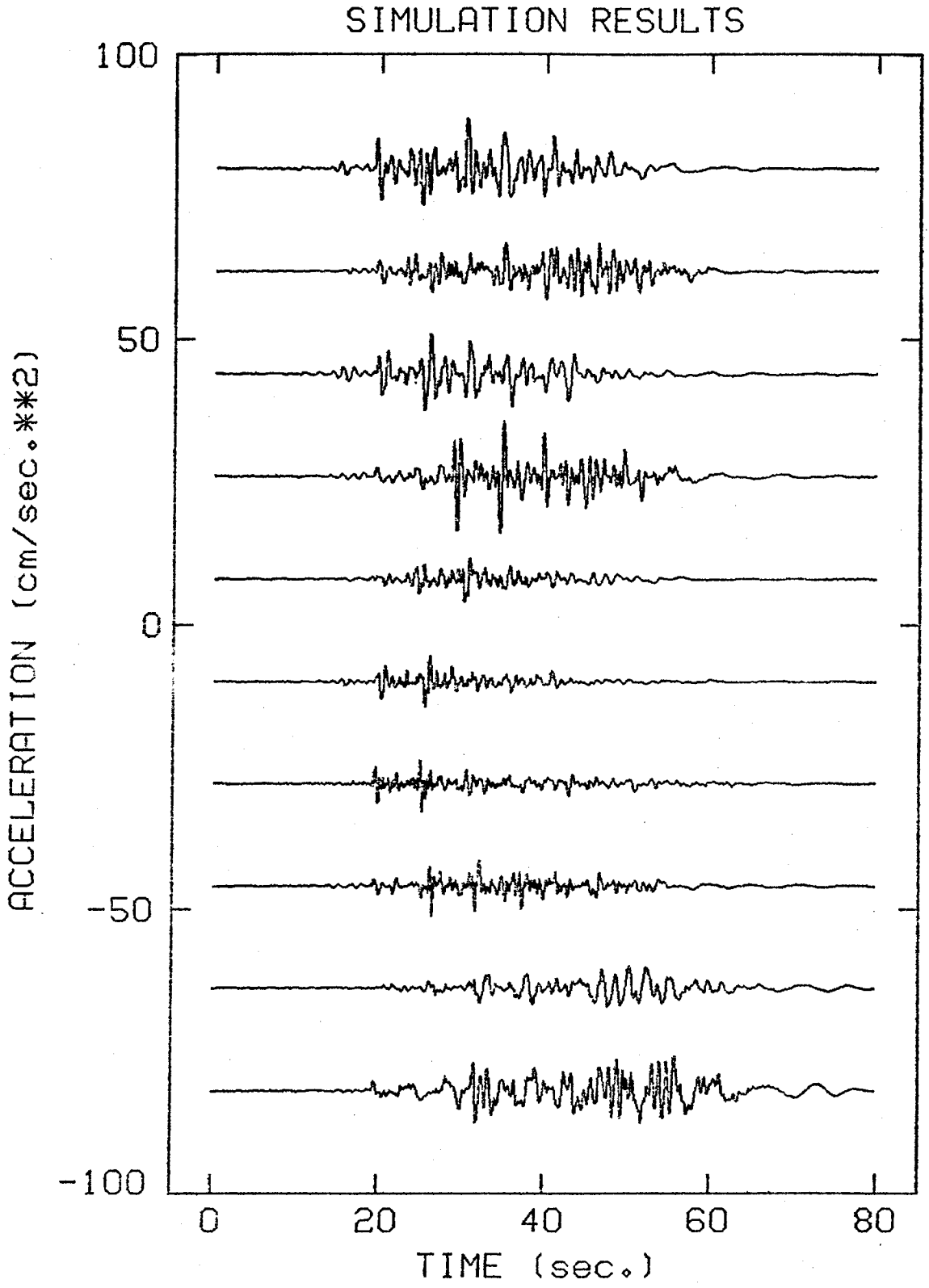


Figure VI.3.6 Time history realization for simulation case 6.

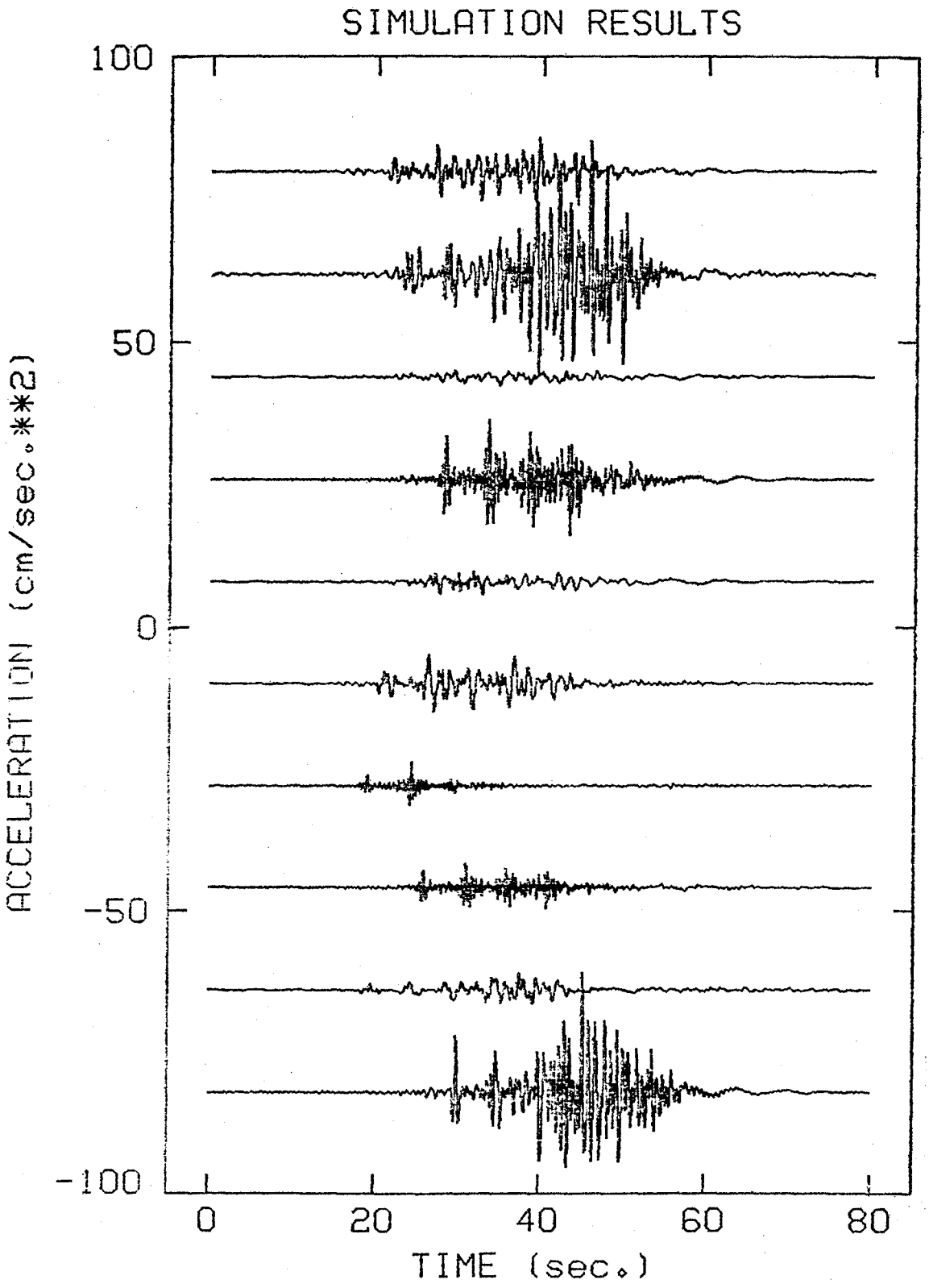


Figure VI.3.7 Time history realization for simulation case 7.

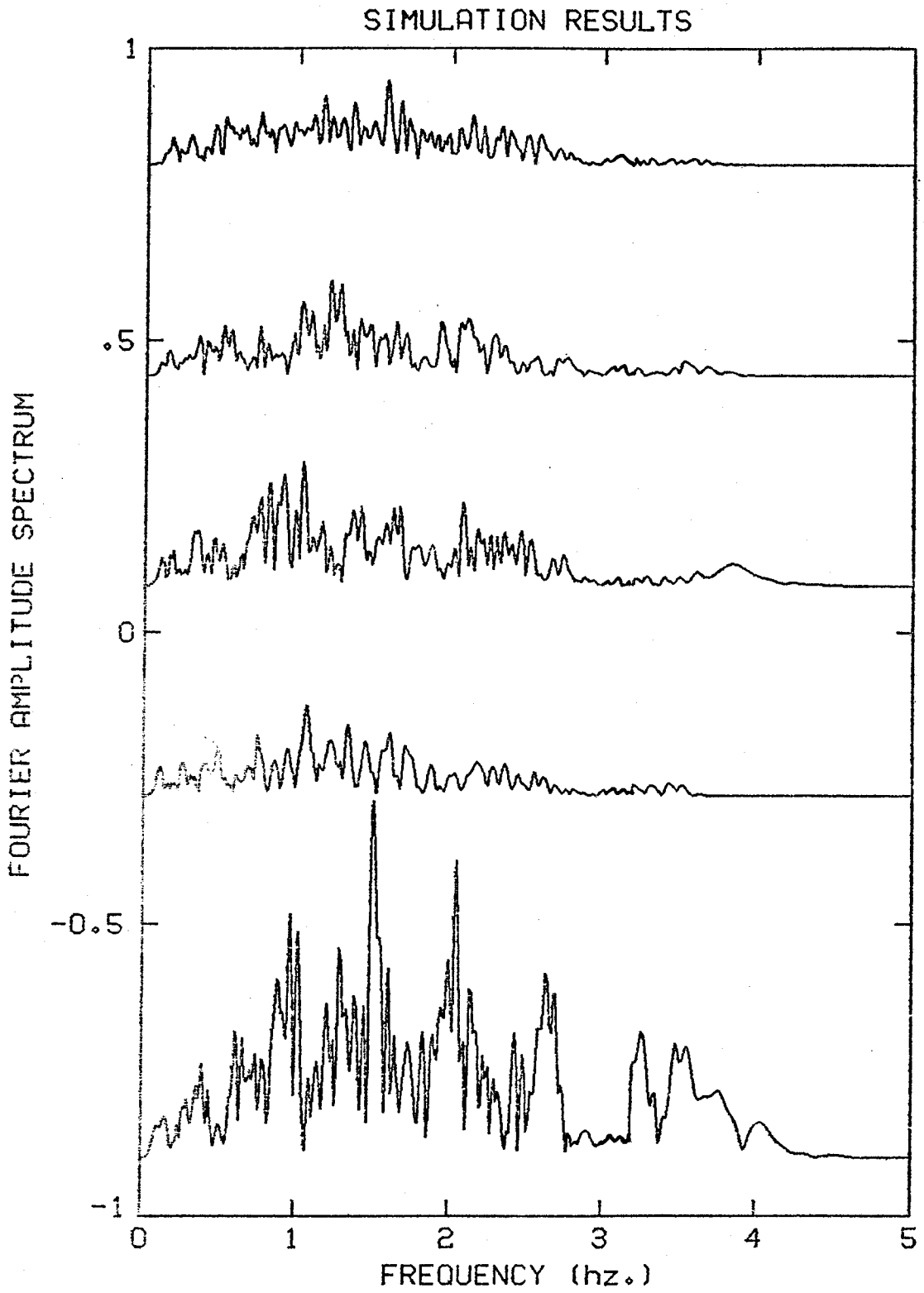


Figure VI.3.8 Fourier amplitude spectrum realizations for case one. The spectra have been normalized.

individually, in a factor of five or more in their extreme effects. Therefore the numerical values reported are significant only in terms of the relative effects of the parameters studied. An important and extensive effort in the future would be to look into the calibration of theoretical models for the prediction of strong ground motion. This study would entail a refinement of the source parameter input. Such refining will involve the development of regional source parameters and a derivation of more realistic probability density functions for the random variables.

# CHAPTER VII - CONCLUSIONS AND RECOMMENDATIONS FOR FUTURE RESEARCH

## VII.1 INTRODUCTION

This chapter summarizes the major conclusions and results of this research effort. In the course of any research work many new and interesting projects are visualized but are secondary to the problem at hand. To aid in continued developments in the area of seismic hazard analysis recommendations for future research are presented.

## VII.2 CONCLUSIONS

This research work consisted of three basic elements, all of which contributed to the development of a Bayesian model for estimating strong ground motion. These three entities were the empirical information on rms acceleration and duration, the development of the Bayesian probability model for ground motion spectra, and the application of the normal mode method for modeling strong ground motion. The major results of this work are the following:

- a Bayesian review of the state of the art in modeling strong ground motion was presented, defining the state of information and the state of practice.

- a Bayesian probability model was developed to incorporate the available sources of information in providing a probabilistic power spectrum at a site.

- the acceleration motion recorded at El Centro during the 1968 Borrego Mountain earthquake was modeled with considerable success indicating that for the Imperial Valley earth structure, the capability exists to use theoretical models to predict future strong ground motion.

- the directivity effect was suggested to have a dominant effect on the motion recorded at the El Centro site.

- sensitivity studies indicate the strong dependence of predicted ground motion on stress drop, rupture velocity and azimuthal location of the site.

## VII.3 RECOMMENDATIONS FOR FUTURE RESEARCH

Topics for future research are suggested based on the findings of this work. Subjects that deserve future investigation are:

- including the P-SV motion or spheroidal modes in the normal mode model so that the complete motion may be determined.

- including a more realistic model for Q, the specific attenuation factor.

- a study of the effect of different earth models on the ground motion, i.e., linear gradient models vs. step gradients.

- application of the normal mode method to other regions.

- incorporation of an occurrence model to develop the total seismic hazard at a site.

## REFERENCES


Abramowitz, M. and I.A. Stegun (1972). Handbook of Mathematical Functions, Dover Publications, New York.

Aki, K. (1966). Generation and Propagation of G Waves from the Nijgata Earthquake of June 16, 1964, 2, Estimation of Earthquake Moment, Released Energy, and Stress-Strain Drop from G-Wave Spectrum, Bull. Earthquake Res. Inst., Tokyo University, 44, 73-88.

Aki, K. (1967). Scaling Law of Seismic Spectrum, J. Geophy. Res. 72, 1217-1231.

Aki, K. (1968). Seismic Displacements Near a Fault, J. Geophy. Res. 73.

Aki,K. and P.G. Richards (1980). Quantitative Seismology, Theory and Methods, W.H. Freeman and Company, San Francisco.

Amin, M. and A.H.S. Ang (1968). Nonstationary Stochastic Model of Earthquake Motions, J. Engr. Mechanics Div. Proc. ASCE 94, 559-583.

Anderson, J.G. and M.D. Trifunac (1977). On Uniform Risk Functionals Which Describe Strong Earthquake Ground Motion: Definition, Numerical Estimation, and an Application to the Fourier Amplitude of Acceleration, A Report of Research Conducted Under a Contract from the U.S. Nuclear Regulatory Commission, Los Angeles, California.

Ang, A.H.S and W.H. Tang (1975). Probability Concepts in Engineering Planning and Design, J. Wiley & Sons, Inc., New York.

Archuleta, R.J. (1979) EOS, American Geophysical Union Meeting Abstracts, San Francisco.

Archuleta, R.J. and R.V. Sharp (1980). Source Parameters of the Oct. 15, 1979 Imperial Valley Earthquake From Nearfield Observations, EOS, American Geophysical Union Meeting Abstracts, Toronto.

Archuleta, R.J. and G.A. Frazier (1978). Three-Dimensional Numerical Simulations of Dynamic Faulting in a Half-Space, Bull. Seism. Soc. Am. 68, 541-572.

Arias, A. (1970). A Measure of Earthquake Intensity in Seismic Design of Nuclear Power Plants, R. Hansen, Editor, M.I.T. Press.

Bath, M. (1973). Introduction to Seismology, J. Wiley & Sons, Inc., New York.

Bayes, T. (1958). An Essay Towards Solving A Problem in the Doctrine of Chances, reprinted in Biometrika 45.

Ben-Menahem, A. (1961). Radiation of Seismic Surface Waves from Finite Moving Sources, Bull. Seism. Soc. Am. 51, 401-435.

Ben-Menahem, A. (1962). Radiation of Seismic Body Waves from a Finite Moving Source in the Earth, J. Geophy. Res. 67.

Bendat, J.S. and A.G. Piersol (1971). Random Data: Analysis and Measurement Procedures, Wiley-Interscience, New York.

Benjamin, J.R. (1968). Probabilistic Models for Seismic Force Design, J. Struc. Div., ASCE 94, No. ST5, Proc. Paper 5950, 1175-1196.

Benjamin, J.R. and C.A. Cornell (1970). Probability, Statistics and Decisions for Civil Engineers, McGraw Hill Book Co., New York.

Biehler, S., R.L. Kovach, and C.R. Allen (1964). Geophysical Framework of the Northern End of the Gulf of California Structural Province, in Marine Geology of the Gulf of California,T.H. van Andel and G.G. Shor, Jr., Editors, Am. Assoc. Petrol. Geologists Mem. 3, 126-143.

Blume, J.A. (1965). Earthquake Ground Motion and Engineering Procedures for Important Installations Near Active Faults, Proceedings Third World Conf. on Earthquake Engineering, Aukland, New Zealand, Vol. III, 56-71.

Boore, D.M. and W. Joyner (1978). The Influence of Rupture Incoherence on Seismic Directivity, Bull. Seism. Soc. Am. 68, 283-300.

Boore, D.M., A.A. Oliver, III, R.A. Page, and W.B. Joyner (1978). Estimation of Ground Motion Parameters, U.S. Geol. Surv. Open File Report 78-509.

Boore, D.M. and M.D. Zoback (1974). Two Dimensional Kinematic Fault Modeling of the Pacoima Dam Strong Motion Recordings of the February 9, 1971 San Fernando Earthquake, Bull. Seism. Soc. Am. 64, 555-570.

Brune, J. (1970). Tectonic Stress and the Spectra of Seismic Shear Waves from Earthquakes, J. Geophy. Res. 75.

Burdick,L.J. and G.R. Mellman (1976). Inversion of Body Waves From The Borrego Mountain Earthquake to the Source Mechanism, Bull. Seism. Soc. Am. 66, 1485-1499.

Campbell, K.W. (1977). The Use of Seismotectonics in the Bayesian Estimation of Seismic Risk, School of Engineering and Applied Science, University of California, Los Angeles, UCLA-ENG-7744.

Clayton, R.W. and G.A. McMechan (1980). Inversion of Refraction Data by Wave-Field Migration, Stanford Exploration Project Report No. 24.

Clough, R.W. and J. Penzien (1975). Dynamics of Structures, McGraw-Hill Book Company, New York.

Cornell, C.A. (1968). Engineering Seismic Analysis, Bull. Seism. Soc.

Am. 58, 1583-1606.

deHoop, A.T. (1958). Representation Theorems For the Displacement in an Elastic Solid and Their Application to Elastodynamic Diffraction Theory, Thesis, Technische Hogescool, Delft.

De Finetti, B. (1951). Recent Suggestions for the Reconciliation of Theories of Probability, Proceedings of the Second Berkeley Symposium on Mathematical Statistics and Probability, Univ. of Calif. Press.

De Finetti, B. (1961). The Bayesian Approach to the Rejection of Outliers, Proceedings of the Fourth Berkeley Symposium on Mathematics and Probability, Univ. of Calif. Press.

Donovan, N. (1974). Earthquake Hazard for Buildings, Dames and Moore Engineering Bulletin 46, Los Angeles.

Esteva, L. (1969). Seismicity Prediction: A Bayesian Approach, Proceedings of the Fourth World Conf. on Earthquake Engineering, 172-184.

Esteva, L. and E. Rosenblueth (1964). Espectros de Templores a Distancias Moderadas y Grandes, Publication Num. 11, Sociedad Mexicana de Ingeniera Sismica.

Eguchi, R.T. and J.H. Wiggins (1979). A Bayesian Seismic Risk Study of California with Loss Estimates, Technical Report No. 79-1328-1, J.H. Wiggins Co.

Fukao, Y. and K. Abe (1971). Multimode Love Waves Excited by Shallow and Deep Earthquakes, Bull. Earthquake Res. Inst., Tokyo University, 49, 1-12.

Geller, R. (1976). Scaling Relations for Earthquake Source Parameters and Magnitudes, Bull. Seism. Soc. Am. 66, 1501-1527.

Geller, R.J. (1976). Geophysics 276, classnotes.

Geller, R.J., G.A. Frazier, and M.W. McCann, Jr. (1979). Dynamic Finite Element Modeling of Dislocations in a Laterally Heterogeneous Crust, J. Phys. Earth 27,395-407.

Gilbert, F. and A.M. Dziewonski (1975). An Application of Normal Mode Theory to the Retrieval of Structural Parameters and Source Mechanisms from Seismic Spectra, J. R. Astron. Soc. 278, 187-269.

Good, I.J. (1952). Rational Decisions, Jrnl. of the Royal Statistical Soc. Ser. B, 14.

Good, I.J. (1965). The Estimation of Probabilities, An Essay on Modern Bayesian Methods, Res. Monog. No. 30, M.I.T. Press.

Gutenberg, B. and C.F. Richter (1956). Earthquake Magnitude, Intensity, Energy, and Acceleration (second paper), Bull. Seism. Soc. Am. 46.

Hanks, T.C. (1975). Strong Ground Motion of the San Fernando, Calif. Eq.: Ground Displacements, Bull. Seism. Soc. Am. 65, 193-225.

Hanks, T.C. and D.A. Johnson (1976). A Geophysical Assessment of Peak Accelerations, Bull. Seism. Soc. Am. 66, 959-968.

Harkrider, D.G. (1964). Surface Waves in Multilayered Elastic Media I. Rayleigh and Love Waves from Buried Sources in a Multilayered Elastic Half-space, Bull. Seism. Soc. Am. 66, 959-968

Haskell, N.A. (1964). Total Energy and Energy Spectral Density of Elastic Wave Radiation from Propagating Faults, Part I, Bull. Seism. Soc. Am. 34, 1811-1841

Haskell, N.A. (1966). Total Energy and Energy Spectral Density of Elastic Wave Radiation from Propogating Faults, Part II, A Statistical Source Model, Bull. Seism. Soc. Am. 56, 125-140.

Heaton, T.H. and D.V. Helmberger (1977). A Study of the Ground Motion of the Borrego Moutain, California Earthquake, Bull. Seism. Soc. Am. 67, 315-330

Heaton, T.H. and D.V. Helmberger (1978). Predictability of Strong Ground Motion in the Imperial Valley: Modeling the M4.9 November 4, 1976 Brawley Earthquake, Bull. Seism. Soc. Am. 68, 31-48

Hermmann, R.B. and O.W. Nuttli (1975a). Ground-Motion Modeling at Regional Distances for Earthquakes in a Continenal Interior, I. Theory and Observations, Earthquake Engineering and Structural Dynamics, 4, 49-58.

Hermmann. R.B. and O.W. Nuttli (1975b). Ground-Motion Modeling at Regional Distances for Earthquakes in a Continental Interior, II. Effect of Focal Depth, Azimuth, and Attenuation, Earthquake Engineering and Structural Dynamics, 4, 59-72.

Hileman, J.A., C.R. Allen, and J.M. Nordquist (1973). Seismicity of the Southern California Region, January 1932 to 31 December 1972, Seismological Laboratory, California Institute of Technology.

Housner, G.W. (1975). Measures of Severity of Earthquake Ground Shaking, Proceedings U.S. National Conference on Earthquake Engineering, EERI, Ann Arbor, Michigan.

Housner, G.W. and P.C. Jennings (1964). Generation of Artificial Earthquakes, Eng. Mechanics Div., ASCE 90, No. EMI, Proc. Paper 3806.

Howard, R.A. (1968). The Foundations of Decision Analysis, IEEE Transactions on Systems, Science and Cybernetics, Vol. SSC-4, No. 3, 1-9

Hradilek, P.J. and J.E. Luco (1970). Dynamic Soil-Structure Interaction, IDIEM Informa Tecnico, No. 14, Instituto de Investigaciones Y Ensayes de Materiels, Universidad de Chile, Santiago.

Hudson, D.E. (1969). Strong Motion Earthquake Accelerograms Digitized and Plotted Data, Vol.II Corrected Accelerograms and Integrated Ground Velocity and Dislpacement Curves, Parts A-W, E.E.R.L. Report, 71-50.

Idriss, I.M. (1978). Characteristics of Earthquake Ground Motions, Proceedings of the ASCE Specialty Conference on Earthquake Engineering and Soil Dynamics, Vol. III, Pasadena, California.

Jaynes, E.T. (1958). Probability Theory in Science and Engineering, Colloquium Lectures in Pure and Applied Science, No. 4, Field Research Laboratory Socony Mobil Oil Company, Inc.

Jeffreys, H. (1961). Theory of Probability, Oxford at the Clarendon Press.

Kanamori, H. (1970). Synthesis of Long-Period Surface Waves and Its Application to Earthquake Source Studies - Kurile Islands Earthquake of October 13, 1963, J. Geophy. Res. 75, 5011-5027.

Kanamori, H. (1979). A Semi-Empirical Approach to Prediction of Long Period Ground Motion from Great Earthquakes, Bull. Seism. Soc. Am. 69, 1546-1670

Kanamori, H. (1980). personal communication.

Kanamori, H. and D.L. Anderson (1975). Theoretical Basis of Some Empirical Relations in Seismology, Bull. Seism. Soc. Am. 65, 1073-1095.

Kanamori, H. and G.S. Stewart (1976). Mode of the Strain Release Along the Gibbs Fracture Zone, Physics of the Earth and Planetary Interior, 312-332.

Keilis-Borok, V.I. (1959). On Estimation of the Displacement in an Earthquake Source and of Source Dimensions, Ann. Geofis. 12, 205-214

Keilis-Borok, V.I. (1960). Investigation of the Mechanism of Earthquakes, Sov. Res. Geophys, 4 (transl. Tr. Geofiz. Inst., 40,1957), American Geophysical Union, Consultants Bureau, 201.

Kiremidjian, A.S. (1976). Probabilistic Hazard Mapping and Development of Site-Dependent Seismic Load Parameters, Ph.D. Dissertation, Dept. of Civil Engineering, Stanford University.

Kiremidjian, A.S. (1979). An Alternating Markov Model for Earthquake Occurrences, Proceedings of the ASCE Specialty Conference on Probabilistic Mechanics and Structural Reliability, Tucson, Arizona.

Koopman, B.O. (1941). Intuitive Probabilities and Sequences, Annals of Mathematics 42.

Langston, C.A. (1978). The February 9, 1971 San Fernando Earthquake: A Study of Source Finiteness in Teleseismic Body Waves, Bull. Seism. Soc. Am. 68, 1-30.

Love, A.E.H. (1927). A Treatise on the Mathematical Theory of Elasticity, Dover Publications, New York.

McCann, Jr., M.W. (1980). RMS Acceleration and Duration of Strong Ground Motion, The John A. Blume Earthquake Engineering Center, Tech. Report No. 46, Dept. of Civil Engineering, Stanford University.

McGuire, R.K. (1974). Seismic Structural Response Risk Analysis, Incorporating Peak Response Regressions on Earthquake Magnitude and Distance, Report R74-51 Dept. of Civil Engineering, M.I.T.

McGuire, R.K. (1978). A Simple Model For Estimating Fourier Amplitude Spectra of Horizontal Ground Acceleration, Bull. Seism. Soc. Am. 68, 803-822.

Molina, E.C. (1931). Bayes Theorem: An Expository Presentation, Annals of Mathematical Statistics II.

Morris, P.A. (1971). Bayesian Expert Resolution, Ph.D. Dissertation, Dept. of Engineering - Economic Systems, Stanford University,

Mortgat, C.P. (1976). A Bayesian Approach to Seismic Hazard Mapping: Development of Stable Design Parameters, Ph.D. Thesis, Dept. Civil Engineering, Stanford University.

Nur, A. (1978). Non-Uniform Friction as a Physical Basis for Earthquake Mechanics, Pure Appl. Geophysics, 116, 964-989.

Pilant, W.L. (1979). Elastic Waves in the Earth, Elsevier Scientific Publ. Co., Amsterdam.

Press, F. (1965). Resonant Vibrations of the Earth, Scientific American.

Raiffa, H. and R. Schlaiffer (1961). Statistical Decision Theory, M.I.T. Press, Cambridge.

Richter, C.F. (1958). Elementary Seismology, W.H. Freeman and Company, San Francisco and London.

Saito, M. (1967). Excitation of Free Oscillations and Surface Waves by a Point Source in a Vertically Heterogeneous Earth, J. Geophy. Res. 72.

Savage, L.J. (1961). The Foundations of Statistics Reconsidered, Proceedings of the Fourth Berkeley Symposium on Mathematics and Probability, University of Calif. Press.

Savage, L.J. (1962). Bayesian Statistics, in Recent Developments in Information and Decision Processes, Ed. R.E. Machol, Paul Gray MacMillan Company, N.Y..

Savage, J.G. (1966). Radiation from a Realistic Model of Faulting, Bull. Seism. Soc. Am. 55, 577-592.

Savy, J.B. (1978). Determination of Seismic Design Parameters: A Stochastic Approach, The John A. Blume Earthquake Engineering Center, Tech. Report No. 34, Dept. of Civil Engineering, Stanford University.

Scanlan, R.H. (1976). Seismic Wave Effects on Soil-Structure Interaction, Earthquake Engineering and Structural Dynamics 4, 379-388.

Seih, K.E. (1979). Slip Along the San Andreas Fault Associated with the Great 1857 Earthquake, Bull Seism. Soc. Am. 68, 1421-1448.

Shah, H.C., C.P. Mortgat, A.S. Kiremedjian and T.C. Zsutty (1975). A Study of Seismic Risk for Nicaragua, Part I, The John A. Blume Earthquake Engineering Center, Tech. Report No. 11, Dept. of Civil Engineering, Stanford University.

Swanger, H.S. and D.M. Boore (1978). Simulation of Strong Motion Displacements Using Surface Wave Modal Superposition, Bull. Seism. Soc. Am. 68, 907-922.

Takeuchi, H. and M. Saito (1972). Seismic Surface Waves, Methods in Computational Physics, Bruce A. Bolt ed., II.

Tribus, M. (1969). Rational Descriptions, Decisions and Designs, Pergamon Press, New York.

Trifunac, M.D. (1974). A Three Dimensional Dislocation Model for the San Fernando, California Earthquake of February 9, 1971, Bull. Seism. Soc. Am. 64, 149-172.

Trifunac, M.D. (1976). Preliminary Empirical Model for Scaling Fourier Amplitude Spectra of Strong Ground Accelerations in Terms of Earthquake Magnitude, Source-to-Site Distance and Recording Site Conditions, Bull. Seism. Soc. Am. 66, 1343-1373.

Trifunac, M.D. and A.G. Brady (1975). On the Correlation of Seismic Intensity Scales with the Peaks of Recorded Strong Ground Motion, Bull. Seism. Soc. Am. 65, 139-162.

Trifunac, M.D. and V. Lee (1973). Routine Computer Processing of Strong-Motion Accelerograms, EERL 73-03, California Institute of Technology.

USGS Open-File Report 79-1654 (1979). Preliminary Summary of the U.S. Geological Survey Strong-Motion Records from the October 15, 1979 Imperial Valley Earthquake.

Vagliente, V.N. (1973). Forecasting the Risk Inherent in Earthquake-Resistant Design, Tech. Report No. 174, Dept. of Civil Engineering, Stanford University.

Wiggins, R.A. (1976). A Fast, New Computational Algorithm for Free Oscillations and Surface Waves, Geophy. J. R. Astr. Soc., 135-150.

Wyss, M. (1977). Earthquake Mechanism: Preparatory Phase and Rupture, Proceedings Sixth World Conf. on Earthquake Engineering, New Delhi.